RL-TR-96-10
In-House Report
February 1996

BIREFRINGENT FIBER DEVICES AND LASERS

James P. Theimer

APPROVED FOR PUBLIC RELEASE; DISTRIBUTION UNLIMITED.

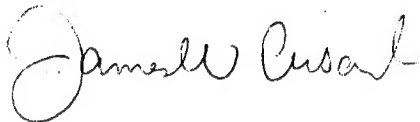**Rome Laboratory
Air Force Materiel Command
Rome, New York**

19960508 091

This report has been reviewed by the Rome Laboratory Public Affairs Office (PA) and is releasable to the National Technical Information Service (NTIS). At NTIS it will be releasable to the general public, including foreign nations.
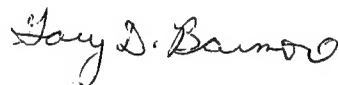
RL-TR-96-10 has been reviewed and is approved for publication.

APPROVED: *James W. Cusack*

JAMES W. CUSACK, Chief
Photonics Division
Surveillance & Photonics Directorate

FOR THE COMMANDER: *Gary D. Barmore*

GARY D. BARMORE, Major, USAF
Deputy Director
Surveillance & Photonics Directorate

If your address has changed or if you wish to be removed from the Rome Laboratory mailing list, or if the addressee is no longer employed by your organization, please notify Rome Laboratory(OCPC), Rome NY 13441. This will assist us in maintaining a current mailing list.

Do not return copies of this report unless contractual obligations or notices on a specific document require that it be returned.

REPORT DOCUMENTATION PAGE

Public reporting burden for this collection of information is estimated to average 1 hour per response, including the time for reviewing instructions, searching existing data sources, gathering and maintaining the data needed, and completing and reviewing the collection of information. Send comments regarding this burden estimate or any other aspect of this collection of information, including suggestions for reducing this burden, to Washington Headquarters Services, Directorate for information Operations and Reports, 1215 Jefferson Davis Highway, Suite 1204, Arlington, VA 22202-4302, and to the Office of Management and Budget, Paperwork Reduction Project (0704-0188), Washington, DC 20503.

1. AGENCY USE ONLY (Leave Blank)	2. REPORT DATE February 1996	3. REPORT TYPE AND DATES COVERED In-House Oct 93 – Oct 95

4. TITLE AND SUBTITLE

BIREFRINGENT FIBER DEVICES AND LASERS

5. FUNDING NUMBERS

PE - 62702F
PR - 4600
TA - P2
WU - 12

6. AUTHOR(S)

James P. Theimer

7. PERFORMING ORGANIZATION NAME(S) AND ADDRESS(ES)

Rome Laboratory/OCPC
25 Electronic Pky
Rome NY 13441-4515

8. PERFORMING ORGANIZATION REPORT NUMBER

RL-TR-96-10

9. SPONSORING/MONITORING AGENCY NAME(S) AND ADDRESS(ES)

Rome Laboratory/OCPC
25 Electronic Pky
Rome NY 13441-4515

10. SPONSORING/MONITORING AGENCY REPORT NUMBER

N/A

11. SUPPLEMENTARY NOTES

Rome Laboratory Project Engineer: James P. Theimer/OCPC/(315)330-4870

12a. DISTRIBUTION/AVAILABILITY STATEMENT

Approved for public release; distribution unlimited.

12b. DISTRIBUTION CODE

13. ABSTRACT (Maximum 200 words)

This report describes the results of computer simulations of optical devices which contain birefringent elements. The physics of pulse propagation in birefringent fiber is summarized first. The behavior of pulses in birefringent fiber amplifiers is examined. These pulses will break up under high amplification. This behavior is shown in the simulations. Simulations of the Nonlinear Optical Loop Mirror are shown. The differences between the behavior of these devices with pulsed and non-pulsed inputs are discussed, and approximate analytical models are derived. The effect of changing polarization controller settings is examined extensively. A fiber ring laser mode-locked with a Nonlinear Optical Loop Mirror is studied. It is shown that the cavity length can be increased greatly if the dispersion of the fiber in the amplifier and in the loop mirror is balanced so that the pulse is nearly a soliton in both elements.

14. SUBJECT TERMS birefringent fiber, Nonlinear Optical Loop Mirror, erbium fiber amplifier, figure-eight laser, fiber laser

15. NUMBER OF PAGES 174

16. PRICE CODE

17. SECURITY CLASSIFICATION OF REPORT UNCLASSIFIED	18. SECURITY CLASSIFICATION OF THIS PAGE UNCLASSIFIED	19. SECURITY CLASSIFICATION OF ABSTRACT UNCLASSIFIED	20. LIMITATION OF ABSTRACT U/L

Table of Contents

List of Figures

iv

List of Tables

ABSTRACT

This thesis presents the results of numerical simulations of mode-locked figure eight lasers and their components: fiber amplifiers and nonlinear optical loop mirrors (NOLMs). The computations were designed to study pulse evolution in optical amplifiers and NOLMs with periodic repetition of these elements. Since fiber laser systems also include birefringent fiber, the effects of fiber birefringence was incorporated into the simulations.

My studies of pulse amplification in non-birefringent amplifiers show pulse breakup when their energies exceed 4.5 fundamental soliton energies. In birefringent fibers pulse breakup is also found, but the two orthogonally polarized pulses propagate together. I find that their behavior is related to the properties of a vector soliton.

I found that vector waves have close to unity transmission through a birefringent NOLM, but the pulse shape is distorted. This shape distortion reduces subsequent transmissions through the NOLM. The energy required for peak transmission of the pulse is predicted by the theory based on vector solitons. The same theory also predicted the low intensity transmission. The performance of the NOLM with birefringent fiber could not be improved by altering the polarization state of the pulse from linear polarization; the polarization controller introduced pulse distortion that resulted in excessive loss.

I found an instability in the steady-state operation of the figure eight laser, which is due to pulse reshaping during propagation in the amplifier section. To remove this instability I introduced the concept of dispersion balancing; by increasing the dispersion in the amplifier section, the pulse can propagate nearly as a fundamental soliton in both the amplifier and the NOLM sections of the laser. This eliminated a major source of dispersive wave shedding and allowed the laser operation to become independent of the amplifier length. Sidebands were found on the pulse spectrum and their maxima corresponded well with the periodic resonance model.

Chapter One : Introduction

This thesis describes the results of simulations of the figure eight laser and its components. The intent has been to improve the understanding of the behavior of these lasers and to propose improvements to their design. A great deal of the behavior of these lasers appears to be controlled by the polarization state of the light. For this reason, the evolution of the polarization state has been extensively studied. The laser simulated is shown in Figure 1.1. It consists of an output coupler, an optical isolator, an amplifier, and a Nonlinear Optical Loop Mirror (NOLM) which serves to mode-lock the laser. The thesis examines how each of the components can be simulated, and then how simulations of the parts are used to model the total system. Propagation of pulses in fiber and their simulation is discussed in Chapter 2. The effects of birefringence are introduced in Chapter 3. Chapter 4 describes how the amplifier is simulated and the NOLM is discussed in Chapter 5. In Chapter 6, all these components are drawn together and simulations of the laser system are described.

It is hoped that these mode-locked fiber lasers will provide a convenient way of producing short optical pulses at high repetition rates. Optical fiber offers an attractive means of producing many useful optical effects. These properties can be used to produce fiber lasers and fiber devices. Since the invention of the laser, optics has been viewed as an attractive means for very high speed data transmission.[1] This is due to the extremely large bandwidths available, compared to traditional electronics. Because of the poor properties of optical transmission through the atmosphere and the inevitable tendency of optical beams to diverge due to diffraction, the development of optical communications had to wait for the invention of low loss optical fibers. In addition to producing a low loss transmission path, fiber also produces amplified nonlinear effects. The fiber continually focuses down the light, overcoming the tendency of light to spread out due to diffraction.[2] Apart from enabling the fiber to act as a means of guiding light from one point to another, this means that light in a fiber is of moderately high intensity

1

for long distances. Since the distances can be made long, large nonlinear optical effects can be produced in standard silica fibers in spite of relatively low nonlinear coefficients. By
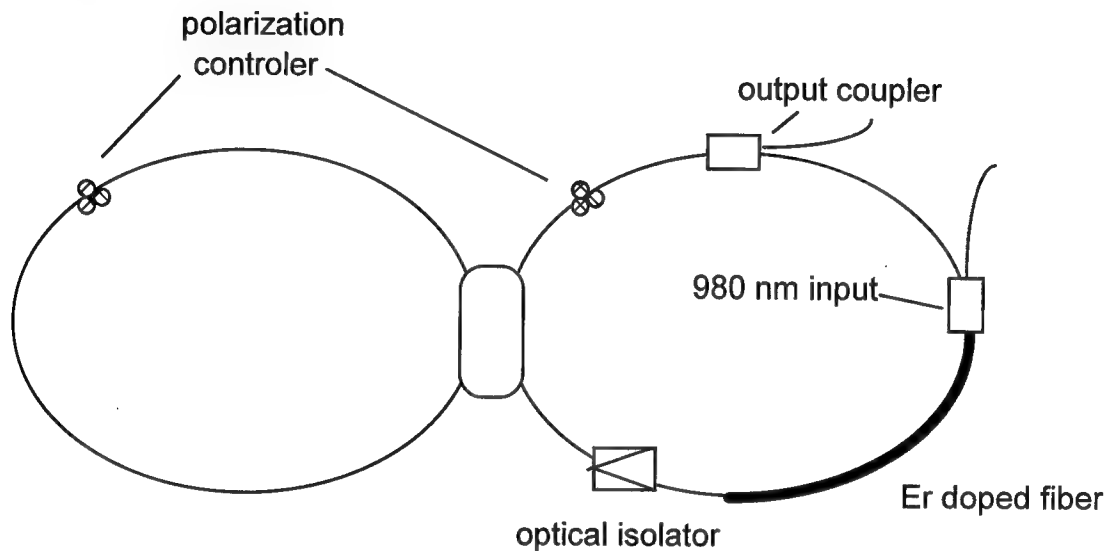
Figure 1.1 NOLM Figure Eight Laser

comparison, an experiment involving light in free space and bulk nonlinear optical material, requires the light to be focused down by a lens.[3] The light near the focal point of the lens can attain very high intensities, but only for a very short distance. Indeed, the more the light is focused down to get high intensities, the shorter this distance becomes.[4] These facts make optical fibers interesting as a system for investigating practical nonlinear optics, involving modest amounts of optical power. The same optical confinement is needed to make efficient optical amplifiers. This means that fibers can make excellent optical cavities for lasers.

The propagation of light in a nonlinear medium makes possible a variety of useful phenomena. Since the light can interact with light from other sources, all-optical switches are possible.[5] Recently, fiber amplifiers have emerged as a practical device.[6,7]

The nonlinear effect in fibers results in the formation of optical pulses known as optical solitons.[8] In a medium in which there is anomalous dispersion, where the group

velocity increases with frequency, the medium will support solitons. In a dispersive fiber, if one ignores nonlinear effects, a short optical pulse will tend to spread in time since light of different frequencies will propagate at different velocities. Optical solitons exist when the nonlinearity of the fiber cancels out the effect of dispersion. In silica fiber, there is anomalous dispersion of light with a wavelength of 1.55 μm. This also corresponds with the wavelength which experiences minimum loss in silica fiber. Since these pulses remain stable, they are of interest for long distance very high speed communications.

Optical nonlinearity in fiber has been used to produce a variety of all optical switches.[5] Loop mirrors work by using the phase difference built up as light of unequal intensities propagates in a Sagnac loop.[9] Dual core fibers have been made in which light in the two cores can interact. This interaction may be used to cause switching behavior.[10] Interaction of light of different polarizations in birefringent fiber causes the frequency of the light in both polarizations to shift so that pulses of light in both polarizations may propagate as one coupled soliton. This phenomenon, known as soliton dragging, has been used to produce a switch.[11] In a birefringent fiber, the polarization of elliptically polarized light evolves at a rate proportional to its intensity, so an optical polarizer can be placed in the system to produce intensity dependent switching. Time division multiplexing has been demonstrated using these devices.

The combination of optical amplifiers and intensity dependent switching makes possible many forms of mode-locked fiber lasers for the production of short optical pulses[6]. Indeed, lasers using Sagnac switches and polarization evolution have been demonstrated experimentally.[12,13,14] Dual core fiber lasers have been proposed and studied by simulations.[15] The appeal of an all fiber laser is that it would appear to offer a robust and inexpensive means of producing short optical pulses. All these are also made possible by the large bandwidth of Erbium doped fiber amplifiers. This wide bandwidth also means that the lasers have a very large saturation energy and this means pulses produced in fiber lasers tend to be highly symmetric and unchirpped. These

advantages, especially as compared to semiconductor lasers, have led commercial firms to examine fiber lasers as a means of producing pulses for long distance communications. In this application, the pulses formed must be close to solitons; any imperfections will result in unwanted background noise. Alternatively, the wide bandwidth, in Erbium doped fiber amplifiers, has been used to produce tunability over a bandwidth of about 30 nm.

This thesis will examine a number of these devices by means of numerical simulation. In the second chapter, the basic physics of pulse propagation in fiber will be examined along with the numerical routines used to simulate it. The third chapter will extend these topics to the case of birefringent fibers. In fact most fibers are birefringent, so this topic must be taken up. Fiber amplifiers are described and the model used in this thesis is discussed in chapter four. The simulations discussed here extend the understanding of pulse amplification in birefringent amplifiers. These chapters lay the groundwork for the simulation of other fiber devices.

Two systems have been examined in detail. They are the Nonlinear Optical Loop Mirror (NOLM), and the figure eight laser. The NOLM is a switch based on the Sagnac effect mentioned above. In addition to its other uses, it can be used as a means of mode-locking a fiber laser. The understanding of the NOLM has been extended by introducing the effect of birefringence. I have examined configurations which produce maximum transmission along with the effect of the switch on the pulses which are being transmitted.

The simulations of the fiber laser carried out for this thesis extend previous work in a number of ways. I have introduced the effect of propagation in the fiber amplifier. This effect has proven to be of great importance to the understanding of the laser. These lasers are marked by a number of different stability regimes. These appear in the simulations. They have been examined, and in one case a means for eliminating one form of the instability has been found. In the final chapter, the conclusions of the research are drawn.

4

Chapter Two : Simulation of pulse propagation

This chapter is intended to serve as an introduction to the physics of pulse propagation in optical fiber. The intention is to show how the basic equations are derived and to discuss the behavior of optical solitons. The major concern is the behavior of light in single-mode step-index silica fiber[1]. This is the sort of fiber used in building the optical devices described in the rest of the thesis. Single mode fiber offers the advantage that transverse modes propagate with different velocities in the fiber so that a multimode signal will break up as it propagates. A step index fiber has a cylindrical core with an index of refraction n_1, in which light is largely confined. This is surrounded by a layer of silica referred to as the cladding which has an index of refraction n_2. If $n_2 < n_1$, light will tend to be confined to the core and the fiber will act as an optical wavguide.

Linear Pulse Propagation in a Fiber

The fundamental component of a simulation of fiber lasers is the simulation of pulse propagation in fiber. Simulation of optical pulses is made more manageable if the function describing the electric field is broken down into components. The electric field of the pulse can be described in the following fashion[1]

$$\vec{E}(\vec{r},t) = \hat{x}A(t)F(x,y)\exp\{i[\omega_0 t - \beta z]\}. \tag{2.1}$$

In this equation, $F(x,y)$ describes the transverse shape of the pulse in the fiber. The exponential term describes the rapid changes of the electric field. The parameter ω_0 is the central frequency and β is the propagation constant. The function $A(t)$ represents the envelope function, that is, the pulse shape. The functions $F(x,y)$ and β are set by properties of the fiber such as the radius of the core, the difference in the index of

refraction between the core and the cladding, and by the central frequency. The envelope function is the part which evolves during propagation through fiber, so it is the focus of further investigation.

The evolution of the envelope function is studied using the nonlinear Schrodinger Equation (NLSE). The linear equations describing propagation in a fiber are derived first. The nonlinear equations are derived as a perturbation to the linear case. This derivation can be found in standard references.[2,16] The starting point for its development is the wave equation

$$\nabla^2 \vec{E}(\vec{r},t) - \frac{1}{c^2} \frac{\partial^2 \vec{E}(\vec{r},t)}{\partial t^2} = -\mu_0 \frac{\partial^2 \vec{P}_L(\vec{r},t)}{\partial t^2},$$
(2.2)

where $\vec{P}_L$ is the linear polarization and $\vec{P}_L = \varepsilon_0 \chi \vec{E}$. We will assume the electric field has the form in Equation 2.1, but it will be considered in frequency space where it becomes

$$\tilde{E}(\vec{r},\omega) = F(x,y)\tilde{A}(\omega - \omega_0)\exp[i(\beta z)].$$
(2.3)

If this is inserted in Equation 2.2, we get

$$\frac{\partial^2 F(x,y)}{\partial x^2} + \frac{\partial^2 F(x,y)}{\partial y^2} + \mu_0 \varepsilon_0 \omega_0^2 F(x,y) - \beta^2 F(x,y) = -\mu_0 \varepsilon_0 \chi F(x,y).$$
(2.4)

Collecting terms this becomes

$$\frac{\partial^2 F(x,y)}{\partial x^2} + \frac{\partial^2 F(x,y)}{\partial y^2} + n^2 k_0^2 F(x,y) - \beta^2 F(x,y) = 0.$$
(2.5)

This equation can be transformed into cylindrical equations. The electric field then becomes

$$\tilde{E}(\rho,z,\omega) = \tilde{A}(\omega)F(\rho)e^{(im\phi)}e^{-i\beta z},$$

and Equation 2.5 becomes

$$\frac{d^2F}{d\rho^2} + \frac{1}{\rho}\frac{dF}{d\rho} + \left(\kappa^2 - \frac{m^2}{\rho^2}\right)F = 0, \tag{2.6}$$

where

$$\kappa^2 = n_i^2 k_0^2 - \beta^2 \,.$$

The variable n_i is the refractive index which takes on values n_1 in the core and n_2 outside the core. Since Equation 2.6 is a Bessel equation, its solutions will be various forms of the Bessel function. The solutions are further constrained by the facts that the field must be finite at the origin and go to zero as ρ goes to infinity. The field must also be continuous at the boundary of the core and the cladding. The first two boundary conditions require that within the core the solution will be

$$F^{(m)}(\rho) = J_m(\kappa\rho)$$

inside the core and

$$F^{(m)}(\rho) = K_m(\gamma\rho)$$

outside the core, where J_m is the Bessel function, K_m is the modified Bessel function and

$$\gamma = \left(\beta^2 - n_2^2 k_0^2\right)^{\frac{1}{2}} \,.$$

The second boundary condition serves to define an eigenvalue equation that sets the values of β, γ and κ for a given set of values of the core radius, n_1, n_2, λ_0, and the order of the solution, m. Values of the propagation constant of order m will be expressed as $\beta^{(m)}$. The normalized frequency, V, is defined by

$$V = k_0 a \left(n_1^2 - n_2^2 \right)^{\frac{1}{2}}.$$

where a is the core radius. The fiber will only support one mode if V is less than about 2.405.

Nonlinear Pulse Propagation

To study the nonlinear phenomena in a fiber, one starts with the nonlinear wave equation

$$\nabla^2 \vec{E} - \frac{1}{c^2} \frac{\partial^2 \vec{E}}{\partial t^2} = -\mu_0 \frac{\partial^2 \vec{P}_L}{\partial t^2} - \mu_0 \frac{\partial^2 \vec{P}_{NL}}{\partial t^2}. \tag{2.7}$$

In the last equation, $\vec{P}_L$ is the linear part of the polarization and $\vec{P}_{NL}$ is the nonlinear part. We will transform this equation by looking for solutions of the form of Equation 2.3,

$$\vec{E}(\vec{r}, \omega) = \hat{x} F(x, y) \tilde{A}(\omega - \omega_0, z) \exp[i(\beta_0 z)]. \tag{2.8}$$

The variable β_0 is the propagation constant. The envelope function is now a function of z, as well as ω because the nonlinear part of the polarization can cause it to evolve as it propagates in the fiber. When this is put into 2.7 we get

$$\frac{\partial^2 F}{\partial x^2} \tilde{A} + \frac{\partial^2 F}{\partial y^2} \tilde{A} + \frac{\partial^2 \tilde{A}}{\partial z^2} F + 2i\beta_0 \frac{\partial \tilde{A}}{\partial z} F + \varepsilon(\omega) k_0^2 F \tilde{A} - \beta_0^2 F \tilde{A} = 0. \tag{2.9}$$

This equation is separable. If we use $\bar{\beta}^2$ as the separation constant, which we will obtain below as the result of solving an eigenvalue problem, the result of the separation is

$$\frac{\partial^2 F}{\partial x^2} + \frac{\partial^2 F}{\partial y^2} + \varepsilon(\omega)k_0^2 F - \overline{\beta}^2 F = 0 \tag{2.10}$$

$$\frac{\partial^2 \widetilde{A}}{\partial z^2} + 2i\beta_0 \frac{\partial \widetilde{A}}{\partial z} + \overline{\beta}^2 \widetilde{A} - \beta_0^2 \widetilde{A} = 0. \tag{2.11}$$

We will first examine Equation 2.10. This will give us the form of the transverse functions. To go further we need to get Equation 2.10 into a form comparable to that of 2.5. To do this we will use the following approximation

$$\varepsilon(\omega) = (n + \Delta n)^2 \cong n^2 + 2n\Delta n \tag{2.12}$$

if Δn is small.

The quantity Δn combines the nonlinear and imaginary parts of the index of refraction

$$\Delta n = n_k I + \frac{i\alpha}{2k_0}, \tag{2.13}$$

where I is the optical intensity. It is assumed that the two additional effects that contribute to Δn are attenuation and the optical Kerr effect. The first term of the last equation describes the optical Kerr effect.[17] The second describes the effect of attenuation or amplification in the fiber. The intensity can be defined as

$$I = \frac{|F|^2 |\widetilde{A}|^2}{\int_{-\infty}^{\infty} \int_{-\infty}^{\infty} |F|^2 \, dxdy}.$$

If we put Equation 2.13 into 2.10, we get

$$\frac{\partial^2 F}{\partial x^2} + \frac{\partial^2 F}{\partial y^2} + n^2 k_0^2 F + 2n\Delta nk_0^2 F - \overline{\beta}^2 F = 0. \tag{2.14}$$

9

Equation 2.14 is a perturbed form of 2.5. It can be solved by first order perturbation theory.[18,19] We seek a value of the eigenvalue of the form

$$\overline{\beta} = \beta(\omega) + \lambda \Gamma \Delta \beta, \qquad (2.15)$$

and eigenfunctions of the form

$$F = F_0 + \Gamma F_1. \qquad (2.16)$$

Where F_0 are the eigenfunctions of the unperturbed problem, F_1 is the function which is the first correction, and Γ is the perturbation parameter. The perturbation parameter is proportional to the nonlinear coefficient n_k and the absorption coefficient α, which are small parameters. If these are substituted into 2.14 and the result is separated into like powers of Γ, we get

$$\frac{\partial^2 F_0}{\partial x^2} + \frac{\partial^2 F_0}{\partial y^2} + n^2 k_0^2 F_0 - \beta(\omega)^2 F_0 = 0 \qquad (2.17)$$

and

$$\frac{\partial^2 F_1}{\partial x^2} + \frac{\partial^2 F_1}{\partial y^2} + n^2 k_0^2 F_1 + 2n \Delta n k_0^2 F_0 - 2\beta(\omega) \Delta \beta F_0 - \beta(\omega)^2 F_1 = 0. \qquad (2.18)$$

Equation 2.17 is the linear propagation equation derived above. The solutions to this equation will be the same as before. The values of F_1 are sought in terms of a series expansion in terms of the complete solutions of 2.17, that is in terms of

$$F_0^{(m)} \qquad m=1,2,3,... \qquad .$$

The expansion can be expressed as

$$F_1 = \sum_m a^{(m)} F_0^{(m)} .$$

This is substituted into 2.18 to obtain

$$\sum_m a^{(m)} \left[\frac{\partial^2 F_0^{(m)}}{\partial x^2} + \frac{\partial^2 F_0^{(m)}}{\partial y^2} + n^2 k_0^2 F_0^{(m)} \right] + 2 n \Delta n k_0^2 F_0^{(n)} - \left[\beta^{(n)}(\omega) \right]^2 \sum_m a^{(m)} F_0^{(m)} = 2 \left[\beta^{(n)}(\omega) \right] \Delta \beta F_0^{(n)} .$$

The last equation reduces to

$$\sum_m a^{(m)} \left[\beta^{(m)}(\omega) \right] F_0^{(m)} + 2 n \Delta n k_0^2 F_0^{(n)} - \left[\beta^{(n)}(\omega) \right]^2 \sum_m a^{(m)} F_0^{(m)} = 2 \left[\beta^{(n)}(\omega) \right] \Delta \beta F_0^{(n)} .$$

This equation is premultiplied by $F_0^{(k)}$ and integrated over all space. Since the functions $F_0^{(m)}$ are orthogonal, we are left with

$$a^{(k)} \left[\beta^{(k)}(\omega) \right] + 2 n k_0^2 \int_{-\infty}^{\infty} \int_{-\infty}^{\infty} \left[F^{(k)} \right]^* \Delta n F^{(n)} dx dy - a^{(k)} \left[\beta^{(n)}(\omega) \right] = 2 \left[\beta^{(n)}(\omega) \right] \Delta \beta \int_{-\infty}^{\infty} \int_{-\infty}^{\infty} \left[F^{(k)} \right]^* F^{(n)} dx dy .$$

In perturbation analysis, one would expand F_1 as a power series of the eigenfunctions of F_0. This case is simple as there is only one mode. If we insert $F_0^{(1)}$ into the last Equation, and define $\beta^{(1)}(\omega) = \beta(\omega)$, the result is

$$n k_0^2 \int_{-\infty}^{\infty} \int_{-\infty}^{\infty} \left[F_0^{(k)} \right]^* \Delta n F_0^{(1)} dx dy = \beta(\omega) \Delta \beta \int_{-\infty}^{\infty} \int_{-\infty}^{\infty} \left[F_0^{(k)} \right]^* F_0^{(1)} dx dy . \tag{2.19}$$

Solving for $\Delta \beta$ and dropping the superscripts this becomes

$$\Delta \beta = \frac{k_0 \int_{-\infty}^{\infty} \int_{-\infty}^{\infty} F_0^* \Delta n F_0 \, dx dy}{\int_{-\infty}^{\infty} \int_{-\infty}^{\infty} F_0^* F_0 \, dx dy} = \frac{k_0 n_k |\tilde{A}|^2 \int_{-\infty}^{\infty} \int_{-\infty}^{\infty} |F_0|^4 \, dx dy}{\left(\int_{-\infty}^{\infty} \int_{-\infty}^{\infty} F_0^* F_0 \, dx dy \right)^2} + \frac{i\alpha}{2} , \tag{2.20}$$

where we have made the assumption that $\beta(\omega) \cong n k_0$.

We may now use the eigenvalue $\overline{\beta}$ in Equation 2.11. We will also make the slowly varying envelope approximation and eliminate the term involving the second derivative. We will further use the approximation

$$\overline{\beta}^2 - \beta_0^{\,2} = (\overline{\beta} - \beta_0)^2 - 2\beta_0^2 + 2\overline{\beta}\beta_0 \cong 2\beta_0(\overline{\beta} - \beta_0). \qquad (2.21)$$

This is justified since the difference is small. This leaves us with

$$2i\beta_0 \frac{\partial \widetilde{A}}{\partial z} + 2\beta_0[\beta(\omega) + \Delta\beta - \beta_0]\widetilde{A} = 0, \qquad (2.22)$$

which can be expressed as

$$\frac{\partial \widetilde{A}}{\partial z} = i[\beta(\omega) + \Delta\beta - \beta_0]\widetilde{A}. \qquad (2.23)$$

The function $\beta(\omega)$ can be approximated by its Taylor expansion

$$\beta(\omega) = \beta_0 + \beta_1(\omega - \omega_0) + \frac{1}{2}\beta_2(\omega - \omega_0)^2 + \frac{1}{6}\beta_3(\omega - \omega_0)^3 + \ldots, \qquad (2.24)$$

where

$$\beta_i = \left(\frac{\partial^i \beta}{\partial \omega^i}\right)_{\omega=\omega_0}.$$

This is substituted into 2.23 to get

$$\frac{\partial \widetilde{A}}{\partial z} = i[\beta_1(\omega - \omega_0) + \frac{1}{2}\beta_2(\omega - \omega_0)^2 + \frac{1}{6}\beta_3(\omega - \omega_0)^3 + \Delta\beta]\widetilde{A}. \qquad (2.25)$$

The inverse Fourier transform of this is taken noting that the inverse Fourier transform of $(\omega-\omega_0)$ is $i\frac{\partial}{\partial t}$. The result is

$$\frac{\partial A}{\partial z} = -\beta_1 \frac{\partial A}{\partial t} - \frac{i}{2} \beta_2 \frac{\partial^2 A}{\partial t^2} - \frac{\beta_3}{6} \frac{\partial^3 A}{\partial t^3} + i\Delta\beta A. \qquad (2.26)$$

When 2.20 is substituted into 2.26, we get

$$\frac{\partial A}{\partial z} = -\beta_1 \frac{\partial A}{\partial t} - \frac{i}{2} \beta_2 \frac{\partial^2 A}{\partial t^2} - \frac{\beta_3}{6} \frac{\partial^3 A}{\partial t^3} + -\frac{\alpha}{2} A + i\gamma|A|^2 A, \qquad (2.27)$$

where the nonlinear coefficient γ is given by

$$\gamma = \frac{n_k \omega_0}{c A_{eff}}, \qquad (2.28)$$

and

$$A_{eff} = \frac{\left(\int_{-\infty}^{\infty} \int_{-\infty}^{\infty} |F|^2 \, dxdy \right)^2}{\int_{-\infty}^{\infty} \int_{-\infty}^{\infty} |F|^4 \, dxdy}. \qquad (2.29)$$

Some additional terms can be added which include effects found in short pulses. In the first place a more extended expansion of $\beta(\omega)$ than was given in 2.24 can be used.[20] One may expand $\beta(\omega)$ in terms of ω and in terms of $|A|^2$ giving

$$\beta(\omega) = \beta_0 + \beta_1(\omega - \omega_0) + \frac{1}{2}\beta_2(\omega - \omega_0)^2 + \frac{1}{6}\beta_3(\omega - \omega_0)^3 +$$

$$\frac{\partial\beta(\omega)}{\partial|\tilde{A}|^2}|\tilde{A}|^2 + \frac{\partial^2\beta(\omega)}{\partial|\tilde{A}|^2 \partial\omega}(\omega - \omega_0)|\tilde{A}|^2 + \dots \quad . \qquad (2.30)$$

If this is put into 2.23 and the inverse Fourier transform is taken, we obtain

$$\frac{\partial A}{\partial z} = -\beta_1 \frac{\partial A}{\partial t} - \frac{i}{2} \beta_2 \frac{\partial^2 A}{\partial t^2} - \frac{\beta_3}{6} \frac{\partial^3 A}{\partial t^3} + -\frac{\alpha}{2} A + i\gamma|A|^2 A - a_1 \frac{\partial}{\partial t}\left(|A|^2 A\right), \qquad (2.31)$$

where $a_1 = \dfrac{\partial^2 \beta(\omega)}{\partial |A|^2 \partial \omega}$. This new term is responsible for the phenomenon know as self-steepening which will be described later.

An additional term is caused by the Raman effect. This is phenomenon known as the self-frequency phase shift. The Raman effect has been found to have a form[5]

$$i\frac{\partial A}{\partial z} = A \int_{-\infty}^{t} f_r(\omega)|A|^2 \, d\omega \,. \tag{2.32}$$

The response function f_r can be approximated by the linear term of its Taylor expansion. If the inverse Fourier transform of the last expression is taken we get

$$i\frac{\partial A}{\partial z} = -a_2 \left(\frac{\partial |A|^2}{\partial t}\right) A. \tag{2.33}$$

The constant a_2 is an experimentally measured value. It is more conventional to refer to the Raman lifetime a_2 as T_R.

The derivation above results in the extended version of the nonlinear Schrodinger equation (NLSE)[21,22] which can be used to describe pulse evolution for pulses as short as about 10 fs. In some places, constants will be changed to make the equations more useful. It is given by

$$\frac{\partial A}{\partial z} + \frac{\alpha}{2} A + \frac{i}{2}\beta_2 \frac{\partial^2 A}{\partial T^2} - \frac{1}{6}\beta_3 \frac{\partial^3 A}{\partial T^3} =$$

$$i\gamma \left[|A|^2 A + \frac{2i}{\omega_0}\frac{\partial}{\partial T}\left(|A|^2 A\right) - T_R\, A \frac{\partial |A|^2}{\partial T} \right]. \tag{2.34}$$

where T is time, as measured in a reference frame moving along with the pulse. That is $T = t - \dfrac{z}{v_g}$ where t is time and v_g is group velocity. The parameters β_2 and β_3 are the second and third order dispersions of the fiber.

14

It is often easier to work with the nonlinear Schrodinger equation in normalized units. This equation is often given in normalized units

$$i\frac{\partial u}{\partial \xi} + \frac{1}{2}\frac{\partial^2 u}{\partial \tau^2} - i\delta\frac{\partial^3 u}{\partial \tau^3} =$$
$$-N^2\left[|u|^2 u + is\frac{\partial}{\partial \tau}\left(|u|^2 u\right) - \tau_R u\frac{\partial}{\partial \tau}\left(|u|^2\right)\right].$$

(2.35)

The variables U, τ, and ξ are given by

$$u = \frac{A}{\sqrt{P_0}}, \qquad \xi = \frac{z}{L_D}, \qquad \tau = \frac{T}{T_0},$$

where P_0 is the peak power of the pulse. The dispersion length is represented by L_D,

where $L_D = \frac{T_0^2}{|\beta_2|}$. The pulse width measured as the full width at half maximum is given

by T_{FWHM}. The pulse width normally used is T_0, given by $T_{FWHM} = 1.763\, T_0$, for a hyperbolic secant shaped pulse. The pulse will be significantly distorted by linear dispersion if it propagates over a distance long relative to a dispersion length. The parameters δ, τ_R, and s describe the effects of higher-order dispersion, Raman scattering and self-steepening, respectively. They are given by

$$\delta = \frac{\beta_3}{6|\beta_2|T_0}, \qquad \tau_R = \frac{T}{T_R}, \qquad s = \frac{2}{\omega_0 T_0}.$$

The parameter N is given by

$$N^2 = \frac{\gamma P_0 T_0^2}{|\beta_2|}.$$

(2.36)

It should be noted that soliton distances are sometimes given in terms of the soliton period, which is

$$z_0 = \frac{\pi}{2}L_D.$$ (2.37)

Normalized distances are also given in terms of dispersion lengths. This second system will be used in this thesis, except when citing the work of others or when the components being simulated had been described by others. In this way the simulations are directly comparable.

When higher order effects are ignored, Equation 2.35 reduces to

$$i\frac{\partial u}{\partial \xi} + \frac{1}{2}\frac{\partial^2 u}{\partial \tau^2} = -N^2|u|^2 u.$$

This equation is known to have soliton solutions.[1,16] The second term on the left hand side of the last equation describes the effect of second order linear dispersion. The term on the right hand side describes the effect of the optical Kerr nonlinearity on the pulse envelope. Optical solitons exist when these two effects are balanced. Solitons have the property that the envelope function evolves in a periodic fashion as it propagates.[4] When the pulse starts with a form

$$u(0,\tau) = N\sec h(\tau)$$

and N is an integer, the pulse will act as a soliton with a period z_0. The work in this thesis focuses on the fundamental soliton, that is when N=1. In practice it has been found that if $0.5 < N < 1.5$, the pulse will evolve into a fundamental soliton. The envelope function of a fundamental soliton is

$$u(\xi,\tau) = 2\eta \sec h(2\eta\tau)\exp(2i\eta^2\xi).$$

It should be noted that the amplitude of the soliton, its width, and how its phase changes as it propagates are all linked.

The work reported in this thesis is expressed in normalized units of the sort accompanying Equation 2.35. At times it is necessary to choose a standard soliton width, in order to convert to physical units. The results have been normalized to a 300 fs soliton, so the times reported here should be multiplied by 300 fs to be converted to real time. The distances are usually given in terms of the dispersion length which is about 4.5 m for the data expressed above. The energy of the soliton will be 26 pJ. Other units can be derived from these.

Table 2.1 Typical data for optical fibers

T_R	6 fsec
β_2	$10^{-28} \text{sec}^2 \text{cm}^{-1}$
β_3	$10^{-42} \text{sec}^3 \text{cm}^{-1}$
n core index	1.46
Δn, core-cladding index difference	0.0036
n_k	$3.2 \times 10^{-16} \text{cm}^2 \text{W}^{-1}$
a, core radius, standard fiber	$4.15 \mu m$
Additional Data for Typical Doped Fiber	
a, core radius	$3.25 \mu m$
N_a	$2 \times 10^{18} \text{cm}^{-3}$
Δn, core cladding index difference	0.0045
τ, metastable lifetime	10 ms
σ_p, pump absorption cross section (980 nm)	$2 \times 10^{-21} \text{cm}^{-2}$
σ, absorption cross section (1.55 nm)	$3 \times 10^{-21} \text{cm}^{-2}$
T_2, polarization relaxation time	60 fs
L_D, dispersion length (300 fs pulse)	450 cm

Numerical Methods

The nonlinear Schrodinger equation was integrated using the split step Fourier transform method. This is an example of a spectral algorithm. These are described by Strang[23] and DeVries.[24] This procedure is described by Agrawal[4] and a FORTRAN program for the algorithm for the simplified NLSE without higher order dispersion, self-steepening, or Raman scattering, is found in the book by Newell and Moloney.[25] This

program, translated into the C programming language, is the basis of the work done here. To set up this algorithm, one rearranges Equation 2.35, and breaks it up into its linear and nonlinear parts. The equation is then expressed as

$$\frac{\partial U}{\partial \xi} = \left(\hat{L} + \hat{N}\right)U,\tag{2.39}$$

where

$$\hat{L} = -\frac{i}{2}\beta_2 \frac{\partial^2}{\partial T^2} + \frac{1}{6}\beta_3 \frac{\partial^3}{\partial T^3} - \frac{\alpha_n}{2},\tag{2.40}$$

and

$$\hat{N}A = i\gamma\left[|A|^2 A + \frac{2i}{\omega_0}\frac{\partial}{\partial T}\left(|A|^2 A\right) - T_R A \frac{\partial |A|^2}{\partial T}\right].\tag{2.41}$$

If this equation is formally integrated, it yields

$$U(\xi + h) \cong \exp\left(\frac{h}{2}\hat{L}\right)\exp\left(\int_{\xi}^{\xi+h}\hat{N}(z)dz\right)\exp\left(\frac{h}{2}\hat{L}\right)U(\xi),\tag{2.42}$$

where h is the step size. The operator for the linear step is carried out in the Fourier domain

$$\exp\left(\frac{h\hat{L}(\omega)}{2}\right)B(\xi,t) = F^{-1}\left[\exp\left(i\frac{h\tilde{L}(\omega)}{2}\right)F\right]B(\xi,t).\tag{2.43}$$

We replace the operator $\frac{\partial}{\partial T}$ with $i\omega$ in Fourier space where F denotes the Fourier transform.

The nonlinear operator is approximated using a variation on the trapezoidal rule. For the first iteration the operator is simply assumed to be

$$\int_{\xi}^{\xi+h}\hat{N}(z)dz \approx h\hat{N}(z).$$

This first guess is used in Equation 2.42 to derive $U(\xi+h)$. This new value of $U(\xi+h)$ is used to derive a second guess for the nonlinear operator. Using the trapezoidal algorithm for integration integration,

$$\int_{\xi}^{\xi+h} \hat{N}(z)dz \approx \frac{h}{2}\left[\hat{N}(z) + \hat{N}(z+h)\right].$$

This new value for the nonlinear operator can be used to form a new guess for U(ξ+h). The process can be repeated as needed. Four or five iterations are sufficient, though for very intense pulses as many as 10 were used for the results reported in this thesis.

The computer program developed for this thesis was checked in a number of ways. Initially it was compared to published results by other groups. This process is described in the remainder of this section. In addition, some results were compared to those of another student, who also needed to simulate a similar system, and who had independently written a computer code to simulate a fiber amplifier. These results were found to be identical. In general, the step size and number of FFT data points were increased until no further changes were observed. For very intense pulses, as many as 8192 FFT data points were used, though often 1024 points proved to be sufficient. The width of the time window of the simulation was varied from 40 to 240 in soliton units, depending on the application. These were set by examining the results in time and frequency space to insure that the intensity of the pulses had fallen to very small amounts at the edges of the time and frequency windows. For a pulse with an amplitude of about 1 in soliton units, 10 steps per dispersion length were found to be sufficient for accurate simulations. As many as 10,000 steps per dispersion length were used when simulating very intense pulses. It was often found that asymmetries of the pulses at the end of a simulation indicated a problem. This was inevitably the case if there was no physical process in the simulation that would produce this. Finally, wherever possible, analytical predictions of the model's results were made. Many of these are reported in the thesis. Rough agreement between the numerical and analytical results also encourages confidence in the simulation. Finally, the simulation reproduces many phenomena observed in experiments. These will be pointed out in latter sections.

Simulation Results

The algorithm described above was carried out for different values of the constants and compared with published results to verify the accuracy of the program. These results also illustrate how the various higher order effects alter the soliton. Figure 2.1 was the result of propagating a fundamental soliton down a fiber when no higher order terms are present. The result is that the pulse retains its hyperbolic secant shape indefinitely. This case ignores the effect of intensity loss, but otherwise this case is approximately correct for pulses longer than about one picosecond.

Figure 2.2 shows the effect of stimulated Raman scattering (SRS). The case given is for $\tau_R = 0.05$ which allows for direct comparison with Figure 9.14 in Agrawal.[1] The parameter T_R can range from 6-8 fs. The effect becomes significant when pulse duration approaches this value. The effect of SRS is a phenomenon known as self-frequency shift, which reduces the carrier frequency of the soliton. This causes the group velocity of the pulse to be reduced in the anomalous dispersion regime. Figure 2.3 shows the result of the phenomenon known as self-steepening. Here, s=0.2, which makes Figure 2.3 comparable with Figure 5.16 in Reference 1. Again, the primary effect is to slow down the propagation of the soliton in the fiber. Figure 2.4 shows the effect of higher order dispersion. Here the pulse is propagated for 6 soliton periods, with δ=0.33 which allows for comparison with the paper by Liu and Puri.[26]
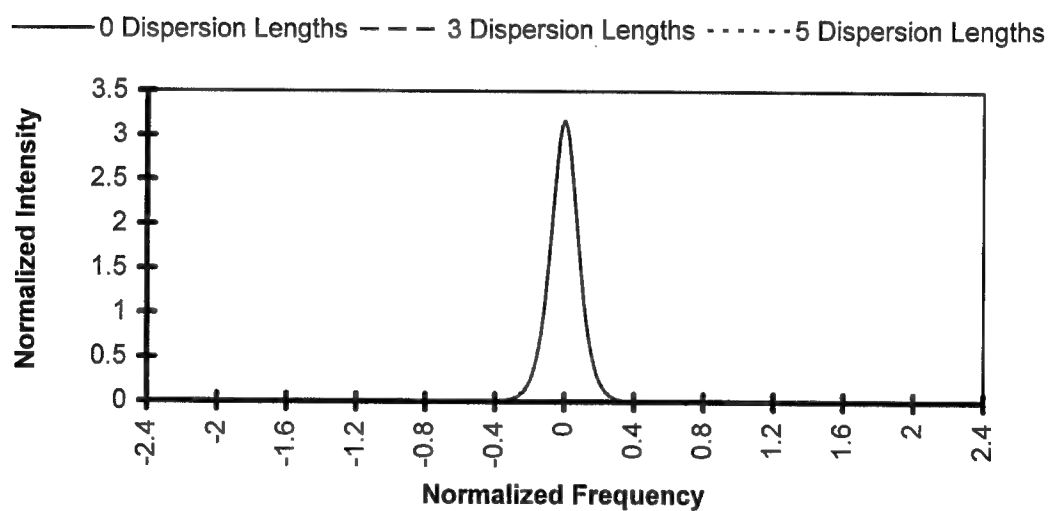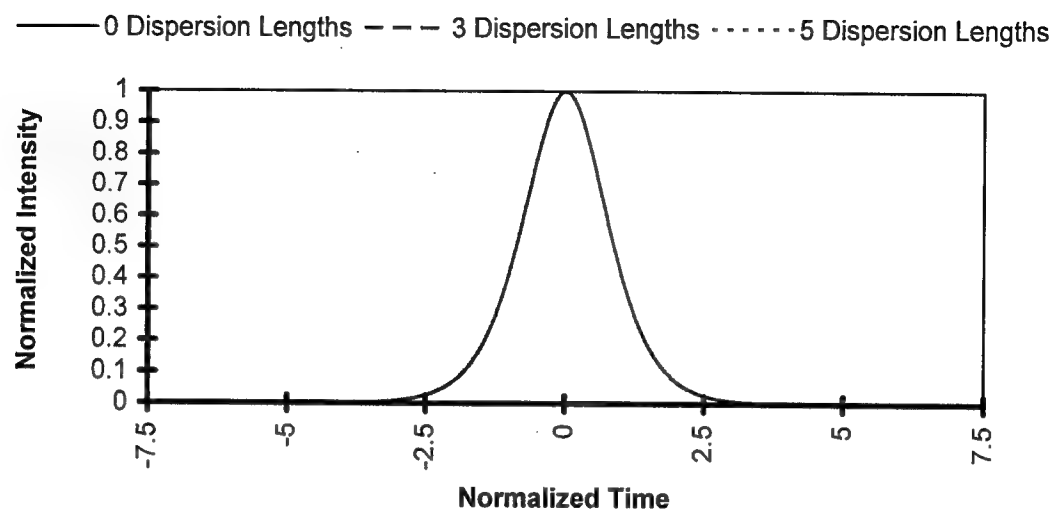
Figure 2.1 Soliton pulse shape with τ_R=0.0, s=0.0, δ=0.0, after traveling 0, 3, and 5 propagation distances. Note that there is a complete overlap of the lines

22
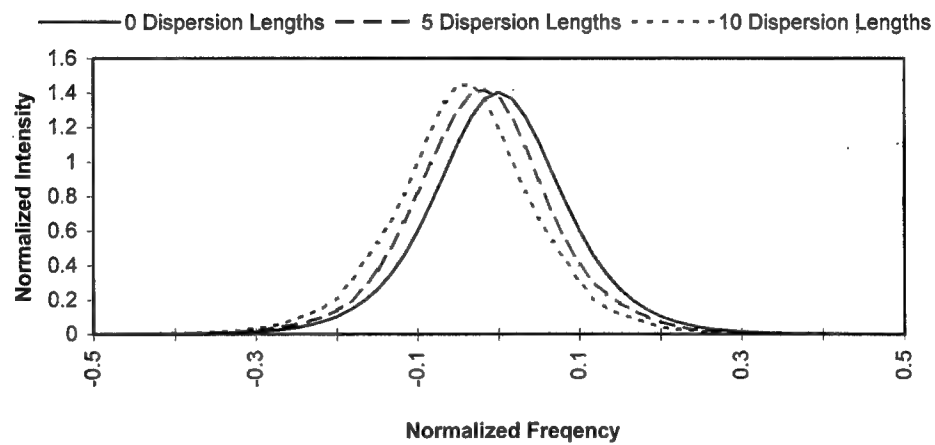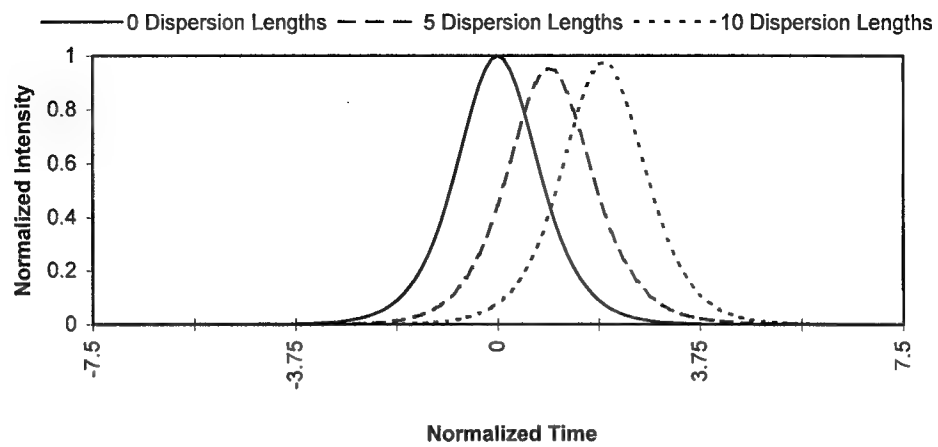
Figure 2.2 **Pulse shapes after 0, 3, and 5 dispersion lengths.** τ_R=0.05. **The Figure shows how the pulse slows down, due to Raman shift.**
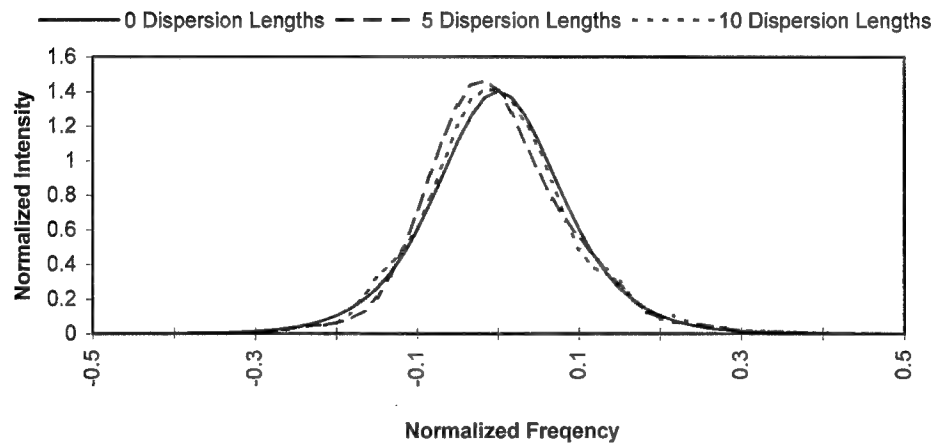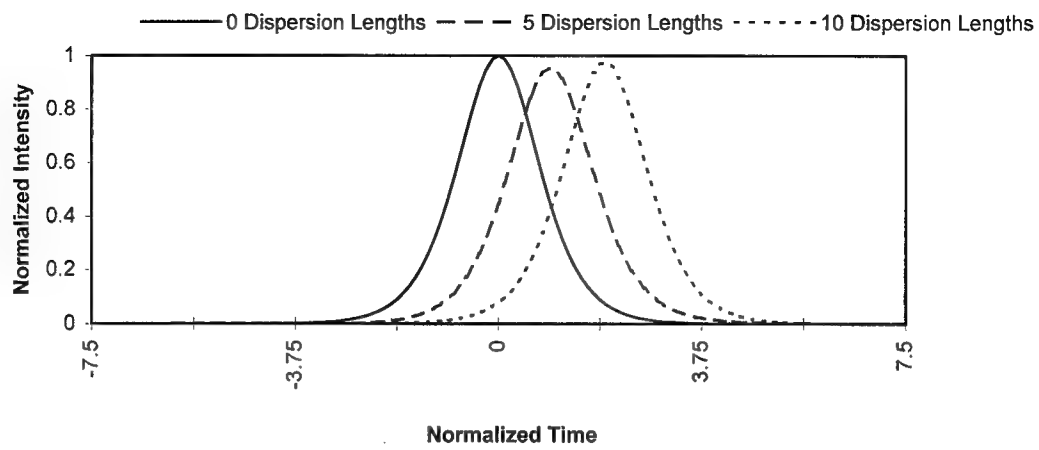
Figure 2.3 Pulse shapes after 0, 5, and 10 dispersion lengths. s=0.2. Figure shows how the pulse slows down due to self-steepening.
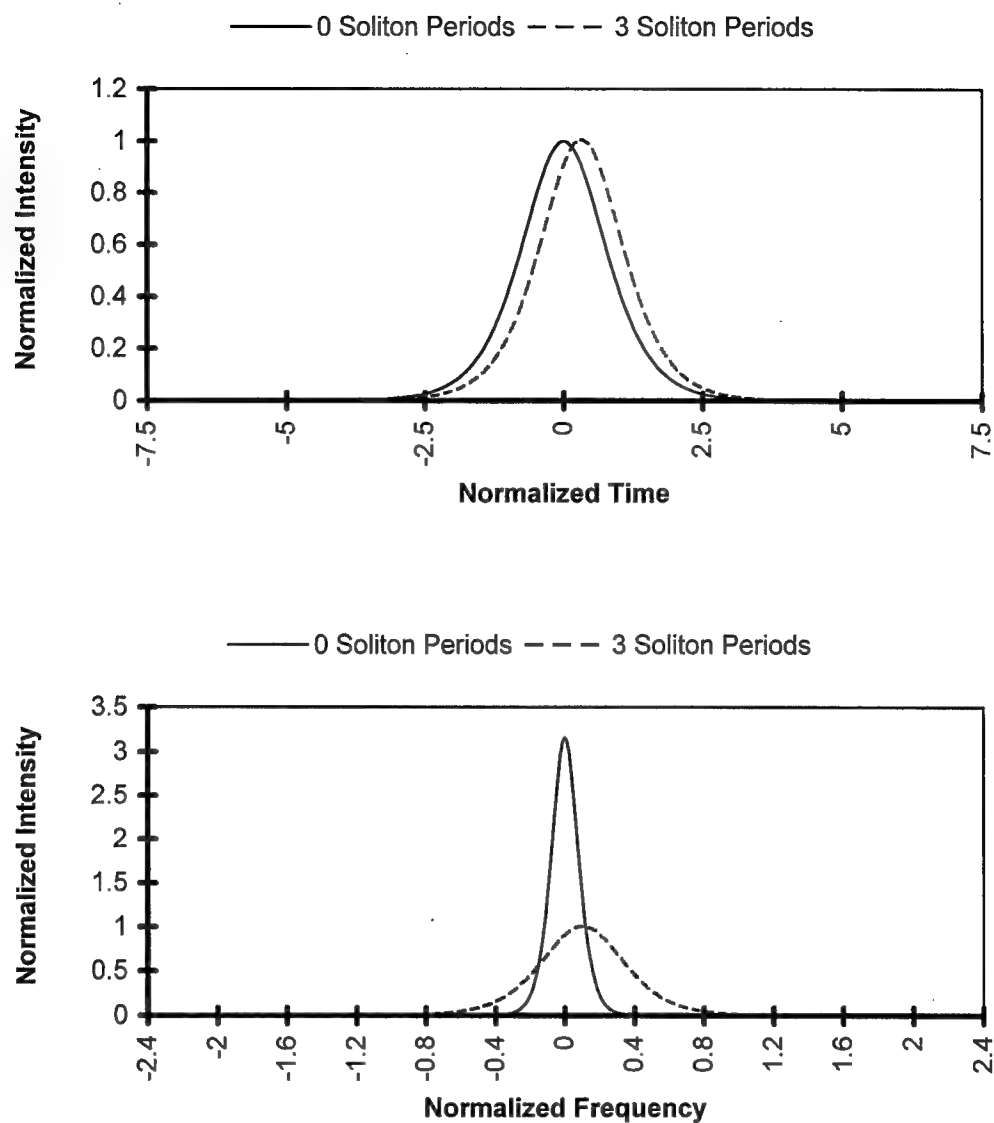
Figure 2.4 Pulse shapes after 0, and 3 soliton periods. δ=0.033. Figure shows the effect of higher order dispersion.

Chapter Three : Propagation in Birefringent Optical Fibers

Normal fibers possess random linear birefringence due to strain or random imperfections in their cores. Linear birefringence of optical fibers has been reviewed by Kaminow.[27] The effect of linear birefringence is that the components of light along the axes of the fiber will have different group velocities. This tends to break up pulses. In the linear regime, power oscillates periodically between the two polarizations with a beat length L_B , where $L_B = \lambda/\Delta n$ and Δn is the difference in index of refraction between the two axes.

In addition to the linear effect, there is a nonlinear contribution to birefringence from self phase modulation.[28,29] The polarization dependent nonlinearities result from a modification to the optical Kerr effect. This will lead to a change in the nonlinear polarization and thus to an altered form of the Nonlinear Schrodinger Equation. The nonlinear polarization will take the form of

$$\vec{P}_{NL}(\vec{r}, t) = \frac{1}{2}\left(\hat{x}P_x + \hat{y}P_y\right)\exp(-i\omega_0 t) + c.\,c., \tag{3.1}$$

where P_x and P_y represent envelope functions and c.c. denotes the complex conjugate of the other term on the right hand side. The components P_x and P_y are given by

$$P_i = \frac{3\varepsilon_0}{2}\sum_j\left(\chi^{(3)}_{xxyy}E_iE_jE_j^* + \chi^{(3)}_{xyxy}E_jE_iE_j^* + \chi^{(3)}_{xyyx}E_jE_jE_i^*\right), \tag{3.2}$$

where the indices i and j can be either x or y. The functions E_x and E_y are the envelope functions as used in Equation 2.1. Due to symmetry relationships, the components of $\chi^{(3)}$ are related by

$$3\chi^{(3)}_{xxxx} = \chi^{(3)}_{xxyy} = \chi^{(3)}_{xyxy} = \chi^{(3)}_{xyyx}.$$

If we use this relationship in Equation 3.2 and 3.1 for the polarization at frequency ω_0 we get the x component

$$\left(\vec{P}_{NL}\right)_x^{\omega=\omega_0} = \frac{3\varepsilon_0}{4}\chi_{xxxx}^{(3)}\frac{1}{3}\left(3E_xE_xE_x^* + E_xE_yE_y^* + E_yE_xE_y^* + E_yE_yE_x^*\right) =$$
$$\frac{3\varepsilon_0}{4}\chi_{xxxx}^{(3)}\left[\left(|E_x|^2 + \frac{2}{3}|E_y|^2\right)E_x + \frac{1}{3}\left(E_x^*E_y\right)E_y\right] \tag{3.3a}$$

and y component

$$\left(\vec{P}_{NL}\right)_y^{\omega=\omega_0} = \frac{3\varepsilon_0}{4}\chi_{xxxx}^{(3)}\frac{1}{3}\left(3E_yE_yE_y^* + E_yE_xE_x^* + E_xE_yE_x^* + E_xE_xE_y^*\right) =$$
$$\frac{3\varepsilon_0}{4}\chi_{xxxx}^{(3)}\left[\left(|E_y|^2 + \frac{2}{3}|E_x|^2\right)E_y + \frac{1}{3}\left(E_y^*E_x\right)E_x\right]. \tag{3.3b}$$

The last result needs to be related to an effective perturbation of the refractive index. We can relate the polarization to the refractive index by

$$P_i = \varepsilon_0\varepsilon_iE_i = \varepsilon_0\left(n + \Delta n_i\right)^2 E_i, \tag{3.4}$$

where the induce i indicates either the x or y axis. The last expression can be approximated by

$$P_i = \varepsilon_0\left(n^2 + 2n\,\Delta n_i\right)E_i. \tag{3.5}$$

If we compare 3.5 to 3.3 we see that

$$\Delta n_x E_x = n_k\left[\left(|E_x|^2 + \frac{2}{3}|E_y|^2\right)E_x + \frac{1}{3}\left(E_x^*E_y\right)E_y\right] \tag{3.6a}$$

and

$$\Delta n_y E_y = n_k\left[\left(|E_y|^2 + \frac{2}{3}|E_x|^2\right)E_y + \frac{1}{3}\left(E_x^*E_x\right)E_x\right], \tag{3.6b}$$

where

$$n_k = \frac{3}{8n}\chi_{xxxx}^{(3)}. \tag{3.7}$$

Equations 3.6 can be substituted into Equation 2.20 to study the effect of polarization on the NLSE. Equation 2.20 showed that

$$\Delta\beta = \frac{k_0 \int\limits_{-\infty}^{\infty}\int\limits_{-\infty}^{\infty} F_0^* \Delta n F_0 \, dxdy}{\int\limits_{-\infty}^{\infty}\int\limits_{-\infty}^{\infty} F_0^* F_0 \, dxdy}.$$

(3.8)

If we substitute Equation 3.6 into Equation 3.8, we get

$$\Delta\beta_i A_i = \frac{k_0 n_k}{\int\limits_{-\infty}^{\infty}\int\limits_{-\infty}^{\infty} F_0^* F_0 \, dxdy}$$

(3.9)

$$\left\{ \left[\int\limits_{-\infty}^{\infty}\int\limits_{-\infty}^{\infty} |F_0|^2 |\overline{E}_i|^2 \, dxdy + \frac{2}{3}\int\limits_{-\infty}^{\infty}\int\limits_{-\infty}^{\infty} |F_0|^2 |\overline{E}_j|^2 \, dxdy \right] A_i + \frac{1}{3}\int\limits_{-\infty}^{\infty}\int\limits_{-\infty}^{\infty} |F_0|^2 \left(\overline{E}_i^* \overline{E}_j\right)\overline{E}_j \, dxdy \right\}.$$

where j is the symbol for the axis orthogonal to the i axis. If we expand the expressions for the electric fields we find

$$\Delta\beta_i A_i = \frac{k_0 n_k \int\limits_{-\infty}^{\infty}\int\limits_{-\infty}^{\infty} |F_0|^4 \, dxdy}{\left(\int\limits_{-\infty}^{\infty}\int\limits_{-\infty}^{\infty} F_0^* F_0 \, dxdy\right)^2}$$

(3.10)

$$\left\{ \left[|A_i|^2 + \frac{2}{3}|A_j|^2 \right] A_i + \frac{1}{3}\left(A_i^* A_j\right)A_j \exp\left[-2i\left(\beta_{1i} - \beta_{1j}\right)\right] \right\}.$$

If we group variables together, we get

$$\Delta\beta_i A_i = \frac{k_0 n_k}{A_{eff}} \left\{ |A_i|^2 + \frac{2}{3}|A_j|^2 + \frac{1}{3}\left(A_i^* A_j\right)A_j \exp\left[-2i\left(\beta_{1i} - \beta_{1j}\right)\right] \right\}$$

(3.11)

where A_{eff} was defined in Equation 2.29. The last equation can be put into Equation 2.26 which was

$$\frac{\partial A}{\partial z} = -\beta_1 \frac{\partial A}{\partial t} - \frac{i}{2}\beta_2 \frac{\partial^2 A}{\partial t^2} - \frac{\beta_3}{6}\frac{\partial^3 A}{\partial t^3} + i\Delta\beta A,$$

(3.12)

to get

$$\frac{\partial A_i}{\partial z} = -\beta_1 \frac{\partial A_i}{\partial t} - \frac{i}{2}\beta_2 \frac{\partial^2 A_i}{\partial t^2} - \frac{\beta_3}{6}\frac{\partial^3 A_i}{\partial t^3} - \frac{\alpha}{2}A_i$$

$$+ i\gamma|A_i|^2 A_i + \frac{2}{3}i\gamma|A_j|^2 A_i + \frac{1}{3}i\gamma\left(A_i^* A_j\right)A_j \exp\left[-2i\left(\beta_{1i} - \beta_{1j}\right)\right].$$

(3.13)

28

The Raman effect[30], and self-steepening are both altered by birefringence. Both of these terms can be added to Equation 3.13. The Raman term will be examined first. It is found that the Raman effect has the general form

$$
\begin{aligned}
i\frac{\partial u(t)}{\partial z}\bigg|_{Raman} = {} & u(t)\int_{-\infty}^{t} f_1(t-t')\big|u(t')\big|^2\,dt' + \\
& u(t)\int_{-\infty}^{t} f_2(t-t')\big|v(t')\big|^2\,dt' + \\
& v(t)\int_{-\infty}^{t} f_3(t-t')u(t')v*(t')dt' + \\
& v(t)\int_{-\infty}^{t} f_3(t-t')u*(t')v(t')\exp(iR\delta z)dt,
\end{aligned}
\tag{3.14}
$$

where the functions u and v are the normalized envelopes introduced in Equation 2.35. In an isotropic medium, $f_1 = f_2 + f_3 + f_4$. It is also found, in general, that $f_2 = f_3 = f_4$. This means that $f_2 = \dfrac{f_1}{3}$. The effect of the last term can be ignored, because the phase mismatch between the terms will make them average to zero. For pulses longer than about 100fs we can approximate the response functions by the first term of their Taylor expansions as was done in the derivation of Equation 2.32. This leaves us with

$$
i\frac{\partial u(t)}{\partial z}\bigg|_{Raman} = T_R\left(u(t)\big|u(t)\big|^2 + \frac{1}{3}u(t)\big|v(t)\big|^2 \right).
\tag{3.15}
$$

The Raman and self-steepening terms can be added to Equation 3.13. The last term of 3.13 can be neglected as it tends to be rapidly varying. The soliton unit normalization introduced for Equation 2.36 can also be used here. The result is

$$
\begin{aligned}
-i\left(\frac{\partial u}{\partial \xi} - \delta\frac{\partial u}{\partial \xi}\right) = {} & \\
& \frac{1}{2}\frac{\partial^2 u}{\partial \tau^2} + \left(\big|u\big|^2 + \frac{2}{3}\big|v\big|^2\right)u + \\
& T_R\left(\frac{\partial\big|u\big|^2}{\partial \tau} + \frac{1}{3}\frac{\partial\big|v\big|^2}{\partial \tau}\right)u - is\frac{\partial}{\partial \tau}\left(\big|u\big|^2 u + \frac{2}{3}\big|v\big|^2 u\right)
\end{aligned}
\tag{3.16a}
$$

and

$$-i\left(\frac{\partial v}{\partial \xi} + \delta \frac{\partial v}{\partial \xi}\right) =$$

$$\frac{1}{2}\frac{\partial^2 v}{\partial \tau^2} + \left(|v|^2 + \frac{2}{3}|u|^2\right)v + \tag{3.16b}$$

$$T_R\left(\frac{\partial |v|^2}{\partial \tau} + \frac{1}{3}\frac{\partial |u|^2}{\partial \tau}\right)v - is\frac{\partial}{\partial \tau}\left(|v|^2 v + \frac{2}{3}|u|^2 v\right).$$

Here $\delta = \dfrac{\pi c \Delta n}{D(\lambda)\lambda_o}$, where Δn is the difference in index of refraction between the two

axes. When higher order terms are neglected, this reduces to

$$-i\left(\frac{\partial u}{\partial \xi} - \delta \frac{\partial u}{\partial \xi}\right) = \frac{1}{2}\frac{\partial^2 u}{\partial \tau^2} + \left(|u|^2 + \frac{2}{3}|v|^2\right)u$$

and $\hspace{10cm}$ (3.17)

$$-i\left(\frac{\partial v}{\partial \xi} + \delta \frac{\partial v}{\partial \xi}\right) = \frac{1}{2}\frac{\partial^2 v}{\partial \tau^2} + \left(|v|^2 + \frac{2}{3}|u|^2\right)v.$$

For a 300fs soliton, normal values of δ will range from 0.02 to 0.20. Fibers with increased birefingence may be used in order to eliminate the effect of random fluctuations in the birefringence.

The question now arises as to whether Equation 3.17 has soliton solutions, and if it does how they behave. In fact, a wide variety of soliton solutions have been found. This question has been examined by Trantnik and Sipe[31], Christodoulides and Joseph[32], Tasgal and Potasek[33], and by Haelterman et al.[34] One form which has been quite useful was found by Ueda and Kath.[35] For the case of equal amplitudes on both birefringent axes, they found the solution

$$u = \eta \sec h\left[\left(1 + \frac{2}{3}\right)^{1/2} \eta\tau\right] \exp\left\{i\left[\left(1 + \frac{2}{3}\right)\frac{\eta^2}{2} + \frac{\delta^2}{2}\right]\xi - i\delta\tau\right\}$$

(3.18)

$$v = \eta \sec h\left[\left(1 + \frac{2}{3}\right)^{1/2} \eta\tau\right] \exp\left\{i\left[\left(1 + \frac{2}{3}\right)\frac{\eta^2}{2} + \frac{\delta^2}{2}\right]\xi + i\delta\tau\right\}.$$

The Equations 3.18 state that the vector soliton should be narrower by $(5/3)^{1/2}$. The phase shift as a function of distance will also be altered. Recently a more general approximate soliton form was found by Afanasjev.[36] The form can have an arbitrary polarization angle and allows study over a wider range of pulse input angles. Since the results have only recently become available, they were not used in this project.

The nonlinear term has two primary effects. One is referred to as soliton dragging.[37,38] If the pulses have an intensity over a certain limit[39], the light on the fast and slow axes is shifted in frequency so that they travel at the same group velocity. This effect is shown in Figure 3.1. It shows the result of the simulation of propagating a soliton of unit normalized intensity 5 soliton periods in a birefringent fiber without higher order terms. In this figure the input amplitude in both polarizations is equal. This effect can eliminate the problem of pulse break up due to linear birefringence. If the pulses do not have equal amplitudes along both axes the behavior changes.[40] If the pulses are intense enough that the dispersion length is less than a beat length the pulse is stable, though energy can be exchanged between the polarizations. If the beat length is less, the energy on the fast axis of the fiber is transferred to the slow axis.

The frequency shift produced by soliton dragging can be used to make a switch.[11] The switch works in the following fashion. If a pulse is launched into a piece of birefringent fiber along one of the birefringent axis, it emerges from the other end with its frequency unaltered. If, however, a second pulse on the other axis is launched along with it, the frequency of the pulses will be altered. A filter is placed at the output such that it will not transmit the unshifted light but will transmit the pulse if it is shifted by soliton

dragging. This combination will act as an And-gate since it will only transmit a pulse if both pulses are present.

A second useful manifestation of nonlinear birefringence is intensity-dependent polarization rotation.[41] The polarization of light which is originally polarized along one of the birefringent axes will not change. This can be seen in Equation 3.16. The polarization will also not change if the pulse originally has equal components along both axes. In this case, the nonlinear change in the index of refraction is the same, so it does not alter the beat length. It should be noted, however, that the factor of 2/3 in the Kerr term means that the self-phase modulation for a pulse with equal components along the birefringent axes will be less than that for a pulse which is polarized along one axis. This will have significance in the study of birefringent fiber devices. For other polarizations, the polarization of light will evolve in a fashion which depends upon its intensity. This effect is greatest if the light is polarized at an angle $\pi / 8$ from one of the birefringent axes. Intensity-dependent polarization rotation has been used to construct switches and to mode-lock lasers.
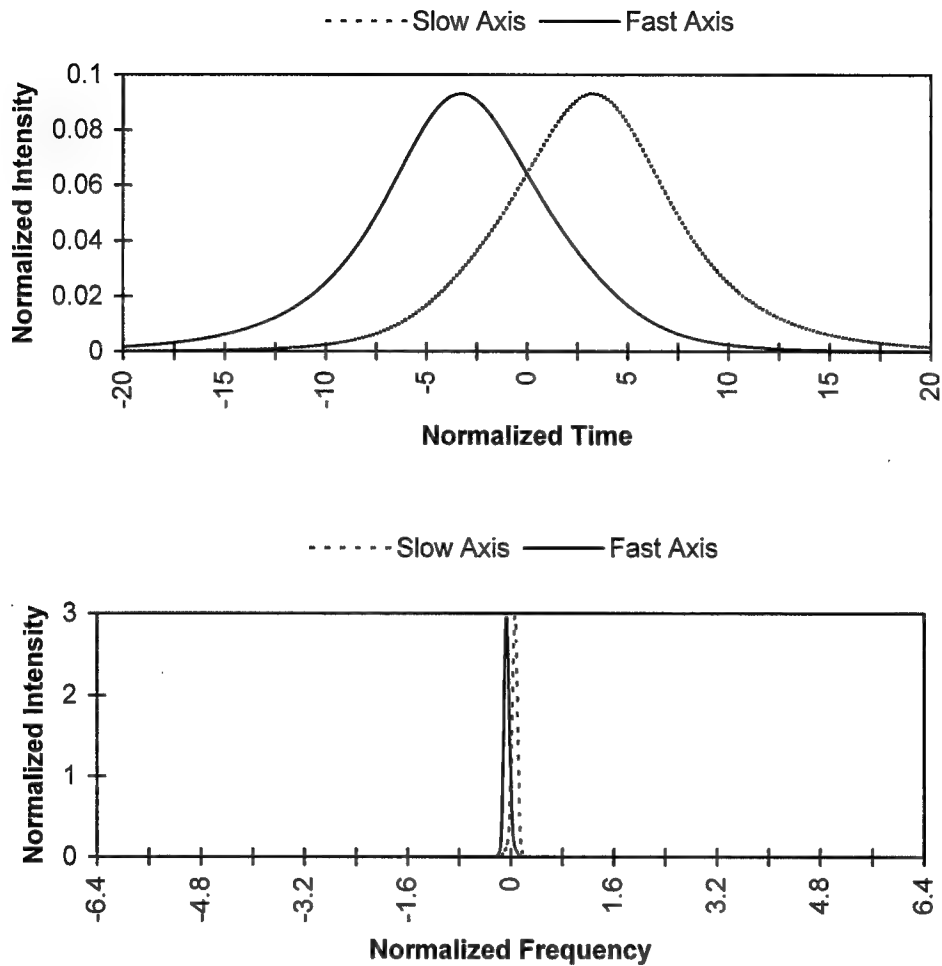
Figure 3.1 Shows the effect of pulse propagation in 5 soliton periods in a birefringent fiber. The birefringence is δ=0.5, The input pulse is a unit amplitude vector soliton with equal amplitude in both polarizations.

Chapter Four : Pulse amplification

Having studied the propagation of pulses in a fiber, we will now examine the propagation of pulses in fibers which act as a gain medium. The fiber amplifier is one of the major devices in a fiber laser. This chapter describes previous work on this topic. The basic equation which I used to simulate the fiber amplifier is derived. While this equation is not new, I have not been able to find a satisfactory derivation in another source. Having done this, I report on novel work I have performed which describes the interaction of the effect of birefingence and pulse break-up due to the amplifier.

Pulse Simulation Theory

The basic properties of erbium doped fibers have been reviewed by Ainslie[42]. Early experimental results were reported by Nakazawa et al.[43], Ainslie et al.[44], and Khrushchev et al.[45] General descriptions of fiber amplifiers can be found in Giles et al.[46] and Desurvire.[47] There are two lines of investigation that have been pursued, to study the amplification of pulses. Both start by using Equation 2.35 to describe how the electric field evolves in the fiber. In addition to this, one needs equations that describe amplification. Mel'nikov et al.[48], Wang and Chi[49], Maimistov[50], Gabitov[51], Nakazawa[52], and Gross and Manassah[53] start with the Bloch equations[3],

$$\frac{d\sigma_{21}}{dt} = i(\omega - \omega_0)\sigma_{21} + \frac{i\mu E_0}{2\hbar}(\rho_{11} - \rho_{22}) - \frac{\sigma_{21}}{T_2} \tag{4.1}$$

$$\frac{d}{dt}(\rho_{11} - \rho_{22}) = \frac{i\mu E_0}{\hbar}(\sigma_{21} - \sigma_{21}^*) - \frac{(\rho_{11} - \rho_{22}) - (\rho_{11} - \rho_{22})_0}{\tau}. \tag{4.2}$$

In these equations μ is the dipole moment in the interaction Hamiltonian, E_0 is the field amplitude of the illuminating light, and ω_0 is the resonance frequency for the transition. The variable T_2 is the decay time of the polarization and τ is the population decay rate.

The variables ρ are the elements of the density of states matrix. The variable σ_{21} is the slowly varying part of ρ, which is related to σ_{21} by

$$\rho_{21}(t) = \sigma_{21}(t)\exp(-i\omega t) \tag{4.3}$$

where

$$\sigma_{21} = \sigma_{12}^{*}. \tag{4.4}$$

The mean dipole moment of the atom is

$$\langle\mu(t)\rangle = 2\mu\left[\text{Re}\,\sigma_{21}(t)\cos(\omega t) + \text{Im}\,\sigma_{21}(t)\sin(\omega t)\right]. \tag{4.5}$$

We can relate this to the mean polarization in the material by

$$P = N\langle\mu\rangle, \tag{4.6}$$

where N is the density of atoms. The population inversion per unit volume is given by

$$\Delta N = N(\rho_{11} - \rho_{22}). \tag{4.7}$$

If we put Equations 4.3-4.7 into Equations 4.1 and 4.2, we see that they form together with Equation 2.35 a set of three Equations with the variables E, P and ΔN. This set of equations can be set up as an initial value problem and solved to model the amplification of a pulse. The Bloch equation approach accurately captures the physics of amplification and can be used to study very short pulses. The problem is that this method takes a great deal of computation and so another method is used where it is possible to do so.

This simpler approach has been used by Hodel et al.[54,55], Gagnon[56], Belanger[57], Nakazawa[58], Romagnoli[59,60], and Agrawal[61,62,63]. If the pulses are longer than the parameter T_2 which is on the order of 100 fs; then this simpler approach can be used. This is the case for all but the shortest pulses. This method has been used for the simulations described in this thesis. Here the gain is approximated by

$$g(\omega) = g_p\left[1 - (\omega - \omega_0)^2 T_2^2\right], \tag{4.8}$$

where g_p is the peak gain. This is sometimes referred to as the parabolic gain approximation. The time dependence of the peak gain is given by

$$\frac{\partial g_p}{\partial t} = \frac{g_0 - g_p}{\tau} - \frac{g_p |A|^2}{E_s}.$$
(4.9)

These equations can be derived from the Bloch equations, when the derivatives are not too large. One starts by assuming that the derivative in Equation 4.1 is zero. Equation 4.1 and its complex conjugate are linearly independent. The sum and difference of Equation 4.1 and its complex conjugate are taken. This leaves us with

$$\left(\sigma_{21} - \sigma^*_{21}\right) = iT_2\left(\omega - \omega_0\right)\left(\sigma_{21} + \sigma^*_{21}\right)$$
(4.10a)

and

$$\left(\sigma_{21} + \sigma^*_{21}\right) = iT_2\left(\omega - \omega_0\right)\left(\sigma_{21} - \sigma^*_{21}\right) + \frac{iT_2 \mu E_0}{\hbar}\left(\rho_{11} - \rho_{22}\right).$$
(4.10b)

When the term involving the sum of the σ_{21} terms is eliminated one is left with

$$\left(\sigma_{21} - \sigma^*_{21}\right) = \frac{iT_2 \mu E_0}{\hbar}\frac{\left(\rho_{11} - \rho_{22}\right)}{1 + T_2^2\left(\omega - \omega_0\right)^2}.$$
(4.11)

Substituting this into Equation 4.2, we get

$$\frac{d}{dt}\left(\rho_{11} - \rho_{22}\right) = -\frac{\mu^2 T_2 E_0^2}{\hbar^2}\frac{\left(\rho_{11} - \rho_{22}\right)}{1 + T_2^2\left(\omega - \omega_0\right)^2} - \frac{\left(\rho_{11} - \rho_{22}\right) - \left(\rho_{11} - \rho_{22}\right)_0}{\tau}.$$
(4.12)

The normalized line shape function in the dipole moment model is given by Yariv[9] in Equation 8.1-20 as

$$g_n(\omega) = \frac{2T_2}{1 + \left(\omega - \omega_0\right)^2 T_2^2}.$$
(4.13)

Substituting this into Equation 4.12, one obtains

$$\frac{d}{dt}\left(\rho_{11} - \rho_{22}\right) = -\frac{\mu^2 g_n(\omega) E_0^2\left(\rho_{11} - \rho_{22}\right)}{2\hbar^2} - \frac{\left(\rho_{11} - \rho_{22}\right) - \left(\rho_{11} - \rho_{22}\right)_0}{\tau}.$$
(4.14)

The gain parameter is defined[17] as

$$g(\omega) = \Delta N \sigma(\omega) = \Delta N \sigma g_n(\omega) = g_p g_n(\omega),$$
(4.15)

where σ is the absorption cross-section. Clearly, the prefactor in Equation 4.8 is

$$g_p = \Delta N \sigma. \tag{4.16}$$

In Reference 9, Equation 8.2-7 states the gain parameter is expressed as

$$g(\omega) = -\frac{k\chi''(\omega)}{n^2}, \tag{4.17}$$

where χ'' is the imaginary part of the atomic susceptibility. It can be expressed[9] as

$$\chi''(\omega) = \frac{\mu^2}{2\varepsilon_0 \hbar} \Delta N g_n(\omega). \tag{4.18}$$

When the last two equations are combined we get an expression for peak gain. When this is compared to Equation 4.15 one sees that

$$\sigma = \frac{\omega\mu^2}{2c n \varepsilon_0 \hbar} = \frac{\omega\mu^2 n}{2c \, \varepsilon\hbar},$$

where the fact that $n^2 = \dfrac{\varepsilon}{\varepsilon_0}$ was also used. When 4.14 is multiplied by $N\sigma$, the result is

$$\frac{dg_p}{dt} = -\frac{\mu^2 g_n(\omega) E_0^{\,2} g_p}{2\hbar^2} - \frac{g_p - g_0}{\tau}.$$

The last equation can be expressed in terms of the variable A, which is described by the square root of the power, instead of E_0. This can be done using the relationship

$$\frac{c\varepsilon}{2nA}|E_0|^2 = I = \frac{|A|^2}{A_{eff}}.$$ We are also interested in using the time average of the electric

field. This can be expressed as $\bar{E} = \dfrac{1}{2}|E_0|^2$. When these expressions are substituted into

the last equation the result is

$$\frac{dg_p}{dt} = -\frac{\mu^2 |A|^2 n g_p}{2\hbar^2 A_{eff} c\varepsilon} - \frac{g_p - g_0}{\tau}.$$

When a factor of σ is factored out of the last expression, the result is

$$\frac{dg_p}{dt} = -\frac{|A|^2 g_p}{E_s} - \frac{g_p - g_0}{\tau}.$$

Which is the expression in Equation 4.9. If τ is much greater than the pulse width, we can ignore the last term on the left hand side. If we integrate we get

$$g_p(\tau) = g_0 \exp\left(-S \int_{-\infty}^{\tau} |A|^2 d\tau\right). \tag{4.19}$$

This last equation allows us to include the effects of saturation which is expressed by the parameter S. Here the saturation energy E_s is

$$E_s = \frac{\hbar \omega_0 A_{eff}}{\sigma}, \tag{4.20}$$

where σ is the transition cross section. If we change $(\omega - \omega_0)$ to the operator $i \frac{\partial}{\partial t}$ in the time domain, we get that the form for α in Equation 2.35 becomes

$$\alpha = g_p(t)\left(1 + T_2^2 \frac{\partial^2}{\partial t^2}\right). \tag{4.21}$$

In normalized units, this becomes

$$\alpha_n = g_0 L_D \exp\left(-S \int_{-\infty}^{\tau} |U|^2 d\tau\right)\left(1 + \tau_2^2 \frac{\partial^2}{\partial \tau^2}\right), \tag{4.22}$$

where $\tau_2 = T_2/T_0$ and $S = P_0 T_0/E_s$. The saturation energy is about 10 μJ. The parameter S should then be around 10^{-6}.

Since amplification in an erbium amplifier is largely independent of polarization, the extension of Equation 4.13 to the case of two polarizations is straightforward. One must remember that both polarizations are contributing to polarization, leaving an amplification of the form

$$\alpha_n = g_0 L_D \exp\left[-S \int_{-\infty}^{\tau} \left(|U|^2 + |V|^2\right) d\tau\right]\left(1 + \tau_2^2 \frac{\partial^2}{\partial \tau^2}\right). \tag{4.23}$$

Simulations of this kind have been carried out by Yang and Wang[64]. They included the effects of Raman response and self-steepening. They demonstrated that light along the

two axes tend to couple and that the spacing between them is reduced as the pulses are amplified.

The equations shown here treat only the longitudinal effects in a fiber amplifier. This is justified in reference 4. It has been found that, in general combining transverse with longitudinal effects makes only a small difference. The importance of studying transverse mode and doping shapes is of importance to optimizing fiber amplifiers. This has been done by Desurvire et al.[65], Ohashi[66], Pedersen et al.[67], and Pfeiffer and Bulow[68]. The results reported show the importance on concentrating the light from the pump, the signal to be amplified, and the dopant ions in the center of the core. For this reason, fiber amplifiers often have smaller cores than normal telecommunications fibers.

Simulation Results

I simulated the propagation of fundamental solitons with a pulse width of 300 femtoseconds introduced into fiber amplifiers with a gain of 10 dB per dispersion length. Here $\tau_2 = 0.2$. Numerically, these were the most difficult simulations performed due to the very high intensities. Results for the amplifier without birefringence were compared with those of another student who independently developed a similar program. The results were the same. The width of the time window of the simulation and the number of FFT points were increased until the pulse was contained in the window in both time and frequency space. The time window was 240 soliton widths wide and 8192 FFT sample points were used. Due to the high intensities 10,000 steps per dispersion length were taken in the simulation. Increasing the number of steps did not alter the results so they were assumed to have stabilized.

The results can be seen in Figures 4.1 - 4.2. The effect of gain dispersion is to limit the height of the pulse and to cause it to break up. The effect seen in both time and frequency space is that side peaks are continually built up after the pulse reaches a critical energy. As the peaks gain intensity they are compressed in time. This causes them to

expand in bandwidth and so eventually two smaller pulses will be energetically favored over one large one.

The effect of gain saturation can be seen in Figure 4.3. Here, everything is the same as with the last Figures except that the saturation constant is set to S=0.01. This was done to illustrate the effect of saturation. As shown above, the actual saturation is much smaller. The saturation tends to reduce the maximum intensity of the pulse, and to cause the leading edge to be built up relative to the trailing edge.
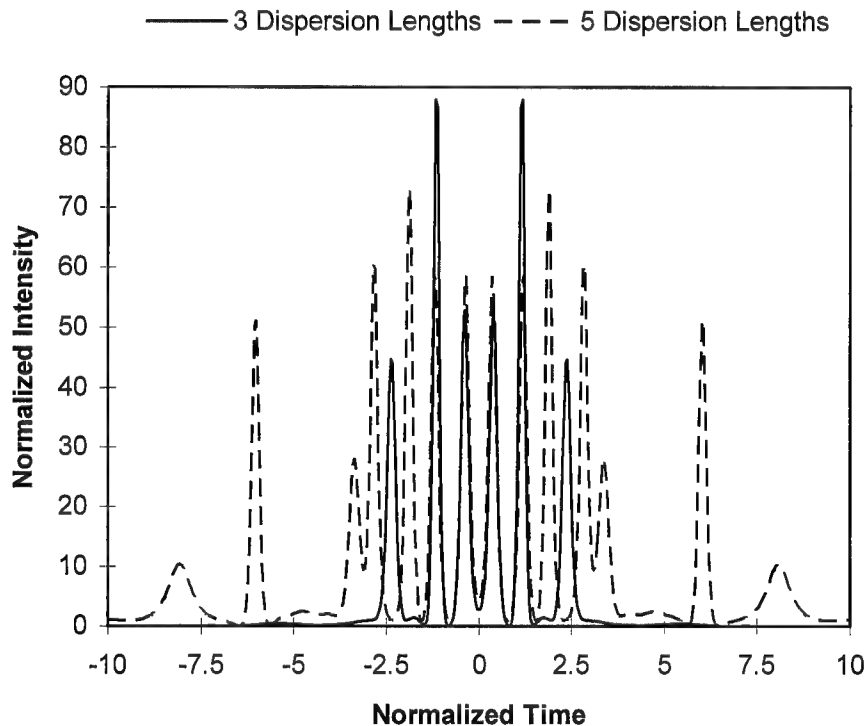
Figure 4.1 Shows how a pulse is modified in an amplifier. The gain is 10 dB per dispersion length. There is no saturation. The results are given in terms of normalized time
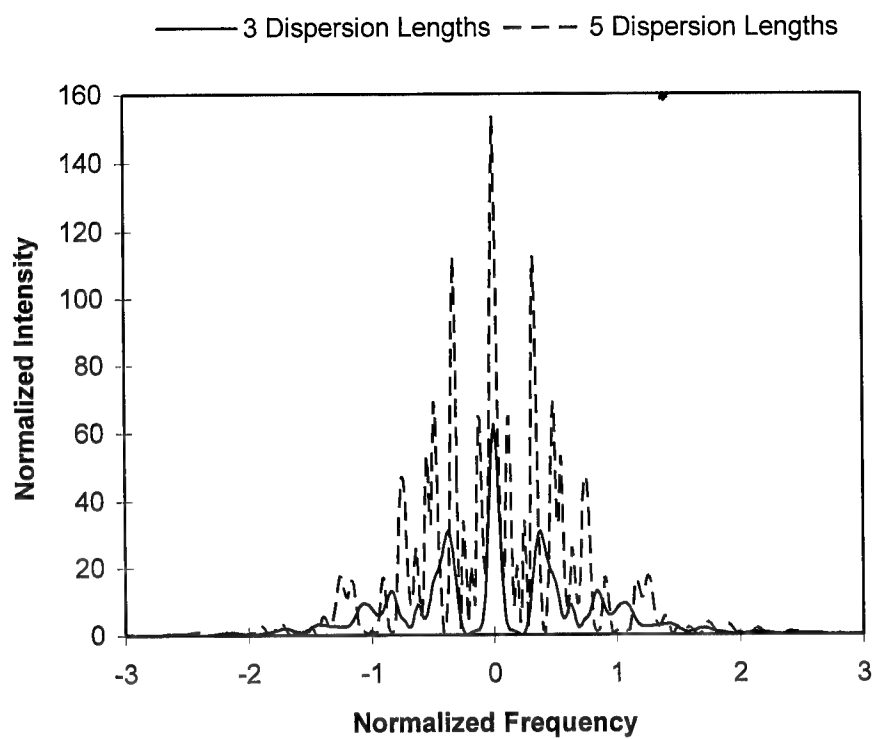
Figure 4.2 Shows the how a pulse is modified in an amplifier. The gain is 10 dB per dispersion length. There is no saturation. The results are given as a function of frequency.
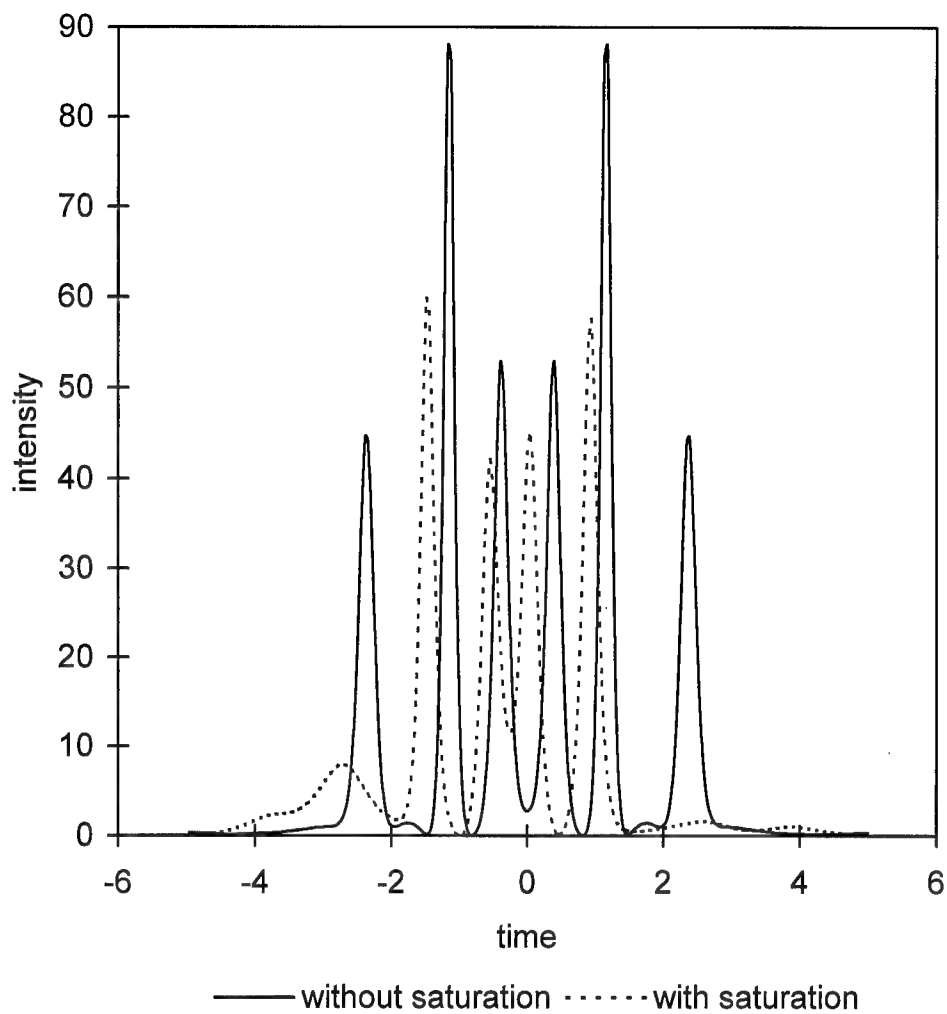
Figure 4.3 Shows the effect of pulse amplification. The gain is 10 dB per dispersion length. Results are given both with no saturation, and for S=0.01. The amplifier is 3 dispersion lengths long. The results are given in terms of normalized time
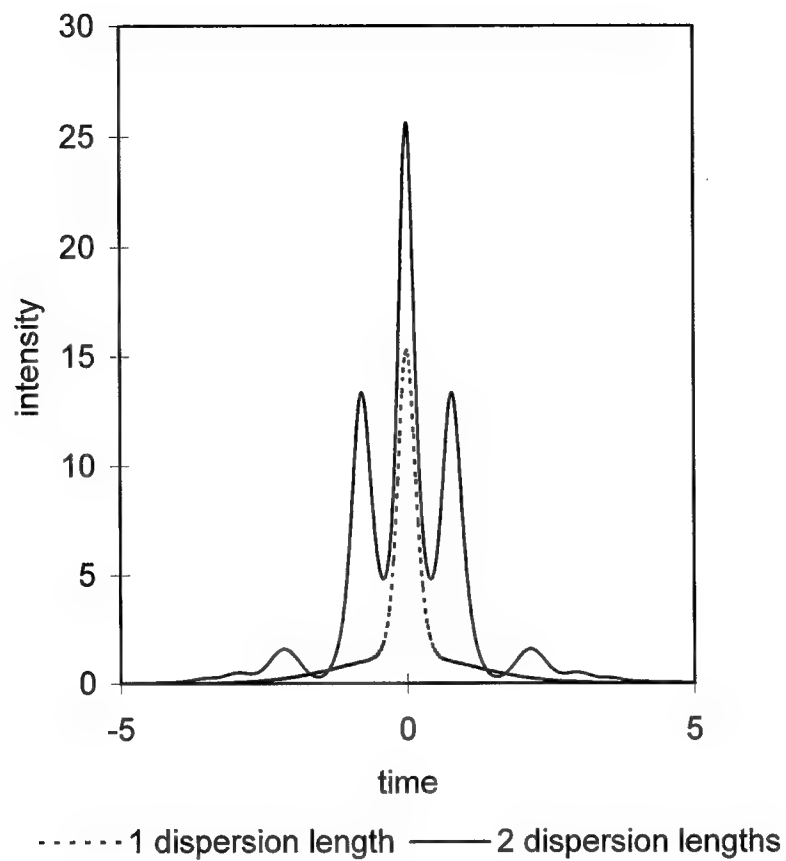
Figure 4.4 Result of pulse propagation in an amplifier. The gain is 10 dB per dispersion length. There is no saturation, and $\delta=0.0$.
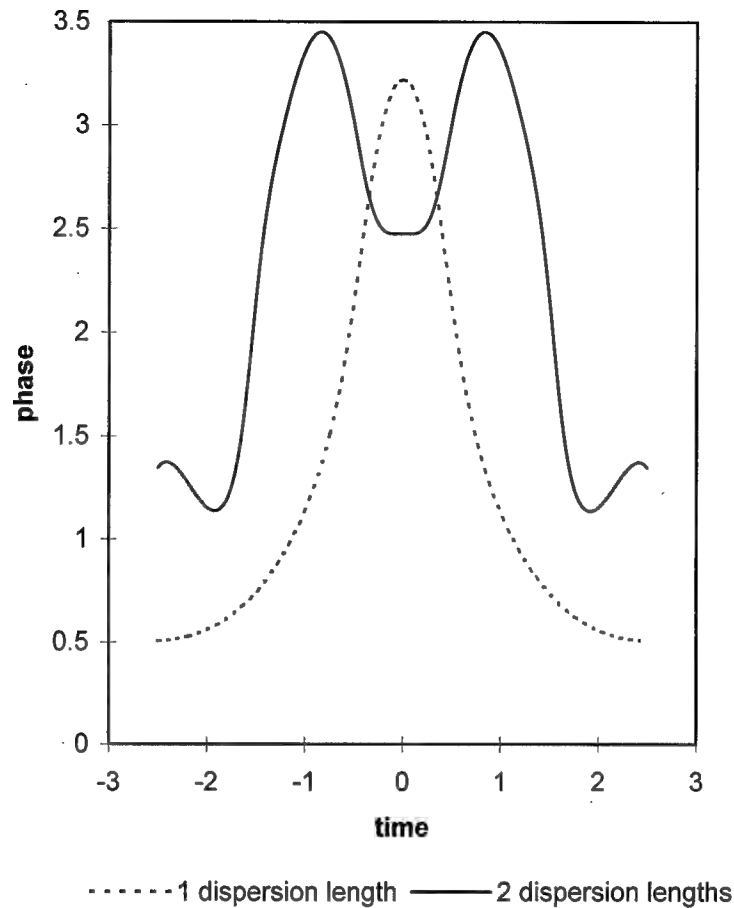
Figure 4.5 Result of pulse propagation in an amplifier. The gain is 10 dB per dispersion length. There is no saturation, and δ=0.0.

The result of polarization was examined in a series of simulations. The amplifier parameters were the same as in the last paragraph. Figures 4.4 and 4.5 show the case in which δ=0.0, where δ is the parameter measuring birefringence given in 3.16. In this case the pulse had equal intensities on both axes of the fiber. The results for both axes were the same. After one dispersion length the pulse has been amplified and compressed. The phase is nearly constant over the high intensity part of the pulse, which is expected for a soliton. The result is that after propagating two dispersion distances the pulse begins to break up as in the case in which we neglected polarization. Before pulse breakup the

phase has a single maximum, but after breakup there is more modulation and multiple maxima. The maxima and the central flat region of the phase correspond to the location of the pulses. Again they are acting like solitons in that they have a uniform phase.

The effect of introducing birefringence is shown in Figures 4.6-4.8. The birefringence was altered so that $\delta=0.5$. The input pulse had an angle of $\pi/8$ to the slow axis of the fiber. The light in the two polarizations is beginning to separate, most notably in that light in the fast axis is beginning to build up in a broad peak in the front of the pulse. Clearly the polarization varies within the pulse. The phase difference between the two polarizations is beginning to increase and it varies by a great deal across the pulse as well. Figure 4.8 can be thought of as the effect of placing a polarizer at the output of the fiber. The amplifier and polarizer working together have the effect of introducing significant distortions. Figure 4.9 shows the effect of introducing saturation into the amplifier. Here, the saturation is $S=0.01$. The pulse has experienced less amplification though this effect is much less pronounced for the light on the fast axis.
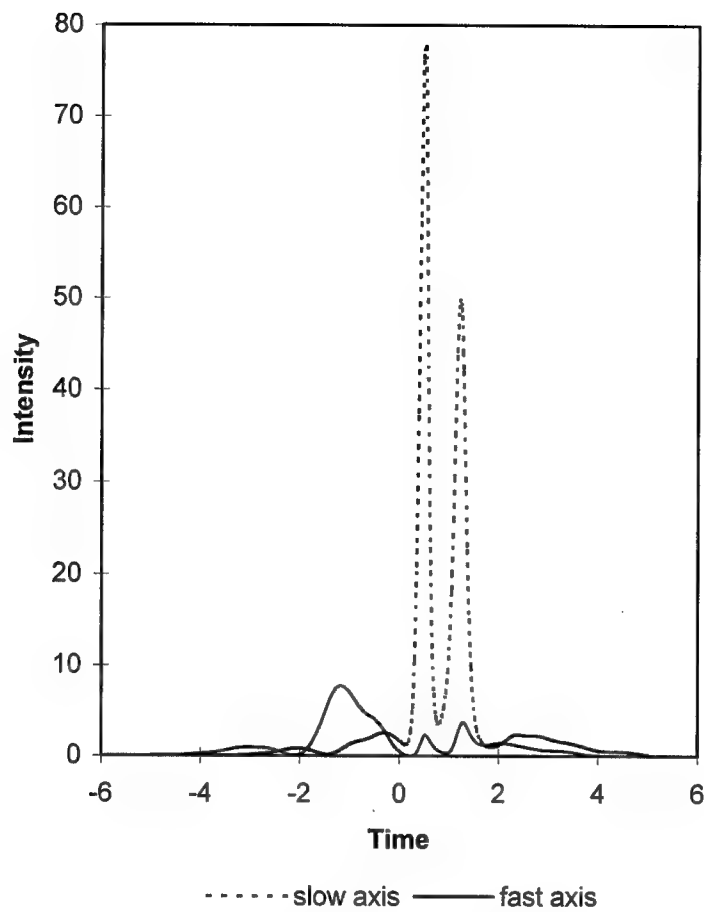
Figure 4.6 Result of pulse propagation in an amplifier. The angle of the input pulse to the slow axis of the fiber is $\pi/8$. The gain is 10 dB per dispersion length. There is no saturation, and $\delta=0.5$.
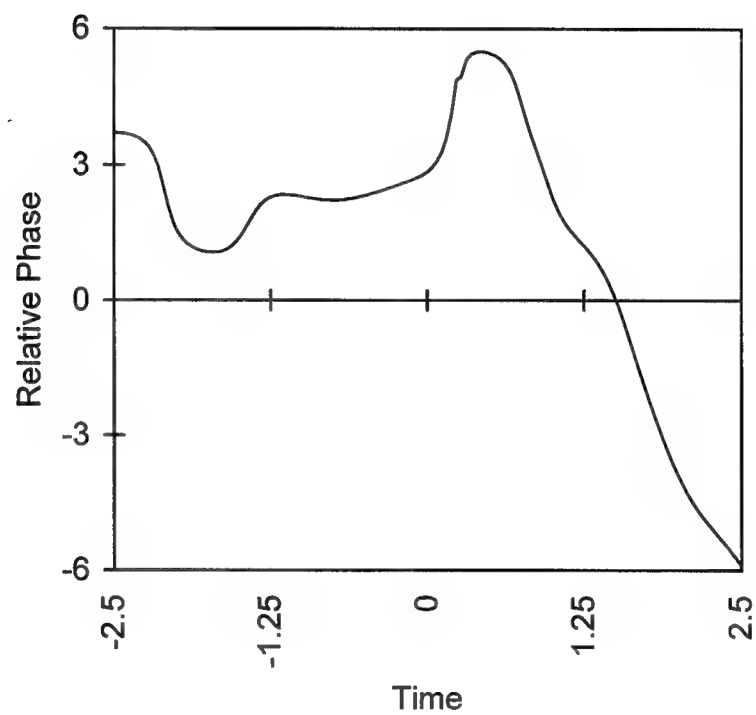
Figure 4.7 Result of pulse propagation in an amplifier. The angle of the input pulse to the slow axis of the fiber is $\pi/8$.   The gain is 10 dB per dispersion length. There is no saturation, and $\delta=0.5$.
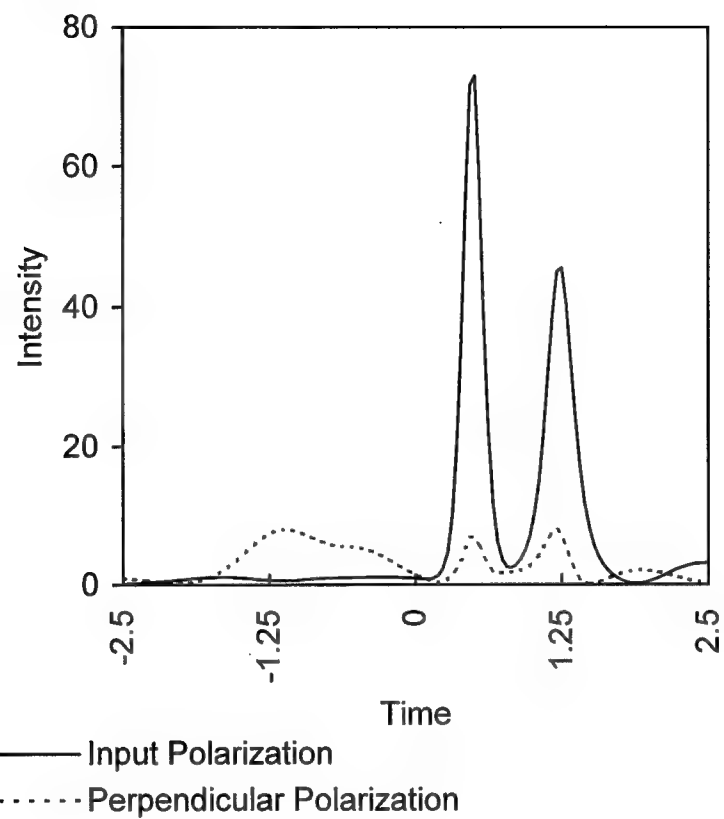
Figure 4.8 Components of the pulse shown in Figure 4.5 either in the input polarization, or perpendicular to the input polarization, as shown.
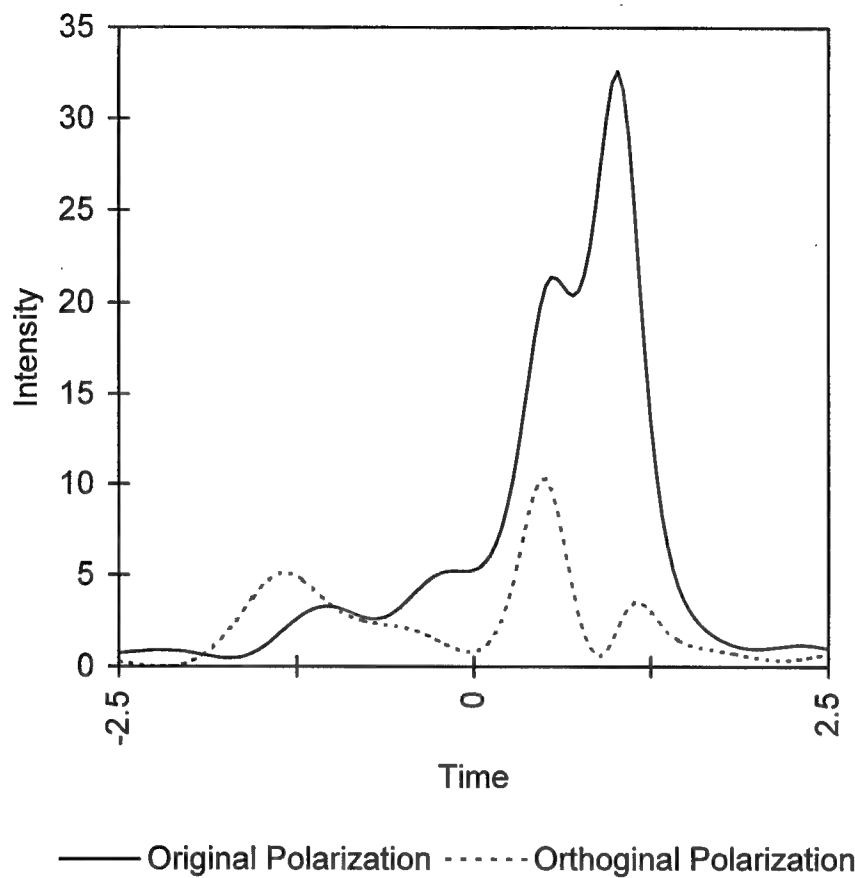
Figure 4.9 Result of pulse propagation in an amplifier. The angle of the input pulse to the slow axis of the fiber is $\pi/8$. Pulse amplification gain is 10 dB per dispersion length. The saturation is S=0.01. The birefringence is δ=0.5.

Fiber amplifiers are a key component that have made possible a number of major advances in optical systems. In particular, they have made fiber lasers practical. A good model of pulse amplification in fiber amplifiers was needed to build a good model of the figure eight laser. A model was described here. It was first applied to the case of the fiber laser without birefringence. This work was verified by comparing it to the results of another student who was independently developing a model of the fiber amplifier. I

carried out novel research in the area of pulse amplification in the birefringent amplifier. I showed that pulses tend to break up in these amplifiers, as they do without birefringence. It is also known, as mentioned in Chapter 3, that the components of a pulse which are along different birefringent axes of the fiber, tend to couple to each other. I further showed that this coupling phenomenon and the pulse break-up effect coexisted. This meant that the amplifier produced a train of coupled fibers. This effect may explain the fact that fiber lasers have been observed to produce bursts of pulses when their amplifiers are being pumped intensely. In carrying out these investigations, the simulation for this essential component of a laser was thoroughly verified.

Chapter Five : Nonlinear-Optical Fiber Loop Switches

The component of a figure eight laser which performs passive mode-locking is the Nonlinear Optical Loop Mirror (NOLM). Because of its critical role in the laser, I carried out very extensive simulations of this device. After duplicating the previous reported work of others, I carried out novel work in simulating how optical pulses were effected by an NOLM constructed of birefringent fiber. The aspects of the loop studied were those that effect the operation of figure eight lasers. In order to be able to predict the pulse energies and widths produced by a laser, one needs to know the energies for which pulses are transmitted by the NOLM. Since the behavior of the laser is sensitive to the pulses being distorted, the effect of the loop on the pulse width was considered. The low intensity transmission of the loop was examined because this will be the state of the system when the laser is starting up. One must also know how the operation of the loop mirror will be effected as the parameters of its components are altered. Specifically, experimentally a great deal of effort is always spent adjusting polarization controllers to optimize the behavior of the laser, so I have examined the impact of the polarization controller on the behavior of the switch. I was able to develop a simple analytical model which allows for the approximate prediction of pulse energy required for switching in these devices. Simple linear analysis of the system proved to be enough under some conditions to predict the low intensity transmission. These models shed light on the physics of the systems and give the ability to do quick analysis for laser design.

Previous Work

I will summarize previous work on these devices and I will mention at least some of their applications. Nonlinear fiber switches were first described by Doran and Wood.[69] The basic idea for a nonlinear switch of this type was proposed by Otsuka.[9] The

Nonlinear-Optical loop mirror works by using the principle of a nonlinear Sagnac interferometer, which is shown in Figure 5.1. Light is passed through one input port of a directional coupler which acts as a beam splitter. The splitting ratio is chosen to be something other than 50/50. The output ports of the directional coupler are then formed into a loop of fiber. This means that the input light is formed into two counter-propagating beams in the loop. Due to the nonlinearity of the fiber, one beam will experience a greater phase shift than the other, since the beams do not have the same amplitude. The intensity difference will be proportional to the input intensity. This phase difference causes switching when the two pulses recombine at the directional coupler. If the beams are in phase, they are passed out the port they came in. Effectively they are reflected. If they are π radians out of phase, the light is switched to the other port, so they are transmitted. The sensitivity of the device can be greatly increased by inserting a fiber Bragg grating into it.[70] This may be useful for demultiplexing applications.

A second form of this device is the Nonlinear Amplifying Loop Mirror (NALM).[71] This device employs a different means of producing beams of different intensities. In this device a fiber amplifier is placed at one end of the loop. The directional coupler can have a 50/50 splitting ratio. If the amplifier is not saturated, light traveling in one direction is amplified at the beginning of its passage through the loop and experiences a greater phase shift than light going in the other direction since this light is amplified only after traversing the loop. The phase difference is caused by the fact that the pulses pass through most of the fiber in the loop with different pulse energies. This phase difference again produces intensity dependent switching.
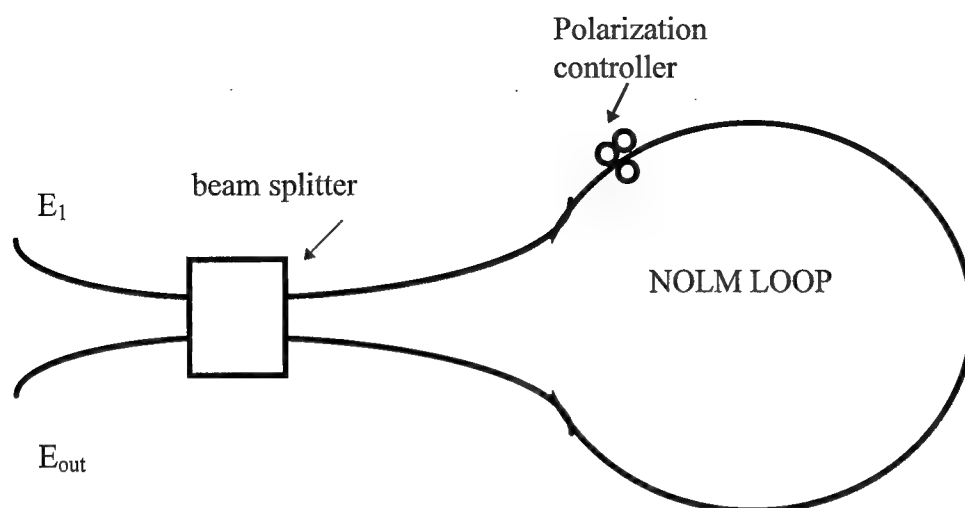
Figure 5.1 Nonlinear Optical Loop Mirror

These devices have been used for a number of applications. The switching of solitons in them was demonstrated experimentally by Blow, Doran, and Wood.[72] The NOLM can be used for many applications in optical communications.[73] Their use in filtering noise in optical systems has also been demonstrated.[74,75] When cw light of two different wavelengths is introduced into such a switch, multigigabit pulse trains can be produced.[76] When properly configured they can be used for the adiabatic amplification of solitons.[77] It has also been studied as a mode-locking device in fiber lasers.[78]

Theory

Most previous work has analyzed these devices in terms of their cw performance. This work will be briefly described here since it helps to shed light on how these devices work. Take E_1 to be the cw input electric field. The variable α is the power transmission of the direction coupler. The electric fields of the signals in the loop become

$$E_3 = \alpha^{1/2} E_1 \tag{5.1a}$$

and

$$E_4 = i(1-\alpha)^{1/2} E_1. \tag{5.1b}$$

Where E_3 and E_4 are the two counter propagating beams. In the optical fiber, light is subject to the optical Kerr effect, so that the phase is shifted by

$$\phi = \frac{2\pi\, n_k |E|^2 L}{\lambda}. \tag{5.2}$$

If the input power is not split evenly between the two directions, the light will undergo a different phase shift as it travels in each of the two directions. This will cause intensity dependent switching when the light is recombined. The transmitted light will be given by

$$E_{out} = \alpha^{1/2} E_3\, e^{i\phi} + i(1-\alpha)^{1/2} E_4 = \alpha E_1\, e^{i\phi} - (1-\alpha)E_1 =$$

$$\{[1+\cos(\phi)+i\sin(\phi)]\alpha - 1\}E_1 \quad , \tag{5.3}$$

where ϕ is a relative phase shift produce in E_3. After the light passes the loop the output power is given by taking the magnitude of Equation 5.3 and rearranging.

$$\frac{|E_{out}|^2}{|E_1|^2} = \{[1+\cos(\phi)+i\sin(\phi)]\alpha - 1\}\{[1+\cos(\phi)-i\sin(\phi)]\alpha - 1\} =$$

$$1 - 2\alpha(1-\alpha)[1+\cos(\phi)] \tag{5.4}$$

If the relative phase shift is produced by the Kerr nonlinearity, in the cw case we get

$$|E_{OUT}|^2 = |E_{IN}|^2 \left(1 - 2\alpha(1-\alpha)\left\{1+\cos\left[(1-2\alpha)|E_{IN}|^2 \frac{2\pi\, n_k L}{\lambda}\right]\right\}\right), \tag{5.5}$$

where L is the length of the loop. By examining Equation 5.5, the general features of the action of the NOLM can be found. The phase shift is clearly dependent on the intensity of the input. The intensity needed for switching can be reduced in a number of ways. The loop can be made longer, which will allow more interaction path over which the phase shift will be built up. The splitting ratio of the directional coupler can be made larger. This will mean that the difference in nonlinear phase shift per unit length will be larger. Finally, one could use a material with a different value of n_k, however, this is not generally practical. These general features carry over to the study of how pulses act when introduced into an NOLM.

It has been found that hyperbolic secant shaped pulses, those with an intensity envelope function of the form

$$A \sec h^2(t),$$

can be almost completely transmitted through an NOLM for a correct value of the amplitude A. It should be noted that unlike the situation with a soliton, the width and height of the hyperbolic secant shaped pulse are not coupled. Pulses of this form can also form solitons if they have enough energy. Solitons have the property that they have uniform phase across their temporal extent. After the input pulse is split by the directional coupler, the counter propagating pulses will form themselves into solitons accompanied by low-intensity pedestal. The pedestal is referred to as dispersive wave radiation. The rate at which the phase changes will depend on the energy of the soliton, hence a phase difference builds up between the two counter-propagating pulses.

Simulation Results: Nonbirefringent NOLM

The transmission of hyperbolic secant shaped pulses was extensively studied. The result of simulations of NOLMs in which the effect of birefringence is not considered will be described here. These results have been already described in length by other researchers.[78] The results are given here because their replication gives confidence that my simulations are working well. The discussion of these results will also make it easier to think about the results for the birefringent NOLM. In addition, the model for predicting the pulse energy needed for maximum transmission is new.   Hyperbolic secant shaped pulses of varying amplitude were introduced into a simulated NOLM. First, the pulses were split into two subpulses using the relationships in Equation 5.1. The propagation of the pulses in fiber was then simulated using the NLSE. The pulses were then recombined. The total energy transmitted was compared to the energy of the input pulse. This was considered to be the transmission. An example of a transmission curve for this type of pulse is given in Figure 5.2. This curve is identical with the results of Duling in reference 78. The figure displays the expected dependence of the energy needed to achieve transmission with loop length. A less intense pulse needs a longer loop to build up a phase difference.
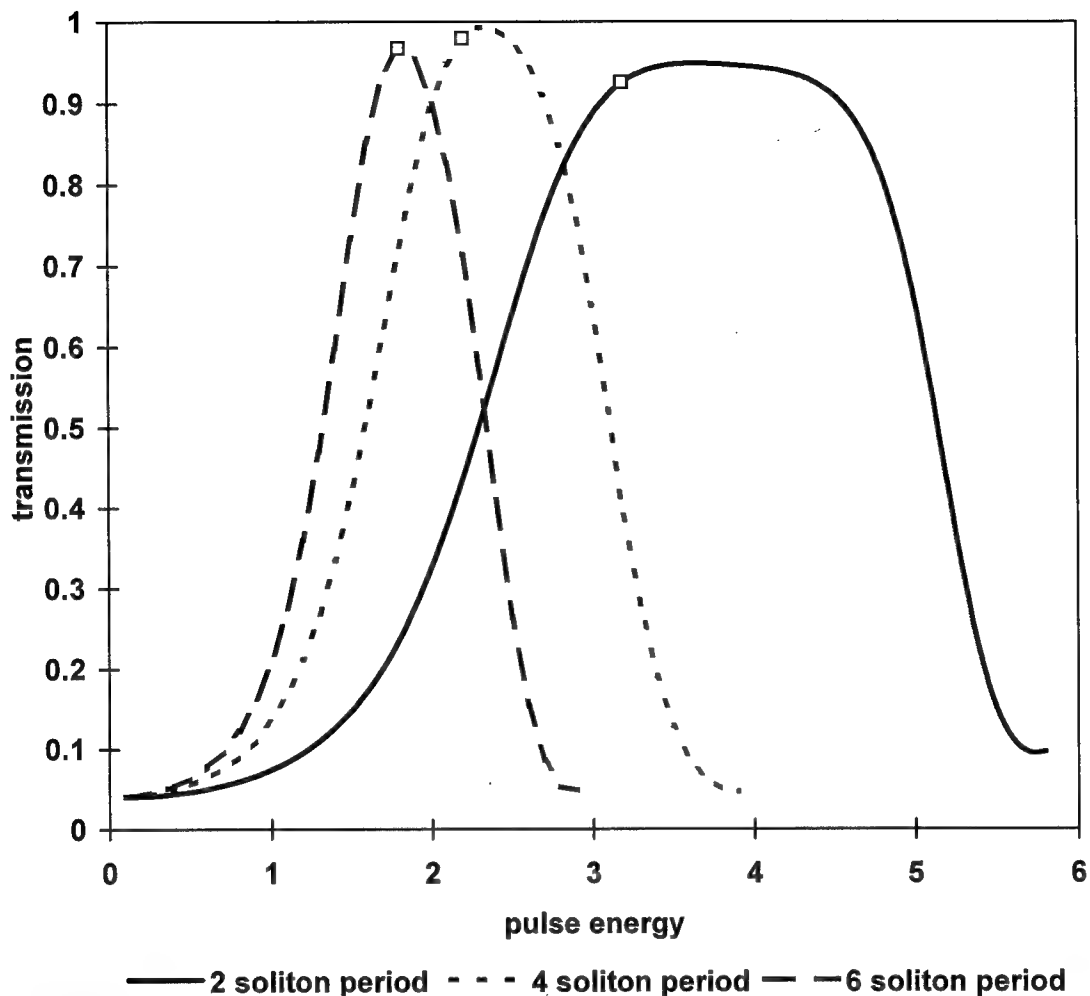
Figure 5.2 Pulse transmission as a function of pulse energy for an NOLM with 60/40 beam splitter and no birefringence. The squares represent the predicted energies required for peak transmission given by Equation 5.13. The figure shows the effect of changing the loop length.

The picture of the pulses in the NOLM forming solitons can be examined quantitatively in that it can be used to predict the location of transmission maxima in Figure 5.2 which is a plot of the transmission curves for solitons with three different lengths of the NOLM. This can be done by using the following simplified picture of how

pulses behave in the NOLM. The pulses will be transmitted when they are out of phase by π radians when they return to the beam splitter. I derived this model in order to help understand the behavior of the NOLM and also to enable me to understand how changing the parameters of the NOLM design would effect their behavior. I needed some way of estimating the phase shift of the pulses as they propagate in the loop. A simple way of doing this is to assume that the pulses immediately turn into solitons with the same energy as the counter-propagating pulses. I can then assume that the pulses will experience a phase shift equal to that the solitons would experience. The assumption that the pulses will become solitons is justifiable since it is observed that hyperbolic secant shaped pulses with amplitudes $0.5<A<1.5$ will evolve into solitons.[4] For the model to hold both of the counter-propagating pulses should have peak intensities in this range. This will be true if the amplitude of the input pulse is greater than $(1-\alpha)/2$ and less than $3\alpha/2$. For a 60/40 beamsplitter, for instance, the range of input intensities will be between 1.25 and 2.5. The assumption that these pulses immediately behave like solitons is an oversimplification and this explains the inaccuracies of the model.

We must now relate the length of the loop to a phase shift. The lengths are chosen in units of the soliton period z_0. The phase shift ϕ of a soliton is given by[79]

$$\phi = \frac{A}{2}\xi,\tag{5.6}$$

where A is the pulse intensity amplitude and the variable ξ is distance in dispersion lengths. As mentioned in Equation 2.36 this is proportional to the pulse width. It is assumed that the input pulses have a hyperbolic secant shape and an energy E_{in}. The width of the input pulses are held constant and only the amplitude is varied. These are rapidly reshaped into solitons of energy E_p for which the amplitude and width are coupled. The quantity E_{in} is given by

$$E_{in} = 2 \int_0^\infty P_{in} \sec h^2[t] dt = 2P_{in}. \tag{5.7}$$

In contrast the energy of the soliton is given by

$$E_p = 2 \int_0^\infty P_p \sec h^2\left[\frac{t}{T_p}\right] dt = 2P_p T_p, \tag{5.8}$$

where P_p and T_p are the pulse height and width of the soliton formed. In the dimensionless soliton units used here these are related by

$$P_p = \frac{1}{T_p^2}. \tag{5.9}$$

If we use Equations 5.7-5.9 and assume that $E_{in} = E_p$, we get

$$P_{in} = \frac{1}{T_p} \tag{5.10}$$

and

$$P_{in} = \left(P_p\right)^{\frac{1}{2}}, \tag{5.11}$$

where T_p is the width of the soliton formed by the input pulse. If Equations 5.6, 5.10, and 5.11 are used, one finds that the phase difference between the two counter-propagating pulses becomes

$$\Delta\phi = \frac{(2\alpha - 1)(P_{in})^2}{2} \xi_1. \tag{5.12}$$

Solving for pulse energy,

59

$$P_{in} = \left[\frac{2\Delta\phi}{(2\alpha - 1)\xi_1} \right]^{\frac{1}{2}}.$$

(5.13)

The results of this analysis are shown as square markers in Figure 5.2. It shows good agreement between the model and the results of the simulations, however, the model does tend to underestimate the energy required for switching. This is to be expected as the pulse will have had less time to be reshaped into a soliton.

Figure 5.2 also shows that transmission is highest if the loop has a length of around 4 soliton periods. For the splitting ratio being examined in this figure, a loop of this length will have maximum transmission for input pulses with an energy slightly higher than twice that of a unit soliton. This means that the pulses formed in the loop by the directional coupler are already close to being unit solitons and there will be relatively little reshaping or dispersive wave shedding in the fiber of the loop. This explains the high transmission.

We expect that the effect of decreasing the splitting ratio will be to require a longer loop for the same degree of switching. This is due to the relatively small difference in the energies of the pulses formed. The effect of making this change is shown in the Figure 5.3. The splitting ratio used was 55/45. The lengths chosen were those that would give nearly the same switching lengths as in Figure 5.2. This was determined by considering Equation 5.13. In the last case the value of the term 2α-1 was 0.2. In the previous case it was 0.1, this implies that one may keep the switching lengths constant by doubling the loop lengths. The predicted locations of first transmission peaks by the soliton model are shown in Figure 5.3 as squares. The model again tends to underestimate the energy needed for switching.
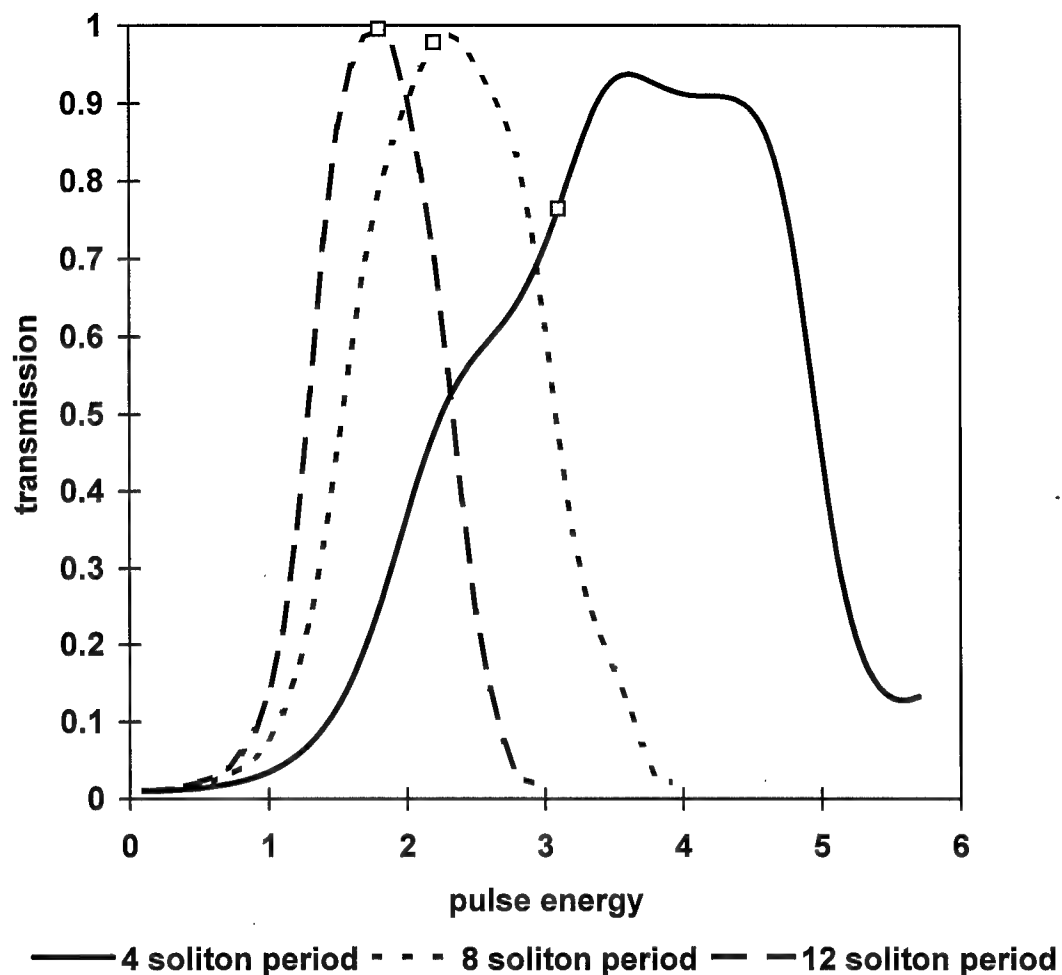
Figure 5.3 Pulse transmission as a function of pulse energy for an NOLM with a 55/45 beam splitter and no birefringence. The squares represent the predicted energies required for peak transmission given by Equation 5.13. The figure shows the effect of changing the loop length.

Simulation Results: Birefringent NOLM

Previous work on NOLMs have either ignored the effect of birefringence in the fiber or have examined their behavior for a nearly constant signal.[80,81,82] I have extended this work by studying pulse propagation in a birefringent fiber NOLM. I have made the idealization of fiber with a uniform birefringence. In particular, since fiber lasers have been noted to be very sensitive to the setting of the polarization controllers, I have studied the impact of the settings of the controllers. This effect has been used to greatly reduce the pump power needed to start a figure eight laser.[83] The propagation of a pulse in the anomalous dispersion regime can be modeled by the coupled Nonlinear Schrodinger Equations (NLSEs).

I modeled the polarization controller in a fashion described by Mortimore[81]. The field components of the pulse are rotated into the coordinate frame of the controller with the controller axes being its fast and slow birefringent axes. A phase delay is imposed on the slow axis and the fields are rotated back into the original coordinate system. The resulting Jones matrix for the controller is

$$
\begin{pmatrix} E'_x \\ E'_y \end{pmatrix} = \begin{pmatrix} J_{xx} & J_{xy} \\ J_{yx} & J_{yy} \end{pmatrix} \begin{pmatrix} E_x \\ E_y \end{pmatrix}. \tag{5.14}
$$

E_x and E_y are the electric field components in the input coordinate frame. The coordinate system used here was that the slow axis of the fiber was the x coordinate axis and the fast axis was the y axis. The elements of the transfer matrix are given by

$$
J_{xx} = e^{i\phi} \sin^2\theta + \cos^2\theta,
$$

$$
J_{xy} = J_{yx} = \left(e^{i\phi} - 1\right) \cos\theta \sin\theta, \tag{5.15}
$$

$$
J_{yy} = e^{i\phi} \cos^2\theta + \sin^2\theta.
$$

The variable θ is the angle between the slow axis of the fiber and the slow axis of the polarization controller. The relative phase shift caused by the controller on its slow axis

when compared to its fast axis is given by ϕ. An additional subtlety of extreme importance was pointed out by Mortimore.[81] The effect of the loop geometry is that the components of the electric field of the counter propagating pulses in the plane of the loop have their orientations reversed relative to each other. This means that their orientations are not the same when they enter the polarization controller. The significance of this will become clear when the results of the simulations are examined.

In general, all angles have been measured relative to the slow birefringent axis of the fiber. There are three other angles of importance. One must define the orientation of the input pulse and the angle of the plane of the loop. As mentioned in the last paragraph, the component of the light in the plane of the loop will have its orientation reversed in one counter propagating pulse relative to the other. Finally, one must define the direction of the slow axis of the polarization controller. These directions are shown in Figure 5.4.

I have sought to find an NOLM configuration which would have a set of desirable properties. Clearly, the device needs to have high transmission, but the loop also needs to transmit pulses which have been undistorted. If the distortions are too great they will cause the pulse to break up in subsequent transmission through fiber or in a subsequent transmission through another NOLM. In addition I would like to be able to change the transmission of the NOLM by adjusting the polarization controller. This is an attractive option since this is often the only adjustment to the NOLM that can be made once it has been assembled. It should be emphasized that almost any desired Jones matrix can be produced within a polarization controller.[84] For this reason, one can assume that in an experiment one could adjust the input polarization into some fixed state.

In order to make the polarization controller function in this way, I need to create an NOLM configuration in which the two counter-propagating pulses are treated quite differently by the controller. This situation can be achieved in the following way. One of the pulses must be aligned with one of the birefringent axes of the polarization controller. There must be an angle of 45 degrees between the orientation of the input pulse and the plane of the loop. This will cause a 90 degree change in the orientation of one of the

orientation of
counterpropagating
pulse

fast axis

input orientation

slow axis
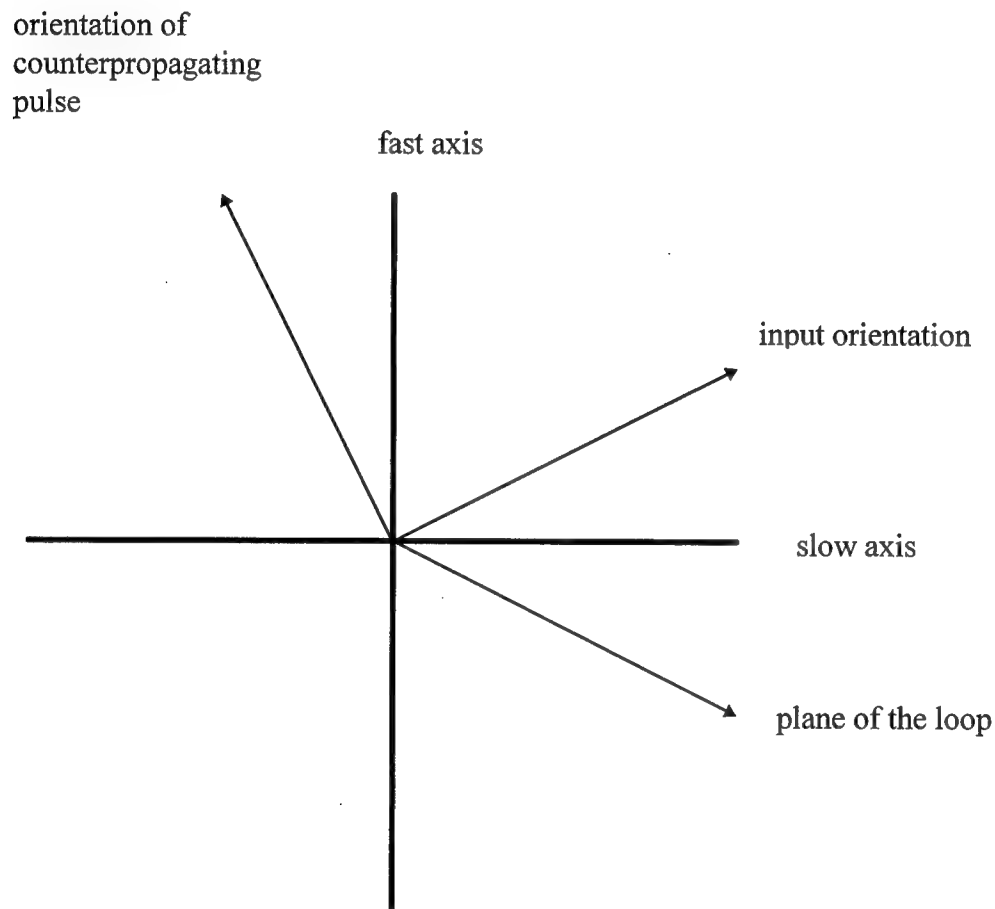
plane of the loop

Figure 5.4 Relative directions of important planes

pulses as it traverses the loop. Hence one of the pulses will be aligned with the slow axis of the controller, and the other with the fast axis. In this configuration, a simple relative phase shift of one pulse relative to the other can be produced.

I have examined situations in which this simple phase shift is produced. Since the polarization controllers can be changed to form any arbitrary Jones matrix, the polarization of the input pulse can be altered to any arbitrary state. Figure 5.5 shows an example of a set of transmission curves where the pulse energy is equally divided between the two birefringent axes of the fiber. The plane of the loop was aligned with the slow axis of the fiber as was the slow axis of the polarization controller. The group velocity difference, δ, was set equal to 0.1. The pulse energy is normalized so that the energy of a unit soliton is unity and the directional coupler had a 60/40 splitting ratio. The input pulse had a form $(A/2)\text{sech}^2[(1+2/3)^{1/2}\tau]$, where A is the amplitude and τ is the normalized time for a unit soliton. This is a form clearly related to that in Equation 3.18. The decision to use this form was guided by the need for the pulses to be at least potentially stable. The loop was two soliton periods long, for the same unit amplitude soliton. The figure indicates that this NOLM configuration can control the loop's switching functions in the fashion which I desire. When the curve describing pulse transmission without phase delay is compared to that when there is a 90 degree phase delay, we find that the energy needed to reach maximum transmission has been cut in half and low energy transmission has been increased by more than ten-fold.
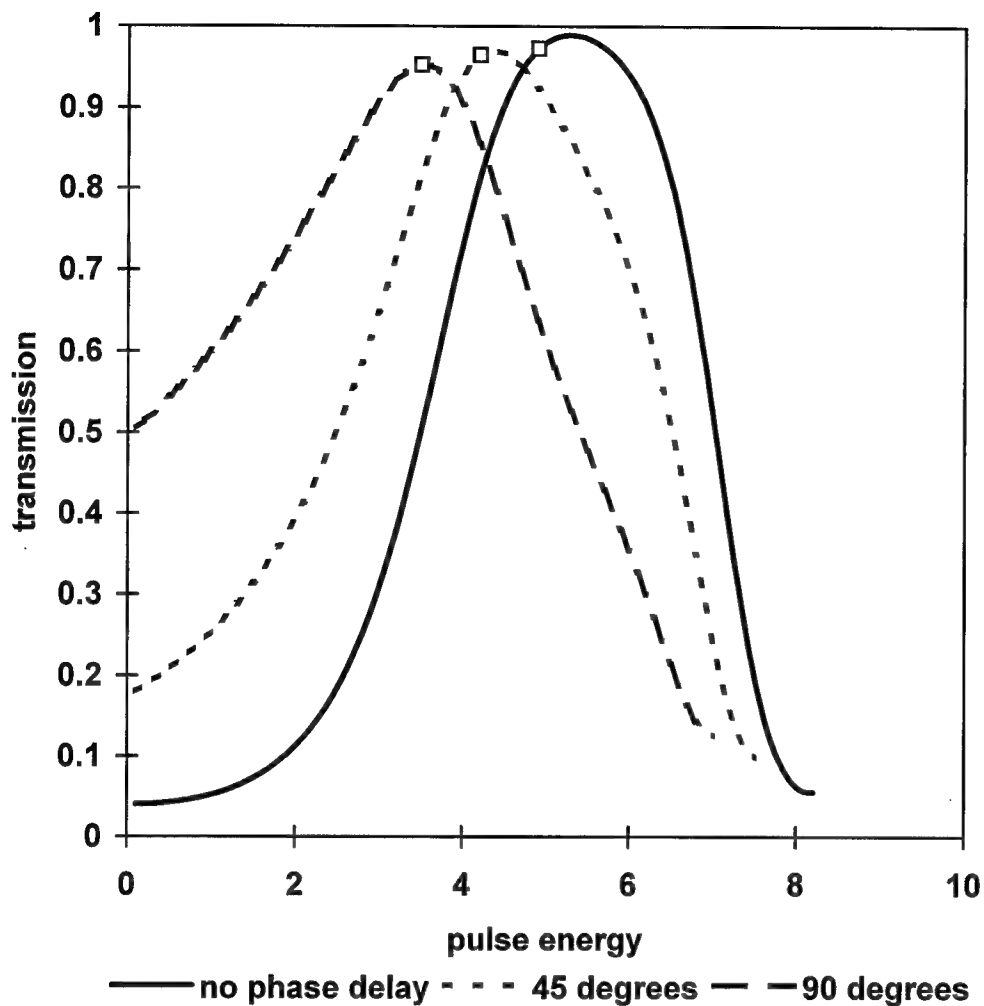
Figure 5.5 Pulse transmission as a function of pulse energy for an NOM with a 60/40 beam splitter. The fiber has a birefringence of δ=0.1, and the loop is 2 soliton periods long. The squares represent the predicted energies required for peak transmission given by Equation 5.20. The figure shows the effect of change in phase delay.

The location of the transmission maximum for the curve will be examined first. At the maximum the two pulses must be out of phase by π. The phase shift a soliton experiences as it propagates is

$$\phi = \left[\left(\frac{5}{3} \right) \frac{\eta^2}{2} + \frac{\delta^2}{2} \right] \xi .$$
(5.16)

The energy of the input pulse is given by

$$E_{in} = 2 \int_0^\infty P_{in} \sec h^2 \left[\left(\frac{5}{3} \right)^{\frac{1}{2}} t \right] dt = 2 \left(\frac{5}{3} \right)^{\frac{1}{2}} P_{in} ,$$
(5.17)

where P_{in} is the pulse height of the input pulse. In contrast the energy of the soliton is given by

$$E_{sol} = 2 \int_0^\infty P_0 \sec h^2 \left[\left(\frac{5}{3} \right)^{\frac{1}{2}} \frac{t}{T_0} \right] dt = 2 \left(\frac{5}{3} \right)^{\frac{1}{2}} P_0 T_0 .$$
(5.18)

This indicates that Equations 5.9-5.11 hold in this case as well. If these are combined with Equation 5.18 one finds that the phase difference between the two counter-propagating pulses becomes

$$\Delta\phi = \frac{\left(\frac{5}{3} \right) (2\alpha - 1)(P_{in})^2}{8} \xi_1 ,$$
(5.19)

where ξ_1 is the length of the loop in dispersion lengths. Solving for pulse energy yields

$$P_{in} = \left(\frac{8\Delta\phi}{\left(\frac{5}{3} \right) (2\alpha - 1)\xi_1} \right)^{\frac{1}{2}} .$$
(5.20)

The results of this simple model and those predicted by numerical simulation are given in Figure 5.5. The results indicate moderately good agreement, especially given the crude approximations made.

The output pulses were compared to the form of the input pulses

$$\left(\frac{A}{2}\right)\sec h^2\left[\left(\frac{5}{3}\right)^{\frac{1}{2}}\frac{\tau}{\tau_0}\right],\tag{5.21}$$

where τ_0 is the altered pulsewidth in normalized units. The output pulses maintained nearly this shape after transmission through the loop. The output values of τ_0 are given in Table 5.1. We see that the effect of changing the phase delay is to make the pulses broader as well. Since the pulses have less energy for maximum switching when a phase delay is added, the pulses will tend to broaden in the loop. This would explain the trend we observe. The NOLM may reshape a pulse transmitted through it.[85] For an NOLM without birefringence, this reshaping is minimized for loops that are four soliton periods long.[86]

The shift in phase delay produces a distortion of the pulse. First, as can be seen in Figures 5.6-5.8 it may be observed that the output pulses are nearly hyperbolic secant shaped pulses. The solid and dashed curves represent the intensities along the fast and slow axes. The wings are built up a bit as the phase delay is increased. The peak intensity is decreased as the phase delay goes up, but this is simply due to that the fact that the input pulses are less energetic. This may be an additional cause of the pulse broadening shown in Table 5.1. This result has been reported before for non-birefringent NOLMs.[78] The pulses appear to propagate as coupled solitons since the polarizations have not separated in time in spite of birefringence.

Table 5.1 Pulse Width as a function of phase delay for a vector soliton in a 2 soliton period long NOLM with a 60/40 beam splitter. The birefringence is δ=0.1.

phase delay	pulse width
0	0.8
π/4	0.9
π/2	1.2

A second feature which can be explained analytically is the minimum transmission. It can be found because the phase delay is only caused by the polarization controller. Equation 5.4 tells us that

$$T_{min} = 1 - 2\alpha(1-\alpha)[1 + \cos(\phi)].$$
(5.22)

The results of this expression and those found from computation are given in Table 5.2. The results show excellent agreement.

Table 5.2 Numerical and analytical low intensity transmission for a 2 soliton period long NOLM with a 60/40 beamsplitter. The birefringence is δ=0.1. The numerical results are compared to the predictions of equation 5.22.

phase delay	numerical	analytical	disagreement
0	0.04	0.04	0%
π/4	0.18	0.18	0%
π/2	0.50	0.52	4%
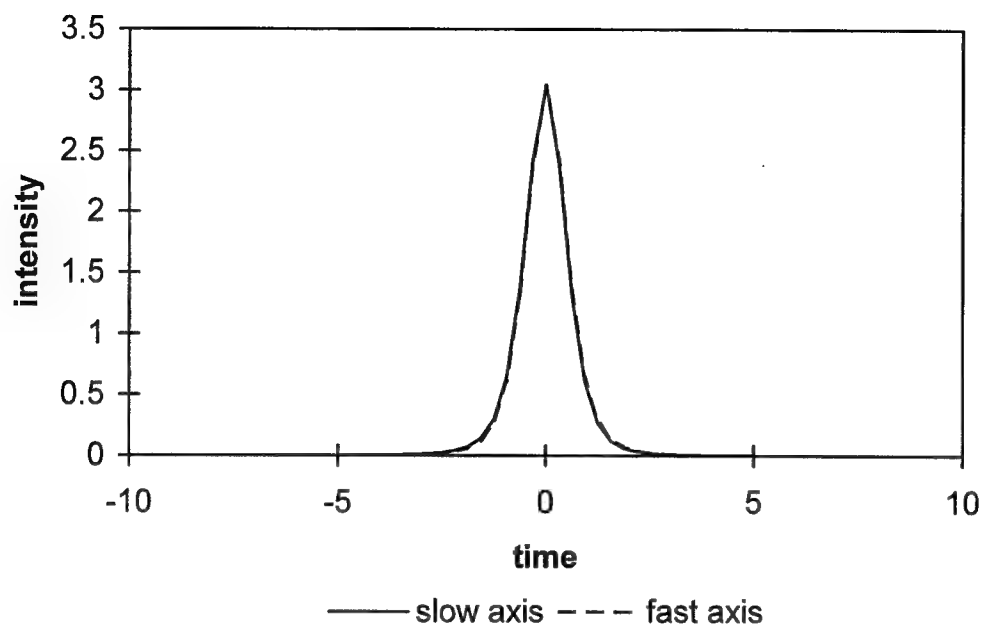
Figure 5.6 Output pulse shape for a 2 soliton period long loop mirror without phase delay. The birefringence of the fiber was δ=0.1.
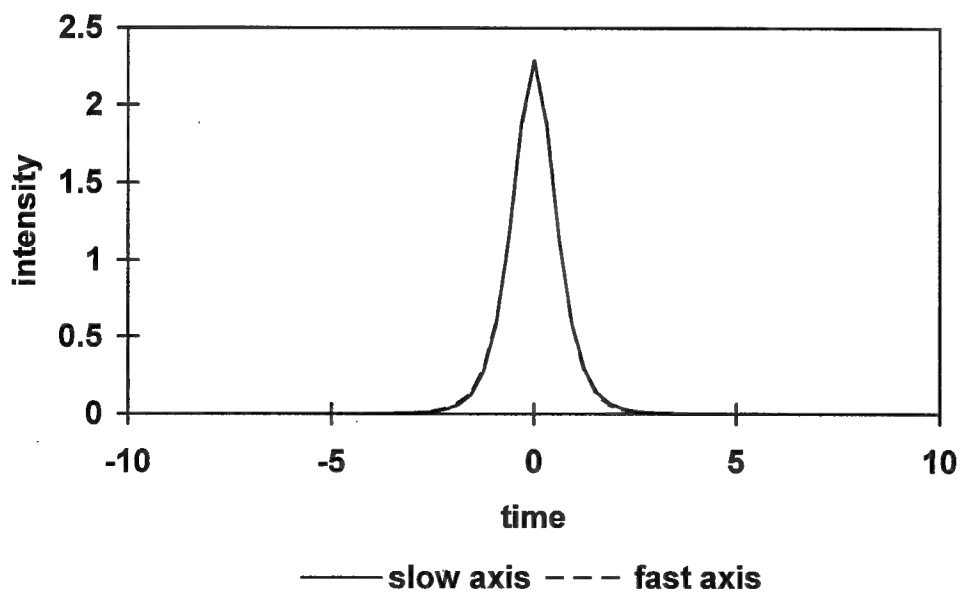
Figure 5.7 Output pulse shape for a 2 soliton period long loop mirror π/4 delay. The birefringence of the fiber was δ=0.1.
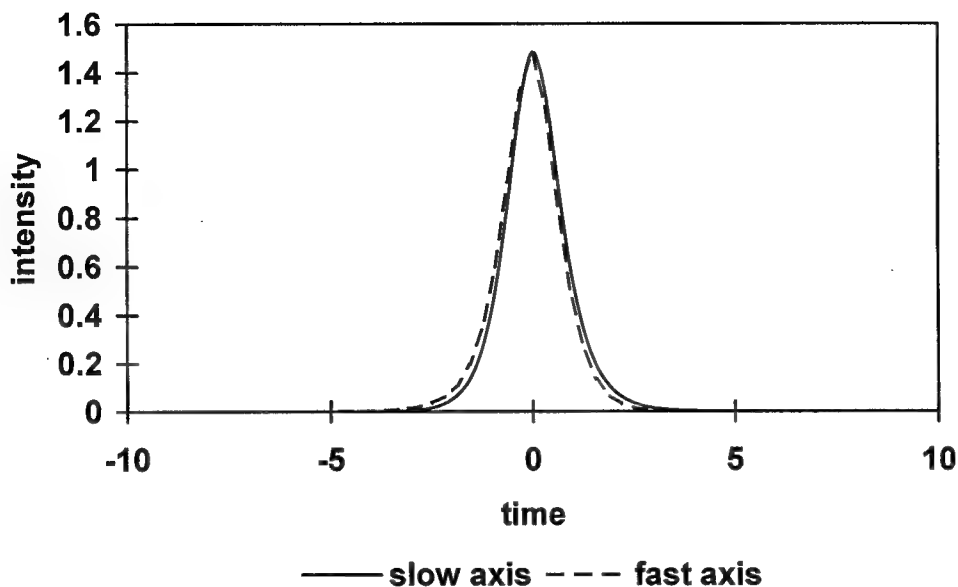
Figure 5.8 Output pulse shape for a 2 soliton period long loop mirror π/2 delay. The birefringence of the fiber was δ=0.1.

A second consequence of pulse reshaping is a reduction in transmission of the pulse, when it is passed through an NOLM a second time. This has been examined experimentally by Nayar, Finlayson, and Doran[87]. They demonstrated that the transmission of their NOLM was about 70% for the first transmission but that two concatenated NOLMs had a transmission of about 50%. They also showed that the pulses appeared to be much more square than the input pulses. Figure 5.9 shows what happens when this is done with an NOLM with the configuration that was discussed above. This phenomenon is a useful thing to study since multiple transmissions through a switch occur in a fiber communications network, or in a laser. In both cases, the pulses would be reshaped by various devices between passes through the NOLM, so this is merely a starting point to the study of these problems. We see that when there is no phase delay, the effect of the second pass is to narrow the transmission peak and to reduce transmission between the peaks. For $\phi=\pi/2$, however the transmission peak is
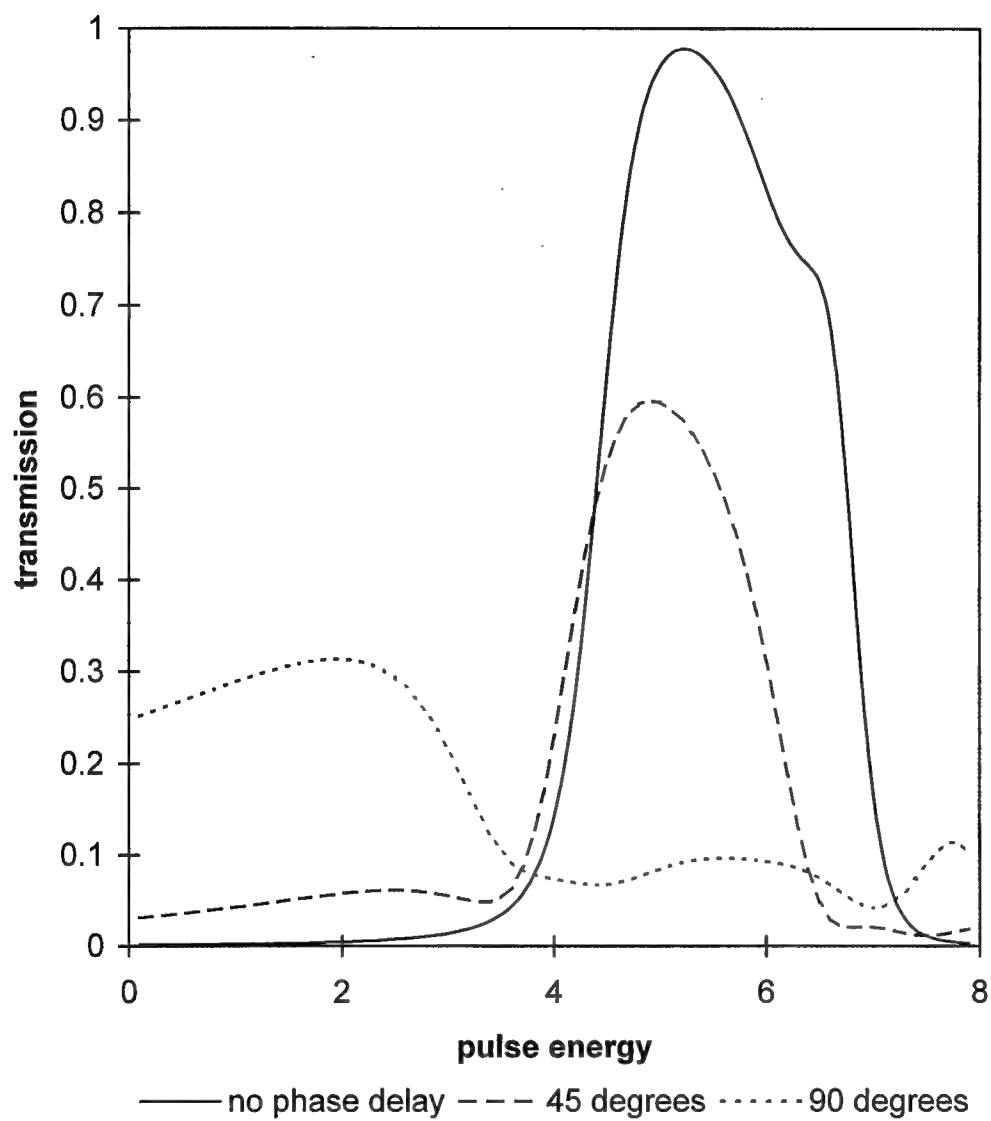
Figure 5.9 Two pass transmission for a 2 soliton period loop. The birefringence of the fiber was δ=0.1

eliminated, and the low intensity transmission is increased. The curve for $\phi=\pi/4$ gives an intermediate result. The low intensity transmission is simply the square of the one pass low intensity transmission.

The explanation for the behavior of the first transmission peak is more complex. This is due to the fact that the system is now nonlinear. The transmission peak for the pulse which does not experience phase delay has been shifted to a lower energy than in the one pass case. It is located at 5.2 rather than 5.3 energy units. The peak transmission in this situation is 0.978. If one simply assumes that the reduction is linear, one multiplies the starting energy by the transmission for that energy and then multiplies the result by the one pass transmission of this intermediate energy. This analysis predicts a two pass transmission of 0.967 or an error of about 1%. So in this case the linear analysis works. If a $\pi/4$ phase delay is imposed, the analysis breaks down. It predicts a transmission of 0.893 which is far higher than the value of .597 predicted by the numerical results. This lower value could be due to pulse reshaping The pulse width, as seen in Table 5.1, is broader than in the case without phase delay. This will certainly alter the transmission somewhat. When the phase delay is increased to $\pi/4$ radians, transmission is greatly reduced. In this case, the pulse is still broader and can be seen to be somewhat distorted.
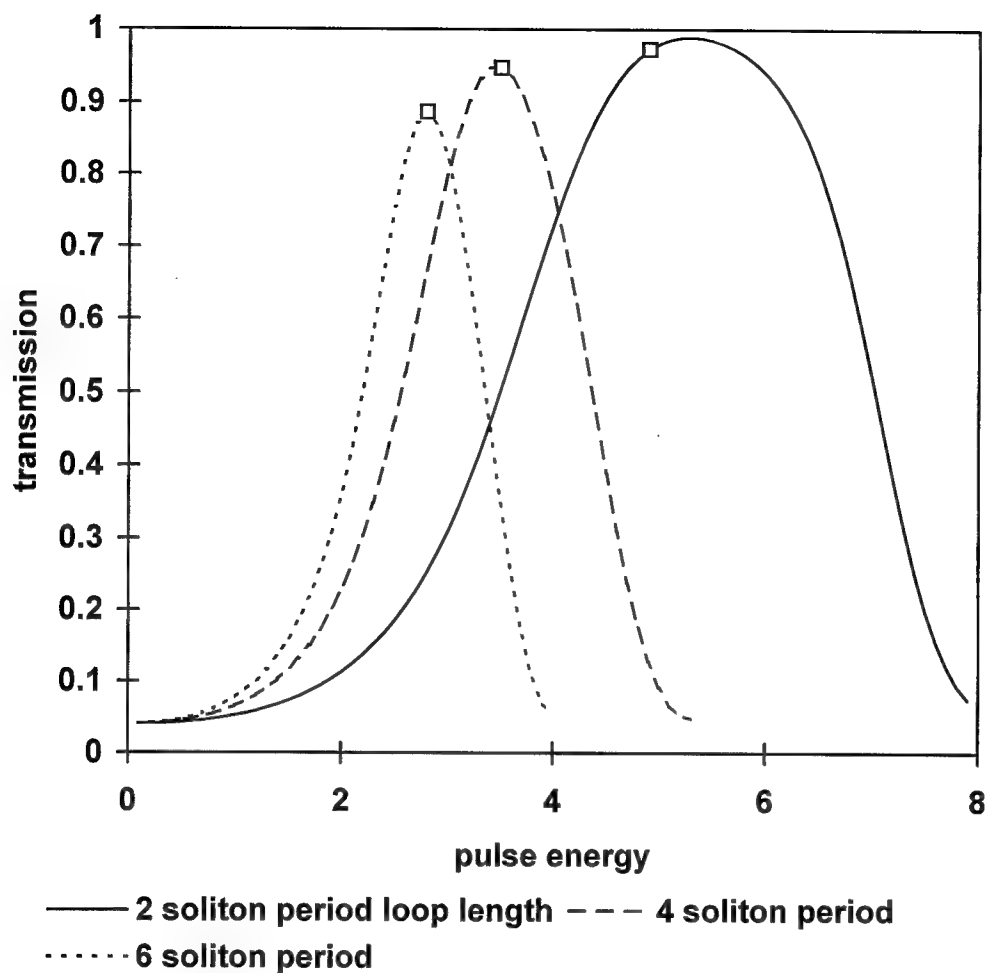
Figure 5.10 Pulse transmission as a function of phase delay in an NOLM without a polarization controller. The birefringence of the fiber was δ=0.1. The NOLM had a 60/40 beam splitter, and a vector soliton input pulse. The figure shows the effect of changing the loop length. The squares show the pulse energies for peak transmission given by equation 5.20.

The expected result of making the loop longer is to reduce the energy required for transmission. Figure 5.10 shows the result of carrying out the simulation of the previous case, by varying the loop length using no phase delay due to the controller. The low intensity transmission is almost exactly what is predicted analytically, as shown in Table

5.2. The results again show good agreement. The comparison of the expected peak location to the results of the simple model improve as the loop becomes longer. This may be attributed to the fact that the pulse is reshaped into a soliton soon after entering the loop and propagates in this form for a longer portion of the total distance. Under these conditions, the assumptions of the simple model are more nearly correct.

The width of the output pulse is dependent on the length of the loop. Table 5.3 shows this effect. The output pulse becomes broader as the length of the loop increases. This is similar to the results in the non-birefringent case. The pulses are less energetic for the longer loops, hence they spread in the loops. This results in longer output pulses.

Table 5.3 Pulse width as a function of loop length for a vector soliton. The loop has a 60/40 beam splitter. The birefringence is $\delta=0.5$.

loop length	T_0
2	0.8
4	1.1
6	1.3
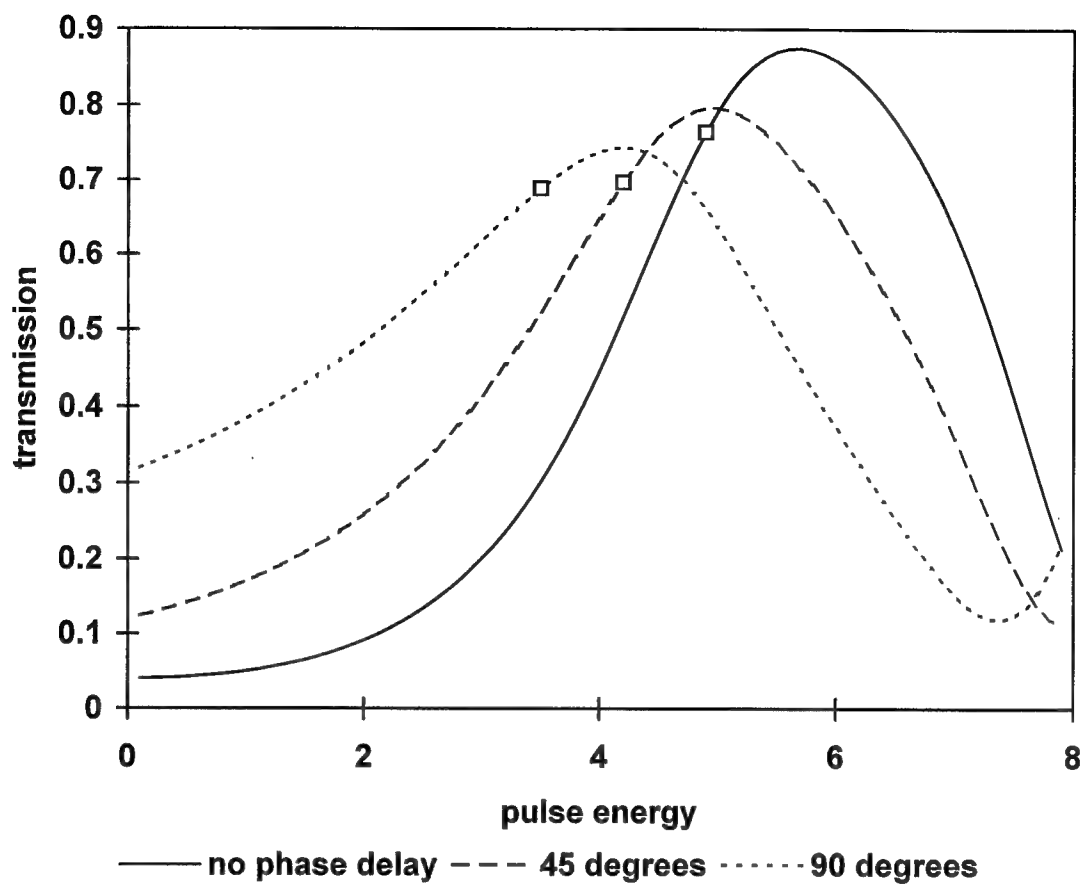
Figure 5.11 Pulse transmission as a function of pulse energy for a 2 soliton period long loop. The NOLM had a birefringence of δ=0.5 and a vector soliton input. The figure shows the effect of changing the phase delay. The squares show the pulse energies for peak transmission given by equation 5.20.

Table 5.4 Low intensity transmission for a 2 soliton period long NOLM with a 60/40 beamsplitter. The birefringence was $\delta=0.5$. The numerical results are compared to the predictions of equation 5.22.

phase delay	numerical	analytical	disagreement
0	0.04	0.04	0%
$\pi/4$	0.12	0.18	50%
$\pi/2$	0.32	0.52	63%

The effect of increasing birefringence, which is described by the parameter δ, has been examined. In general, the effect of increased birefringence is to reduce the functionality of the NOLM switch. This is due to the tendency of birefringence to distort the vector solitons, making them less stable. The primary form of distortion is that the light in the two polarizations separate;that is to say, the sub-pulses along the two birefringent axes tend to separate from each other. This tendency is reduced by the soliton trapping effect which causes light in the two polarizations to couple. The degree of separation is dependent upon the birefringence and on the energy in the soliton. This effect was described in the chapter on birefringence. This effect has a variety of manifestations, as will be seen. Figure 5.11 shows the result of making $\delta=0.5$ and examining the effect of changing the phase delay. The first effect to be noted is that the low intensity transmission no longer agrees with the cw analysis. This is shown in Table 5.4, which shows that the pulse width is relatively insensitive to changes in phase delay for this case.   In addition,we can see that the predictions of the location of the transmission peaks become far worse. These predictions are indicated in Figure 5.11.

Table 5.5 Pulse width as a function of phase delay for a 2 soliton period long NOLM with a 60/40 beamsplitter. The briefringence is δ=0.5.

phase delay	pulse width
0	1.1
$\pi/4$	1.0
$\pi/2$	1.0

The explanation for the reduction in low intensity transmission can be found by examining how the polarization controller affects pulse shape. Figures 5.12-5.14 show the case of a hyperbolic secant pulse in the low intensity case. The dashed and solid lines represent intensity along the two birefringent axes. The loop is two soliton periods long. The polarization controller is on one end of the loop. Of the two pulse traveling in the loop mirror, one will encounter the controller first, and then be modified by the fiber in the loop. The other will be altered by the polarization controller only after passing through the loop. The pulse which first is passed through the polarization controller and then passes through the loop is undistorted. The pulse which passes through the loop first, however is dramatically distorted by the polarization controller. Figure 5.12 shows the pulse after it has passed through the loop but before it is affected by the polarization controller. It has been broadened by linear dispersion and the two polarizations are separating, but it still has a hyperbolic secant shape. This is the same as the counter propagating pulse which first passes through the polarization controller and then through the fiber. Figure 5.13 shows the the pulse which has been passed through the fiber through the controller. Large satellite pulses have been produced. The origin of these satellites can be found in Equations 5.14 and 5.15, which describe the polarization

controller. In the case where the pulse energy is equal along both axes ($\theta=\pi/4$), the polarization controller will not change the polarization orientation of the pulse but simply acts to impose a phase delay on one axis. Figure 5.12 shows however, that the pulse does not in general have equal intensities along both axes at any given moment. Under this condition, the controller couples light between the two input polarizations. This explains the distorted pulse. The distortion in the output pulse is shown in Figure 5.14.
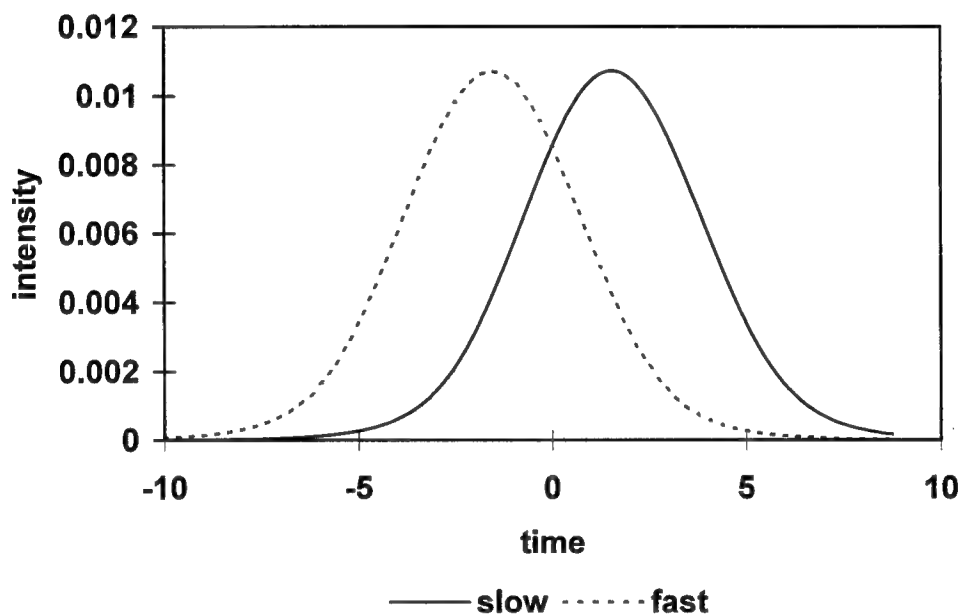
Figure 5.12 Shape of a low energy pulse in the loop. This pulse was affected by the polarization controller at the beginning of its passage through the fiber loop.   The birefringence of the fiber was $\delta=0.5$. There is a phase delay of $\pi/4$. The loop is two soliton periods long.
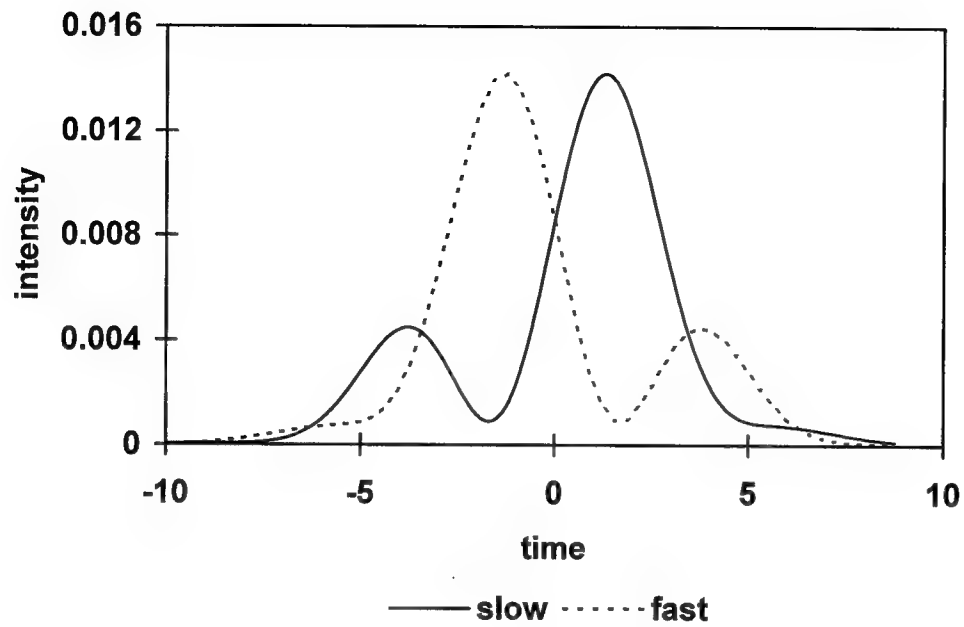
Figure 5.13 Shape of a low energy pulse in the loop. This pulse was affected by the polarization controller at the end of its passage through the fiber loop. The birefringence of the fiber was $\delta=0.5$. There is a phase delay of $\pi/4$. The loop is two soliton periods long.
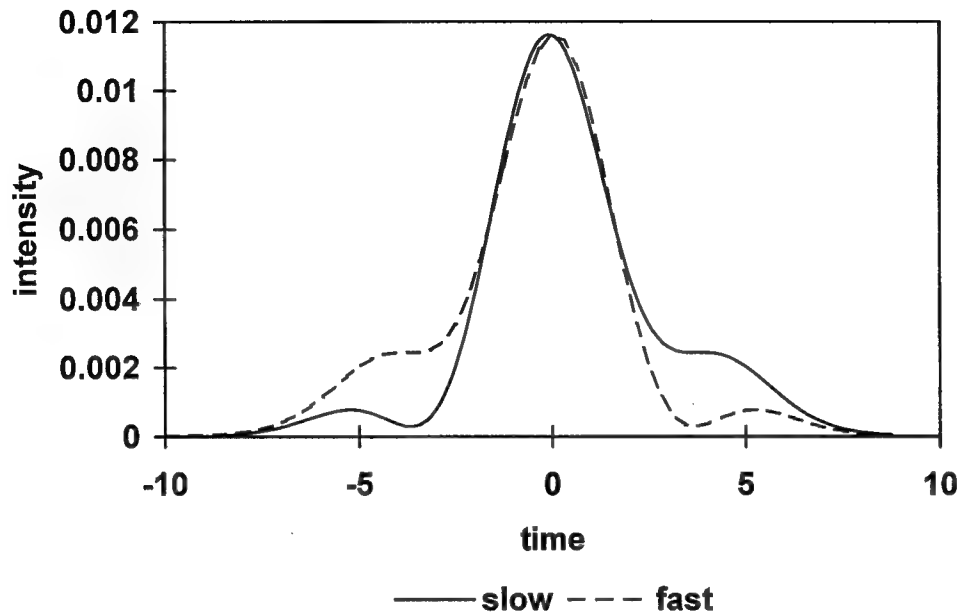
Figure 5.14 Shape of a low energy pulse transmitted by an NOLM. The birefringence of the fiber was δ=0.5. There is a phase delay of π/4. The loop is two soliton periods long.

The distortion of one of the counter propagating pulses causes the change in transmission. The relationship between the two can be seen by taking the magnitude of both sides of Equation 5.3 to obtain

$$\left|E_{out}\right|^2 = \alpha\left|E_3\right|^2 + (1-\alpha)\left|E_4\right|^2 - 2\,\mathrm{Re}\left[i\,\alpha^{\frac{1}{2}}\,(1-\alpha)^{\frac{1}{2}}\,E_3 E_4^* \,e^{i\phi}\right]. \tag{5.21}$$

This equation expresses the output of the NOLM, where the last term describes the effect of interference of the two counterpropagating pulses. If the magnitude of the pulses can be related to the input fields by Equation 5.1, then Equation 5.21 reduces to Equation 5.4. But since one of the pulses is distorted by the polarization controller, the instantaneous transmission is altered. The low intensity transmission cited in Table 5.4, represents the averaging of the instantaneous transmission over time. Indeed if one uses Equation 5.1 in the last equation, but assumes that coherence between the two pulses has been eliminated,

one obtains a transmission of 0.52 if α=0.6. This is what we see in Table 5.4 for the case where ϕ=π/2. So in this case the interference term is making no net contribution to the pulse transmission.

The reason that this phenomenon did not appear for the case of δ=0.1, can be seen in Figures 5.15-5.17. The dashed and solid lines represent intensity along the two birefringent axes and the loop is two soliton periods long. The NOLM has a 60/40 beamsplitter. These show the pulses under the same conditions except with this lower value of δ. We can clearly see here that under these conditions the light in the two polarizations separate less. The pulses in Figure 5.15 display only about one fifth the separation as in Figure 5.12. This is to be expected from the difference in birefringence. Soliton trapping does not occur due to the low pulse intensities. The much smaller pulse separation means that Equation 5.22 is a much better approximation and the simple theory holds more exactly. The effect of the controller can be seen in Figure 5.16. It is manifested in an increase in pulse separation rather than by the large wings shown in Figure 5.13, which is the higher birefringence case. The final output pulse is shown in Figure 5.17. The pulse appears undistorted in the δ=0.1 case. The δ=0.5 results, shown in Figure 5.14, again show large wings.
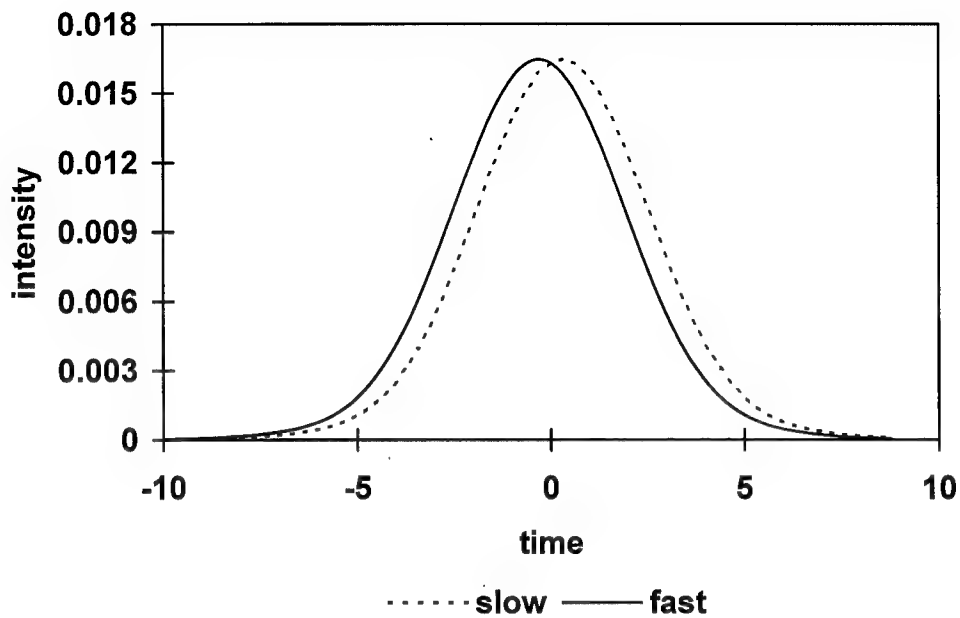
Figure 5.15 Shape of a low energy pulse in the loop. This pulse was affected by the polarization controller at the beginning of its passage through the fiber loop. The birefringence of the fiber was $\delta=0.1$. There is a phase delay of $\pi/4$. The loop is two soliton periods long.
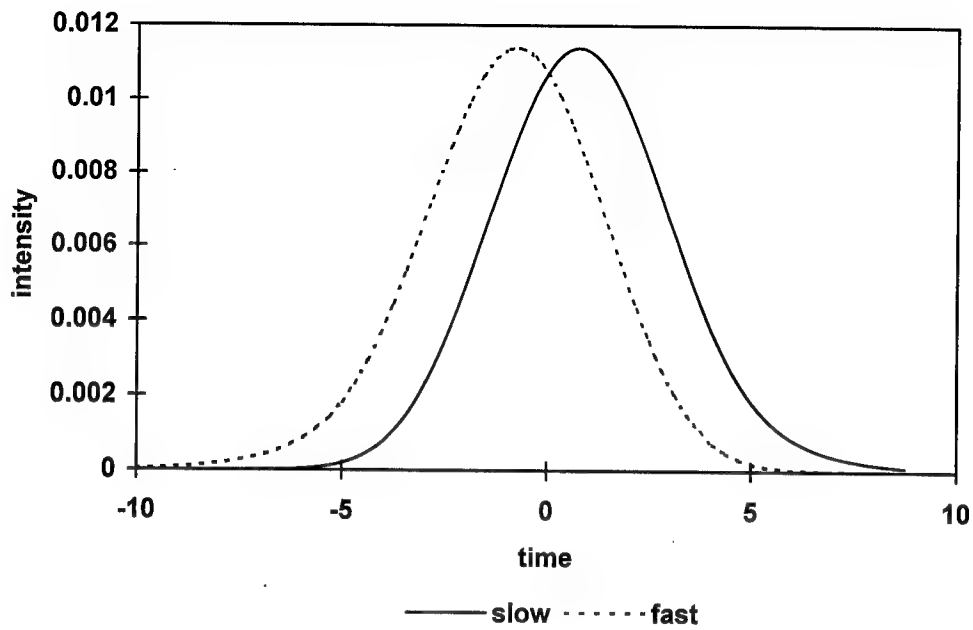
Figure 5.16 Shape of a low energy pulse in the loop. This pulse was affected by the polarization controller at the end of its passage through the fiber loop. The birefringence of the fiber was $\delta=0.1$. There is a phase delay of $\pi/4$. The loop is two soliton periods long.
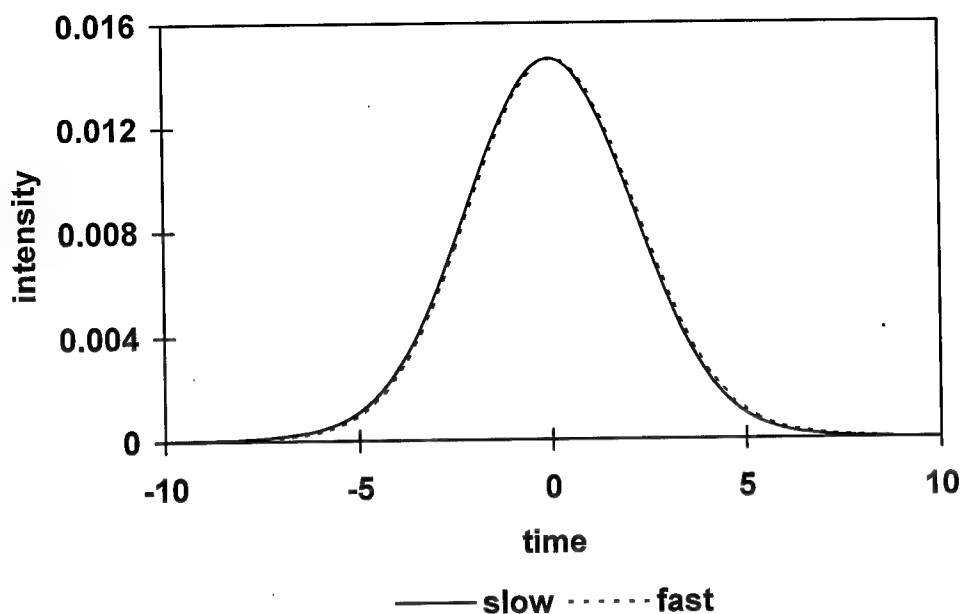
Figure 5.17 Shape of a low energy pulse transmitted by an NOLM. The birefringence of the fiber was δ=0.1.   There is a phase delay of π/4. The loop is two soliton periods long.

The same pulse reshaping phenomenon helps to explain the fact that the peak transmission for the δ=0.5 case declines as the phase delay increases. It also manifests itself by the altering of the NOLM pulse output shape. This is seen in Figures 5.18-5.20. These figures show the output pulses transmitted by the NOLM as the phase delay is increased. The loop is two soliton periods long and it has a 60/40 beam splitter. The solid and dashed lines indicate intensity along the two birefringent axes. These show the effect of adding more phase delay. The difference between the results shown here and those seen for low intensity pulses is that the pulses in the two polarizations will couple. This nonlinear effect will reduce the separation and hence the distortion of the pulse by the polarization controller. At first there is simply some separation of the polarizations. When the delay is π/4, the pulse has a hyperbolic secant shape which has reduced

polarization separation. This shows clearly how the soliton dragging effect helps the NOLM function in this case. In the $\pi/2$ case, however, there is increased separation and satellite pulses develop. The satellites are still much smaller, relatively, than in the low intensity case.
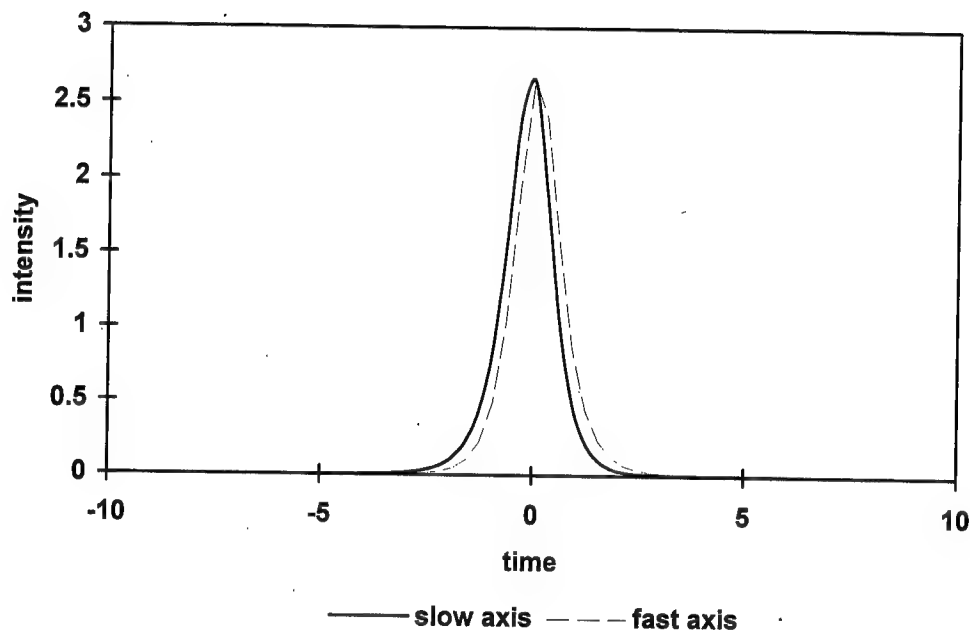
Figure 5.18 Output pulse shape for a 2 soliton period long loop mirror. There is no phase delay. The birefringence of the fiber was $\delta=0.5$.
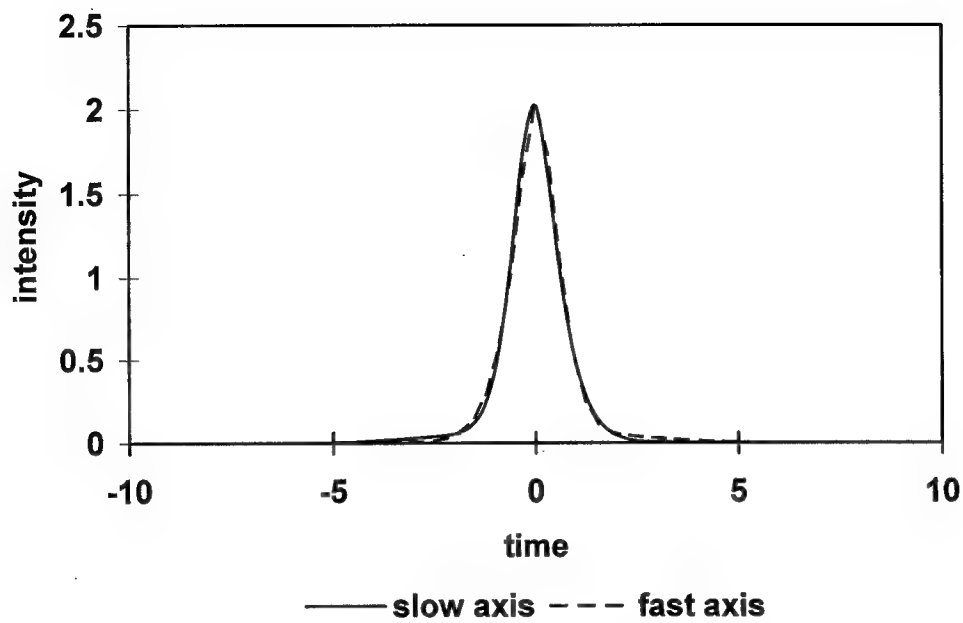
Figure 5.19 Output pulse shape for a 2 soliton period long loop mirror. The birefringence of the fiber was δ=0.5. There is a phase delay of π/4.
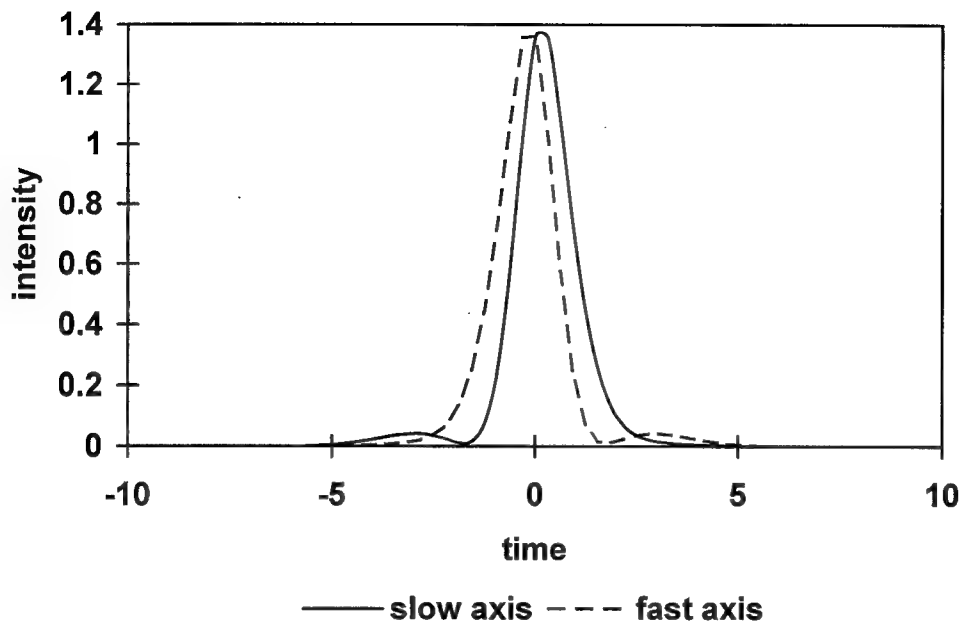
Figure 5.20 Output pulse shape for a 2 soliton period long loop mirror. The birefringence of the fiber was δ=0.5. There is a phase delay of π/2.

The fact that the polarization controller distorts the pulse can also be clearly seen in the way it reduces the multiple pass transmission, as seen in Figure 5.21. In comparison to Figure 5.9, the transmission peak for a π/4 phase delay has been almost eliminated. The low intensity transmission has increased, as is expected. The peak transmission for the switch without phase delay has been reduced due to pulse distortion.
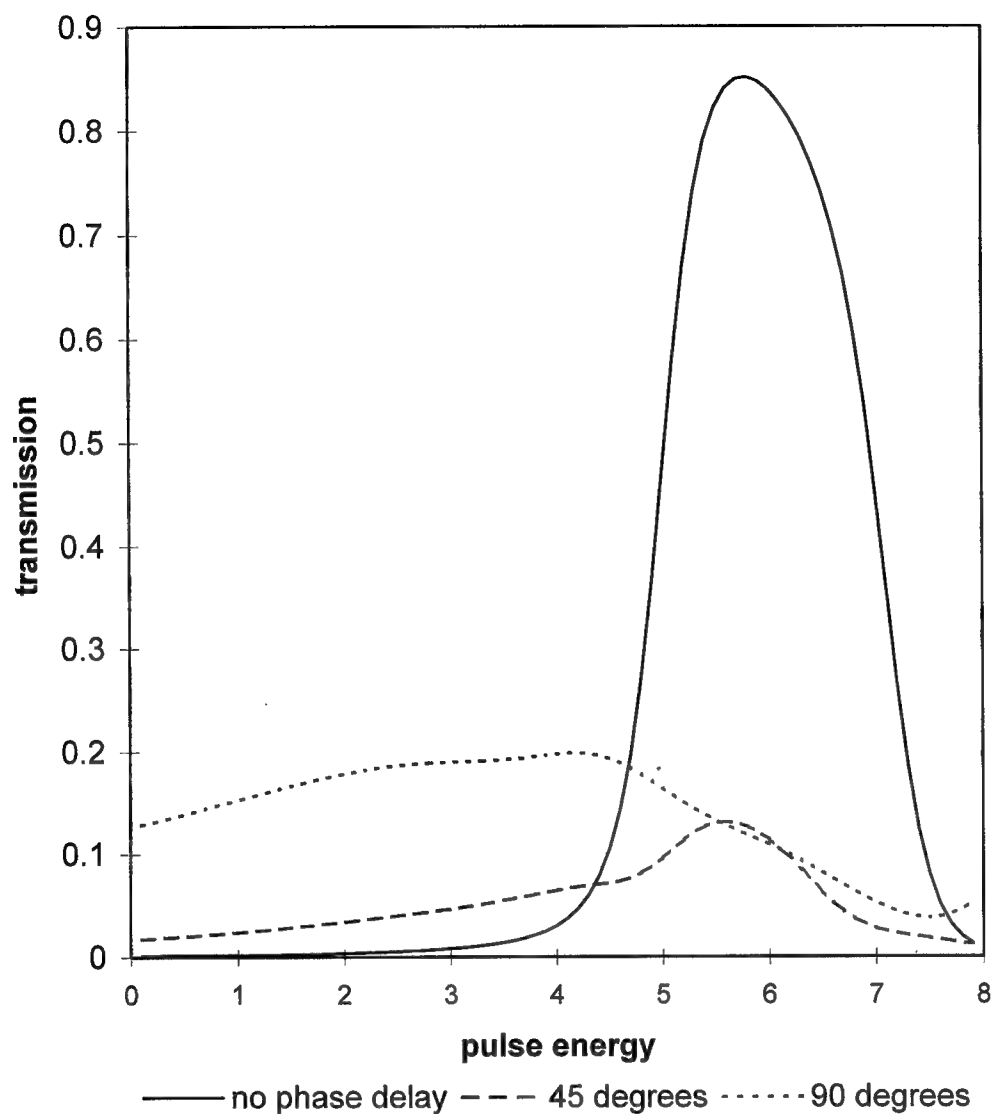
Figure 5.21 Two pass pulse transmission for a vector soliton in a 2 soliton period loop. The birefringence of the fiber was δ=0.5.

Figure 5.22 shows the effect of changing the loop length for the case of an NOLM with δ=0.5. The behavior of the NOLM is much the same as in the other cases. The effect of the birefringence is to increase the energy required to switch pulses. The peak

transmissions are reduced due to pulse distortion. This also appears in Table 5.6 which shows how the pulse widths increase as the loop becomes longer. Comparison with Table 5.3 shows that this effect is greater than in the case with less birefringence. The increased birefringence causes the pulses along the two birefringent axes to separate more in time. For this reason, when they are recombined by the polarization controller the output pulse will be wider. The increase in birefringence also means that the pulses will propagate like solitons for a reduced part of their passage through the loop. The degree to which the pulses in the loop do not behave like true solitons contributes to the breakdown in the accuracy of the soliton model for predicting pulse energies for switching, as seen in Figure 5.22. It should be noted that the energies needed for peak transmission are increased from the $\delta=0.1$ case. This indicates that the phase difference builds up more slowly when the birefringence increases. Since the birefringence parameter does not appear in Equation 5.20, which predicts the transmission energy, we must attribute the change to increased non-soliton like propagation.
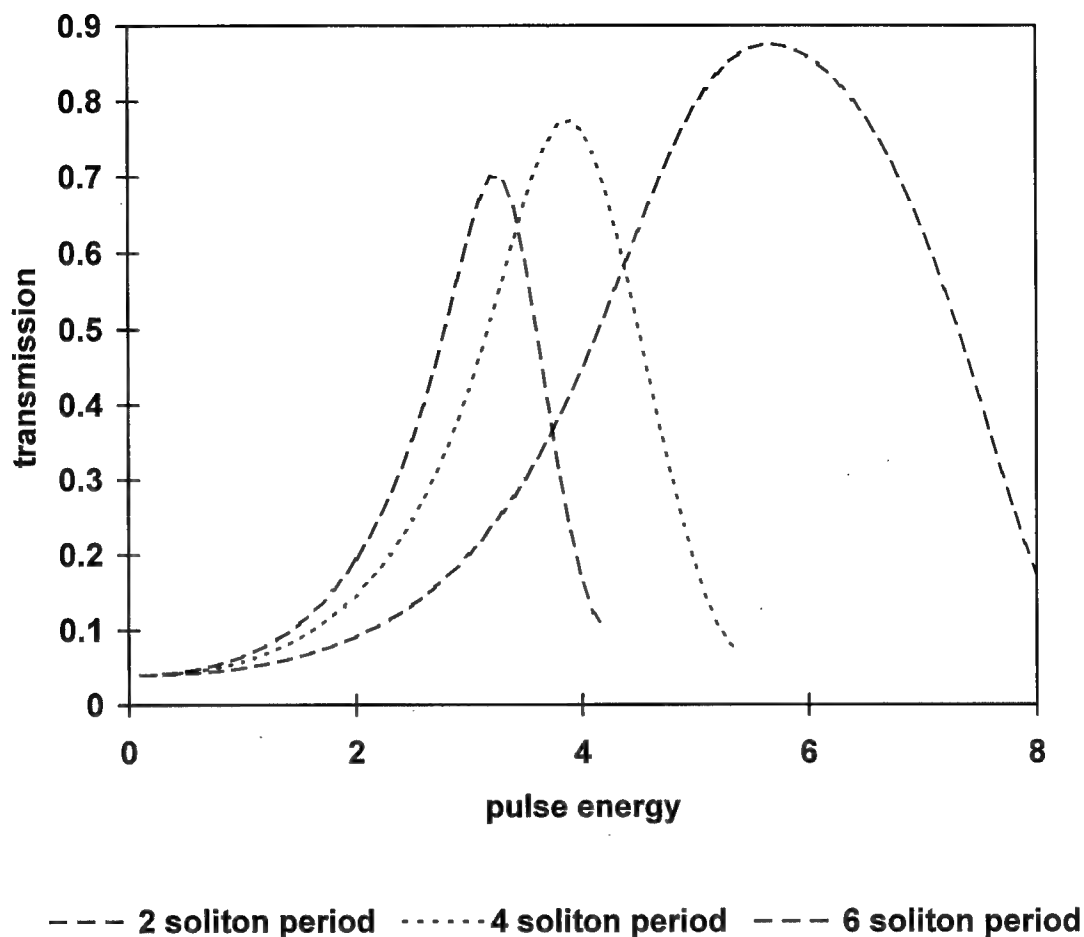
Figure 5.22 Transmission of a vector soliton as a function of soliton energy. The birefringence of the fiber was δ=0.5. The figure shows the effect of changing the loop length. The squares represent the predicted energies required for peak transmission given by Equation 5.20.

Table 5.6 Pulse width as a function of loop length soliton for an NOLM with a 60/40 beamsplitter. The birefringence is $\delta=0.5$.

loop length	T_0
2	1.1
4	1.4
6	1.8

The configuration that has been examined, with the input pulse energy evenly divided between the two birefringent axes, is not the only one that displays switching. The general requirement is that the input pulse be at a $\pi/4$ angle to the plane of the loop and that one of the axes of the polarization controller be aligned with the input pulse. Other configurations will be examined much more briefly. Figure 5.23 shows the case in which the input pulse is aligned with the slow axis. The central change in this configuration, compared to the last is that the counter-propagating pulses are now moving with different group velocities. For this reason, the interference between them is reduced when they recombine. This is manifested in the reduced peak transmissions observed in Figure 5.23 when compared to Figure 5.5. This effect also appears in the increased low intensity transmission displayed. Figure 5.24 shows the two-pass transmission when $\delta=0.1$. It indicates that this configuration is less sensitive to pulse distortion in the polarization controller than the case in which the light is evenly divided between the birefringent axes, especially in the case where the phase delay is $\pi/2$. The pulse distortion in the vector soliton case was caused by the light of different polarization separating. In this case, however, this does not happen, so the polarization controller can not distort the pulse. This explains why the one pass transmission is more uniform. The energy required for peak two-pass transmission is not greatly altered by the polarization controller, so it may not be a useful adjustment.

The effect of increasing birefringence is far more dramatic. Figure 5.25 displays this effect. Here the increased pulse separation greatly reduces pulse transmission. This effect can be understood in terms of the ideas given above. The pulses separate, and hence they do not interfere as much. This would lead to the dramatic reduction in peak transmission shown in the figure. Figure 5.25 also indicates that the two pass transmission is insensitive to changing the phase delay as is the low intensity transmission. Hence the utility of adjusting the polarization controller is lost in this case.
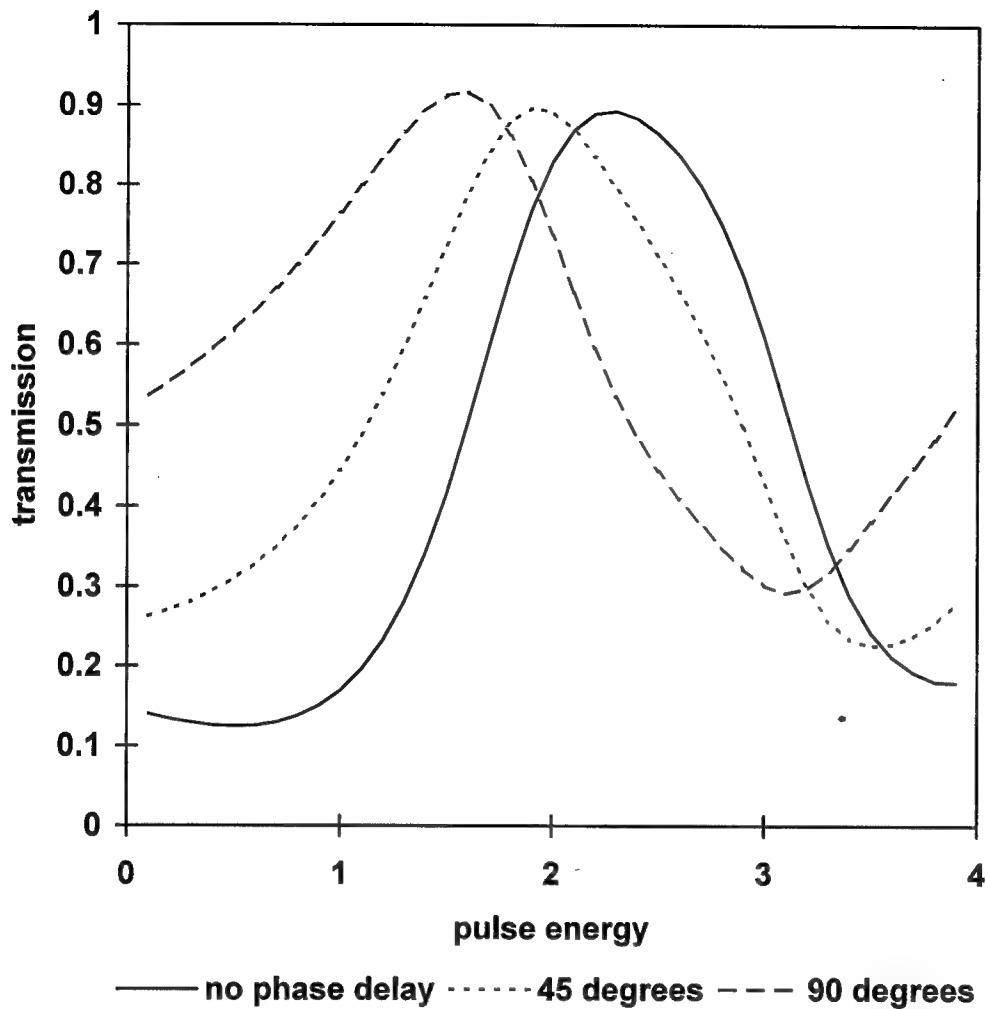
Figure 5.23 NOLM pulse transmission for an input pulse and polarization controller aligned to the slow axis of the fiber. The plane of the loop is tilted by $\pi/4$ from this and the birefringence of the fiber was $\delta=0.1$. The loop is four soliton periods long. The figure shows the effect of change the phase delay.
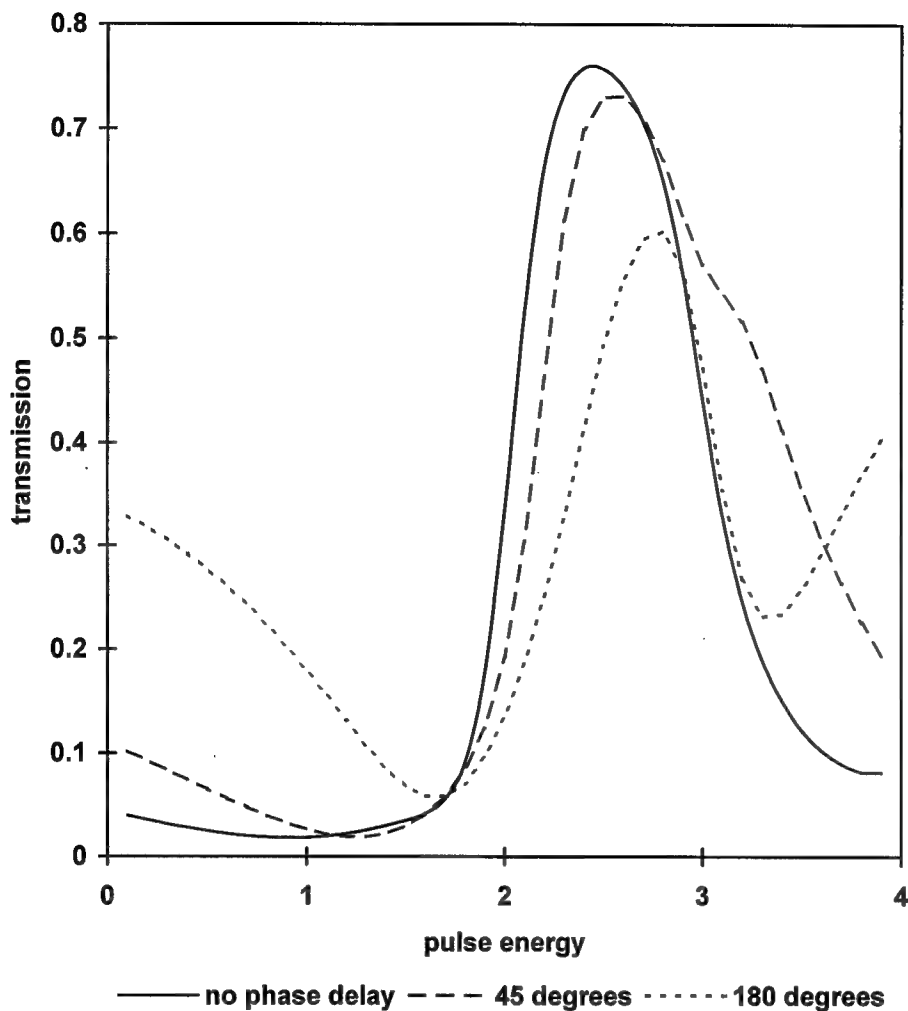
Figure 5.24 Two pass NOLM pulse transmission for an input pulse and polarization controller aligned to the slow axis of the fiber. The plane of the loop is tilted by $\pi/4$ from this and the birefringence of the fiber was $\delta=0.1$. The loop is four soliton periods long.
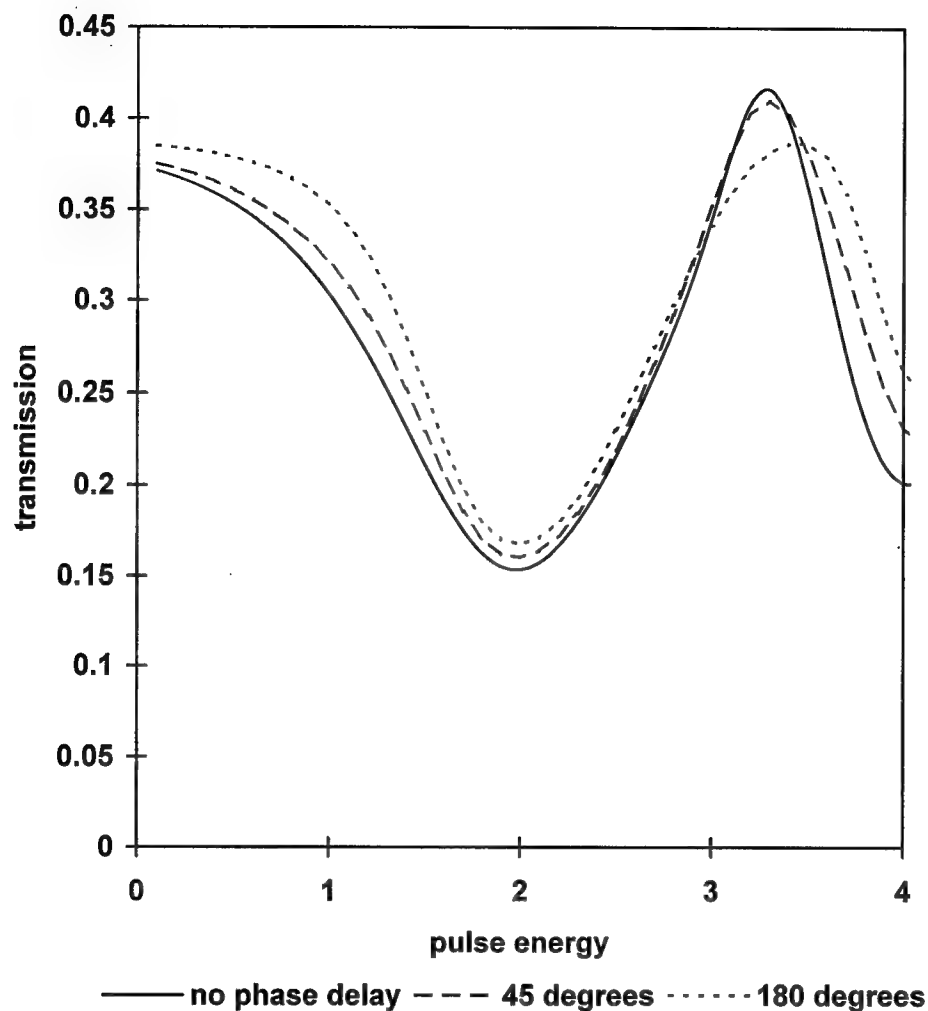
Figure 5.25 Two pass NOLM pulse transmission for an input pulse and polarization controller aligned to the slow axis of the fiber. The plane of the loop is tilted by $\pi/4$ from this and the birefringence of the fiber was $\delta=0.5$. The loop is four soliton periods long.

Transmission curves for an arbitrary input polarization can be expected to be more complex since the pulses will experience polarization rotation as well as separation of light in different polarizations. Figure 5.25 shows the polarization curves for the situation

in which the input pulse is at an angle of $\pi/8$ to the slow axis of the fiber. The slow axis of the controller is aligned with the pulse and the plane of the loop is at an angle of $-\pi/8$. Pulses with this input angle will be subject to intensity dependent polarization rotation. Their behavior can be expected to be quite complex. In addition, their pulses will be subject to distortion by the polarization controller. We observe that the peak transmission is reduced. This may be ascribed to reduce interference at the beamsplitter due to the alteration of the polarization in the loop and to the separation of the light along the two different axes. The separation of light along the two axes manifests itself in increased low intensity transmission, compared with the cw case.
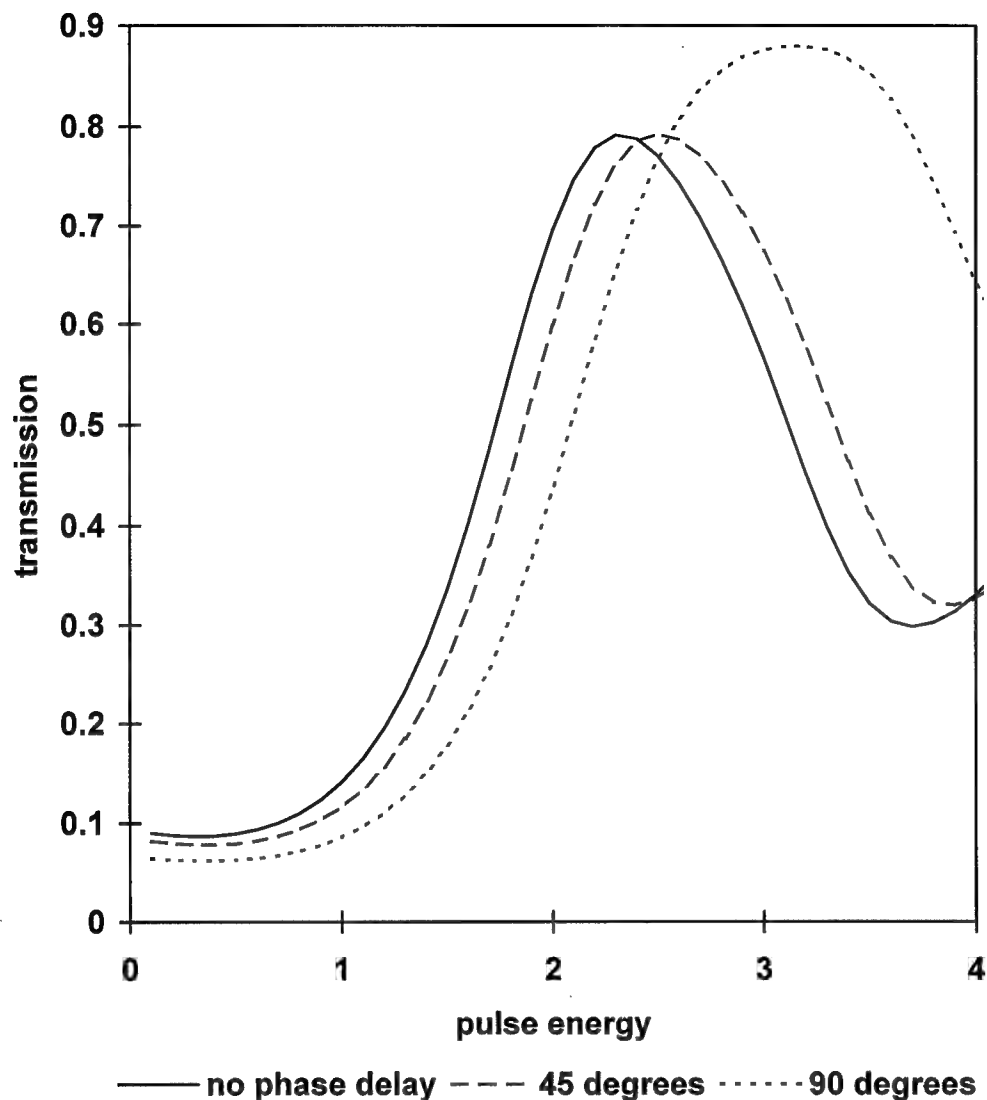
Figure 5.26 NOLM pulse transmission for an input pulse and polarization controller at a π/8 angle from the slow axis of the fiber. The plane of the loop is tilted by -π/8 from this and the birefringence of the fiber was δ=0.1. The loop is four soliton periods long.

Figure eight lasers are mode-locked using nonlinear optical loop mirrors. These fiber components have also been used for a number of other applications as discussed in the beginning of this chapter. The operation of the NOLM was simulated and compared

to previously published computational results to verify the models validity. A novel model was developed to predict the input pulse energy, and the maximum amount of the input energy to be transmitted by the loop. I then extended these results by examining the effects of birefringence on the functioning of the loop. It was found that the transmission of low energy pulses could be increased by changing the relative phase delay between the two counter-propagating pulses in the loop. This effect could be explained quantitatively as long as the birefringence was not too large. The break down of the model was explained. In addition, a model was developed to predict peak pulse transmission energies, based on vector soliton propagation. The distortion of pulses by the NOLM and the effect of this on further transmissions through the loop was examined. These effects have an influence on the behavior of the figure eight laser. Hence a good foundation has been established for the simulation of this system.

Chapter Six : Figure Eight Fiber Lasers

The components described in previous sections can be combined to form a fiber laser. This chapter starts with a short review of previous work on fiber lasers. The theory of sideband formation is reviewed in greater detail. This is the most successful theory in this field and it has been used to help design other lasers. I then go on to simulate a fiber laser mode-locked by an NOLM switch. I show that I can reproduce in the simulation many of the phenomena observed experimentally. With insights gained by this task I have proposed the concept of a dispersion balance figure eight laser which overcomes some of the limitations of previous figure eight designs. I have extensively simulated a laser of this type and the concept appears to work well. I then compare the results of this work to the sideband formation theory described before.

Previous Work

A laser which uses the NOLM switch is shown in Figure 5.1. Such a laser was first built by Avramopoulos et al.[88] Another laser of the same type was recently reported by Wu.[89] A similar type of laser, based on the NALM switch, has also been built, and much more work has been done on these. The NALM lasers were first demonstrated by Duling[12,90,] and by Richardson et al.[91] Pulses as short as 100 fs have been produced in these systems.[92]

These lasers can have very erratic pulse repetition rates.[93] This is one of the most significant problems in making them practical. Others have found that the NALM laser has several distinct repetition rate regimes which change as pump power is increased. At first, the laser will support one pulse in the loop which means that the output repetition rate of the laser will be the round trip time. If the pump power is increased, one observes a chaotic pulse output rate. This is characteristic of harmonically mode-locked lasers.[94]

If the pump power is increased even more, bursts of chaotically spaced pulses are observed. It will be shown that I can explain all three operating regimes.

A number of means have been used to stabilize the repetition rate. A fiber sub-ring can be introduced into the cavity.[95,96] The sub-ring acts like a Fabry-Perot etalon to stabilize the modes of the laser. This is similar to the means used to stabilize actively mode-locked fiber lasers.[97] It has also been found that introducing a small amount of extracavity feedback can help to stabilize a figure eight laser.[98] Fiber lasers in a ring geometry have been stabilized with phase modulation.[99] A ring laser was stabilized by adjustments made to polarization controllers in the loop.[100] The author attributed this stabilization to a long range repulsive interaction between the solitons.
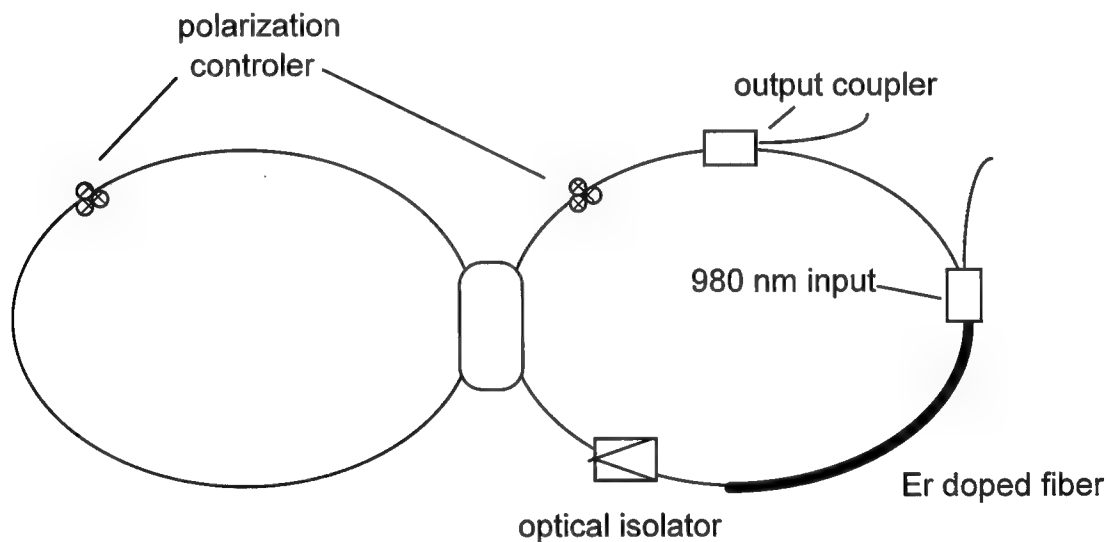
Figure 6.1 NOLM Figure Eight Laser

In addition to mode-locking with loop mirrors, passive mode locking in fiber lasers has been demonstrated by means polarization rotation filtering. This has been shown in a Fabry-Perot geometry.[13,101] Polarization rotation for mode-locking has been extensively studied in a ring geometry and has been used to develop a type of laser known

as the stretched pulse ring laser.[14] Nonlinear switching has been demonstrated in dual-core optical fibers.[10] This has been proposed as a means of mode-locking a laser as well.[15]

The model developed here involves the simulation of the laser by modeling the propagation of a pulse through optical fiber. Little work has been done to simulate figure eight lasers in this way. Bulushev et al.[102] simulated a figure eight laser mode-locked by an NOLM loop. They modeled pulse propagation in the loop but not in the amplifier, which they treated as a lumped gain. It will be shown that pulse shaping in the amplifier is quite important. They also assumed an unrealistically high value of saturation energy. This allowed them to demonstrate self-starting. Specifically, they assumed an amplifier of the form

$$A_{in}^{n+1} = \frac{\Delta N \sigma(\omega)}{1 + \varepsilon \int_{-\infty}^{\infty} |A_{out}(\omega)|^2 \, d\omega},$$

where their variable ε corresponds to the saturation energy. They used a value of 1.8. As was shown in chapter 4, even when using a 300 fs pulse as the basis of the normalized units, the saturation energy should be about 10^{-6}. Hence their results are invalid.

Some numerical results were reported by Stentz and Boyd.[103] They did not describe their model except to say that it involved birefringent pulse propagation. They assumed that the birefringent axes of the fiber rotated at random intervals in the fiber. They demonstrated that this eliminated the effect of nonlinear polarization rotation in the fiber.

The NALM laser was modeled by Tzelpis et al.[104] They included the effect of propagation in the amplifier, however, they also used a very high value of saturation energy. This renders their results suspect as well.

A model was described by Chen et al.[105] which used pulse propagation through a stretch of birefringent fiber to show the effect of pulse rotation in an actively mode-locked laser. They use a lumped amplifier model along with a lumped saturable absorber. They incorporated a Fabry-Perot etalon in order to stabilize the pulse repetition rate. They were able to foresee the need to incorporate active mode-locking into this laser in spite of the saturable absorption used.

Theoretical and experimental results have been reported by Richardson et al.[106] They studied the result of amplifying pulses after they have been emitted by the laser. They demonstrated that when the total gain of the amplifier is increased, one can obtain short pulses due to pulse compression in the amplifier.

An alternative method is to study the laser by means of an NLSE with cyclical perturbations.[107,108,109,110,111,112] These papers show how the periodic amplification of the pulse can generate spectral sidebands and study the role of dispersion in breaking up pulses. The spectral side bands are built up by constructive interference between the soliton-like pulse in the laser and the cw background. The background is built up by the process of dispersive wave shedding. When the pulse is perturbed from being a soliton if the perturbation is small, the pulse will be reshaped back into a soliton. The process will result in some light being shed by the pulse as cw background. The amount of light shed will be proportional to the size of the perturbation.

The location of the sidebands can be located analytically for ring lasers. This analysis will be adapted to figure eight lasers, so it is included here. The frequencies at which the dispersive wave radiation interferes constructively with the soliton must be found. The phase shift of the dispersive wave radiation will be $\beta(\omega)L$ where L is the length of the ring. The soliton phase shift is $\xi_l/2$ as discussed above. The variable ξ_l is the length of the cavity in dispersion lengths. The soliton envelope function only contains the slowly varying information, which is dominated by the second order term of the expansion of the dispersion. I must add other components which have been left out. The

actual soliton field phase will contain the factor of exp[-i$\beta(\omega_0)$L]. If this is expanded to first order, the phase difference becomes

$$\Delta\phi(\omega + \delta\omega) = \left[\beta_0 + \beta_1(\delta\omega) + \frac{1}{2L_D} - \beta(\omega + \delta\omega)\right]L,$$ (6.1)

where $\delta\omega = \omega - \omega_0$ and L_D is the dispersion length. For constructive interference we must have

$$\Delta\phi = 2m\pi,$$ (6.2)

where m is some integer. If the term $\beta(\omega + \delta\omega)$ is expanded as a Taylor series and inserted in the last equation, we obtain

$$\left[\frac{1}{2L_D} - \frac{\beta_2(\delta\omega)^2}{2}\right]L = 2m\pi.$$ (6.3)

Solving for $\delta\omega$, the result is

$$\sqrt{\frac{1}{L_D\beta_2}\left[\frac{4m\pi L_D}{L} - 1\right]} = \delta\omega.$$ (6.4)

The soliton pulse width is $T_0^2 = L_d\beta_2$, so the last equation can be expressed as

$$\left(\frac{4m\pi L_D}{L} - 1\right)^{\frac{1}{2}} = \delta\Omega, \tag{6.5}$$

where $\delta\Omega$ is in normalized units.

The analysis done by others has shown that, in general, stable operation with a fiber laser can not be achieved if

$$L \leq 4\pi L_D \tag{6.6}$$

This is equivalent to saying that the spacing of the sidebands can not be allowed to be reduced to zero, from Equation 6.5. That is, the phase change for the soliton must be less than 2π. I have found that this seems to hold for situations in which perturbations are producing a moderate amount of dispersive wave radiation, however, if the perturbations are reduced, the limit can be eliminated.

A model known as additive pulse mode locking has been the basis of a great deal of research. Figure eight lasers are an example of additive pulse mode locking (APM) and have been analyzed in this fashion.[113] The vast majority of work involving additive pulse mode-locking has addressed ring lasers. APM theory involves constructing a master equation of the laser and finding solutions to it. The master equation is constructed by assuming that the pulse is subject to only small perturbations as it goes through the loop. This is not the case for figure eight lasers since the pulse in the amplifier will have approximately twice the amplitude of the pulse in the loop mirror. A vast amount of work has recently been done involving this method, largely by Haus and his co-workers. This includes work on conditions necessary for self-starting[114] and the effect of third-order dispersion on pulses in a ring laser.[115] This method has been used to develop a type of laser known as the stretched pulse ring laser.[14] This method addressees the observation that the loop length must be kept less than eight soliton periods. This was done by inserting positive dispersion fiber into the loop. The pulse in this fiber will spread out and its phase shift per unit length will fall. When the pulse reenters the

negative dispersion fiber it will be compressed again. These two effects were balanced out so that the pulse is undistorted in one round trip. Recently the additive pulse mode-locking formalism has been extended into regimes where the pulse undergoes larger distortions.[116] Similar work has been done to analyze mode-locking of a Ti:sapphire laser.[117] Other research groups have examined conditions under which stable pulses could be formed in ring lasers.[118,119]

The side-band theory has been used to study figure eight lasers. Dennis and Duling have made extensive investigations into this experimentally.[120] They found that by reducing the product dispersion and the cavity length, they could reduce the width of the shortest pulse that could be formed in their laser in the same fashion as in the ring laser. They found that the minimum pulse formed, τ_{min}, could be found by

$$\tau_{min} \approx \sqrt{L\bar{\beta}_2} \, ,$$

where L is the length of the total cavity and $\bar{\beta}_2$ is the average dispersion of the cavity. The form of this relationship can be deduced if one inserts the expression of the dispersion length into equation 6.6. This yields

$$T_0 = \sqrt{\frac{L\bar{\beta}_2}{4\pi}} \quad .$$

This theory concludes that the shortest pulse producable by a laser is limited by the laser length and by its average dispersion.

Sideband generation is of concern in telecommunications as well. The effect occurs when solitons are maintained by a large number of optical amplifiers. It has been shown that sideband generation is reduced by introducing NOLMs along with the amplifiers to eliminate the dispersive wave radiation.[121] This implies that dispersive wave radiation should have only a reduced role in the lasers that will be studied here.

It has also been shown that third-order dispersion limits the length of pulses in figure eight lasers.[122] Pulses could be shortened considerably by compensating for this effect.

Simulation Results: Figure Eight Laser

I simulated the behavior of an NOLM mode-locked figure eight laser extensively. The goal was to analyze the steady-state behavior of the laser. This was done by inserting a seed pulse into the laser shown in Figure 6.1. The seed chosen was a hyperbolic secant shaped pulse which provided maximum transmutation in the results given in the last chapter. It was assumed that this would be a good approximation of the steady-state pulse shape. The function of the NOLM was simulated in the fashion described in Chapter 5. The pulse was then amplified as in Chapter 4. The amplifier was assumed to have uniform gain along its length and that it fully recharged between passes of the pulse. The effect of the output coupler was simulated as a linear loss. For instance, for a 10% output coupler, the intensity of the light at all points was multiplied by 0.9. The resulting pulse was then reintroduced into the NOLM and the cycle was continued. The pulses were examined at the end of the cycle, that is after the output coupler. It was found that after fewer than 10 cycles the pulses had assumed their final shape in time and frequency space. This was determined by propagating a sample case for 10, 20 and 30 cycles and comparing the results. In general, the pulses were assumed to have reached equilibrium if the total integrated energy in the simulation was stable to within less than 5% for successive cycles.

To start the investigation of the NOLM laser, the nonbirefringent case was examined. The loop length was assumed to be four soliton periods and the directional coupler had a 60/40 splitting ratio. A 10% output coupler was used and the amplifier was assumed to recharge completely between passes of the pulse. The effect of the

polarization controller was ignored. The first fact that appears is that one cannot use simply any length for the amplifier. The results in Figure 6.2, show the maximum and minimum gain for which stable pulses can be produced. In this case gain is defined as the ratio of the power out to the power in. It is given by $e^{-\gamma L}$ where L is the length of the amplifier and γ is the gain parameter. To demonstrate this pulses corresponding to those for the maximum transmission through the NOLM were introduced into the laser and allowed to pass through its loop ten times. If the gain was insufficient the pulses would decay away exponentially. The explanation for this behavior is simply that the loss per pass through the loop is greater than the gain. When the gain grew to be too great a more unexpected result occurred. The pulse energy would first oscillate and only decay away at a later time. An explanation for this behavior can be derived from examining an NOLM transmission curve such as Figure 5.2. If the amplification of the pulse is too great, the pulse energy will be such that the pulse will experience a great deal of loss in the NOLM in subsequent passes and ultimately be extinguished. Under these conditions the pulse energy after each pass through the system would oscillate several times but finally decay away. The amount of tolerable excessive gain parameter appears to be about 0.1 in this case. This corresponds to an excess gain of about 10%. It should be noted that behavior like this is observed in lasers experimentally. As noted before, it has been found that figure eight lasers transition through several stability regimes. As pumping is increased, they transition from having one pulse in the loop to having several. The observation here of a maximum stable gain make sense in this context. When the amplification becomes too great, the existence of this maximum will force the laser to produce two small pulses rather than one pulse with greater energy. Saturation due to the second pulse will eliminate the excess amplification. When the amplification is even greater, the pulse can breakup into many pulses, as shown in the chapter on amplifiers. This would produce the chaotic bursts of pulses which are observed.

For short amplifiers, the gain parameter needed corresponds to an amplification of about 10%. This means that for these short amplifiers, only enough gain is needed to

compensate for losses from the output coupler. For longer amplifiers, there is a loss which is dependent on the amplifier length. Behavior of this sort has been noted by a number of groups in studying lasers in a ring geometry. In that case, it is thought to be caused by the repetitive amplification of dispersive wave radiation.[123] The exact role of this phenomenon in the NOLM is problematic, as noted above.[121] Dispersive wave radiation would appear as a weak pedestal about the pulse. In the case of the NOLM laser, however, this should be eliminated by the switch. Gordon[123] also found that loss increased very rapidly as the loop length approached 8 soliton periods. My investigations show that stable operation was impossible if the amplifier was longer than about 0.83 dispersion lengths.

The shape of the pulse in the laser is of interest in itself and it also sheds light on the phenomena described in the last paragraph. Figures 6.3 and 6.4 show how the shape of the pulse is altered as the length of the amplifier is increased. In this simulation, the pulse first passes through the NOLM, is amplified, and then is reduced by 10% due to the output coupler. These pulses were the result of 10 passes through the laser. The pulse in the Figures 6.3 and 6.4 is in the state it has just before reentering the NOLM. The pulses in both figures show some pedestal corresponding to some dispersive wave radiation. The pulse produced when the amplifier is 0.1 dispersion length is much closer to being in the the form

$$P_0 \sec h^2(\tau).$$

which will be referred to as a hyperbolic secant shaped pulse. The pulse for a 0.8 dispersion length amplifier much more closely resembles a soliton. In this form the argument of the hyperbolic secant has the form (τ/T_0) where P_0 and T_0 have the standard fixed relationship. As we saw in the last section, the output pulse is almost the right shape for optimal transmission by the NOLM, if it were immediately fed back into it. The transmission is very sensitive to pulse shape. Hence, any pulse shaping by the

amplifier fiber will tend to create loss. A longer amplifier will obviously create more loss and this will create the length dependent loss we observe.
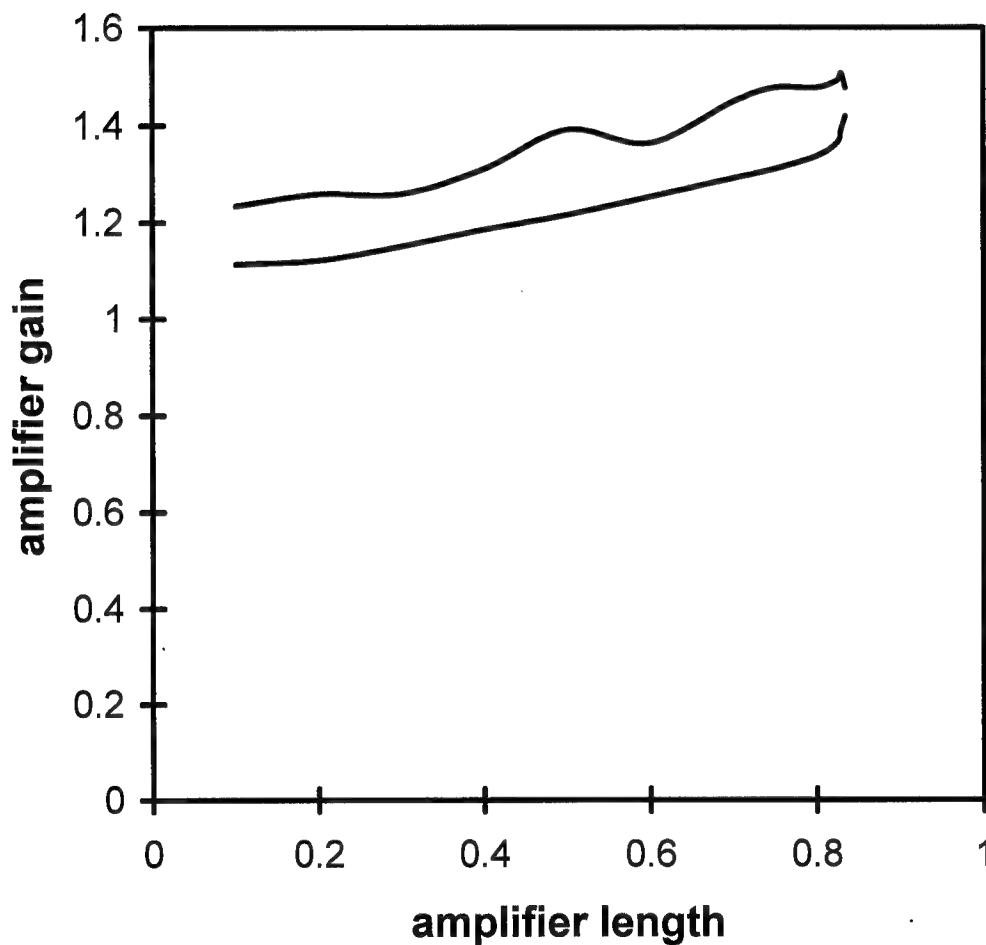
Figure 6.2 Stable pulse formation could take place between the curves in a nonbirefringent NOLM laser with a 60/40 beamsplitter, and a 4 soliton period long loop mirror. The output coupling is 10%. Amplifier length is given in dispersion lengths.
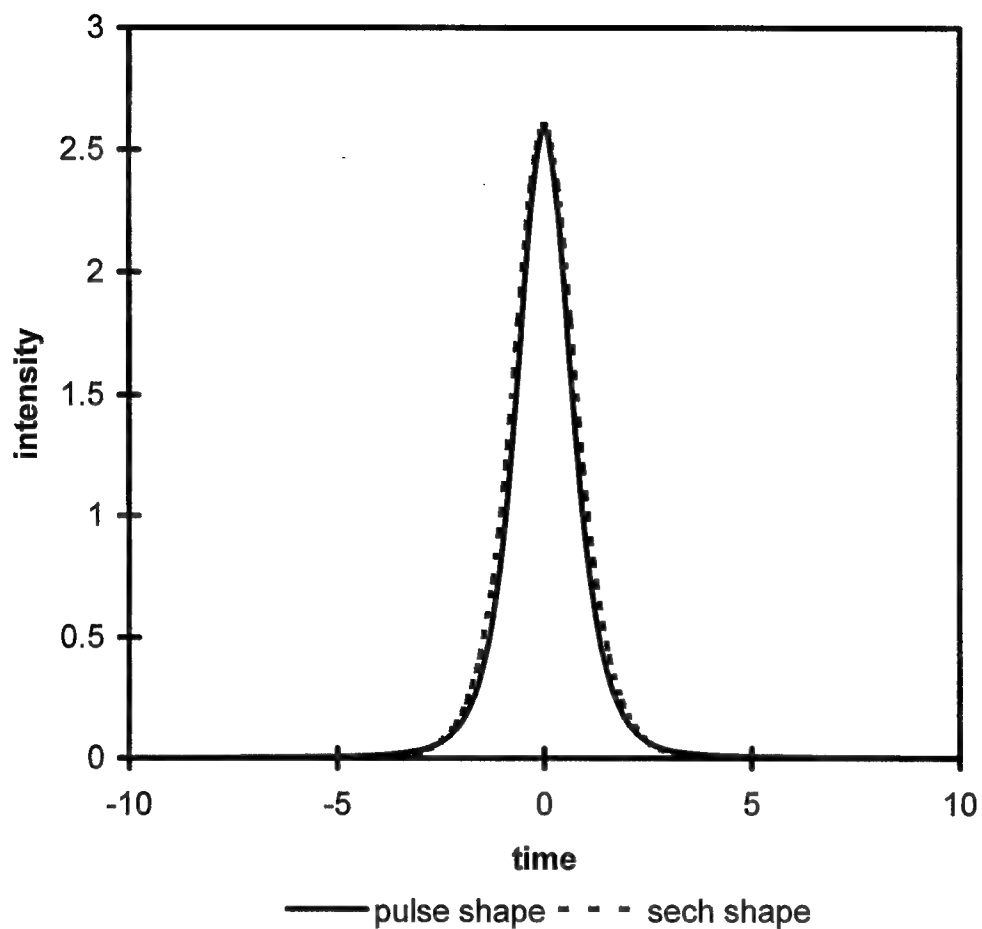
Figure 6.3 Pulse shape in a nonbirefringent NOLM laser with a 60/40 beamsplitter, and a 4 soliton period long loop mirror. The output coupling is 10%. The amplifier is 0.1 dispersion lengths long. The power of the pulse is shown as a function of time. Both are in soliton units.
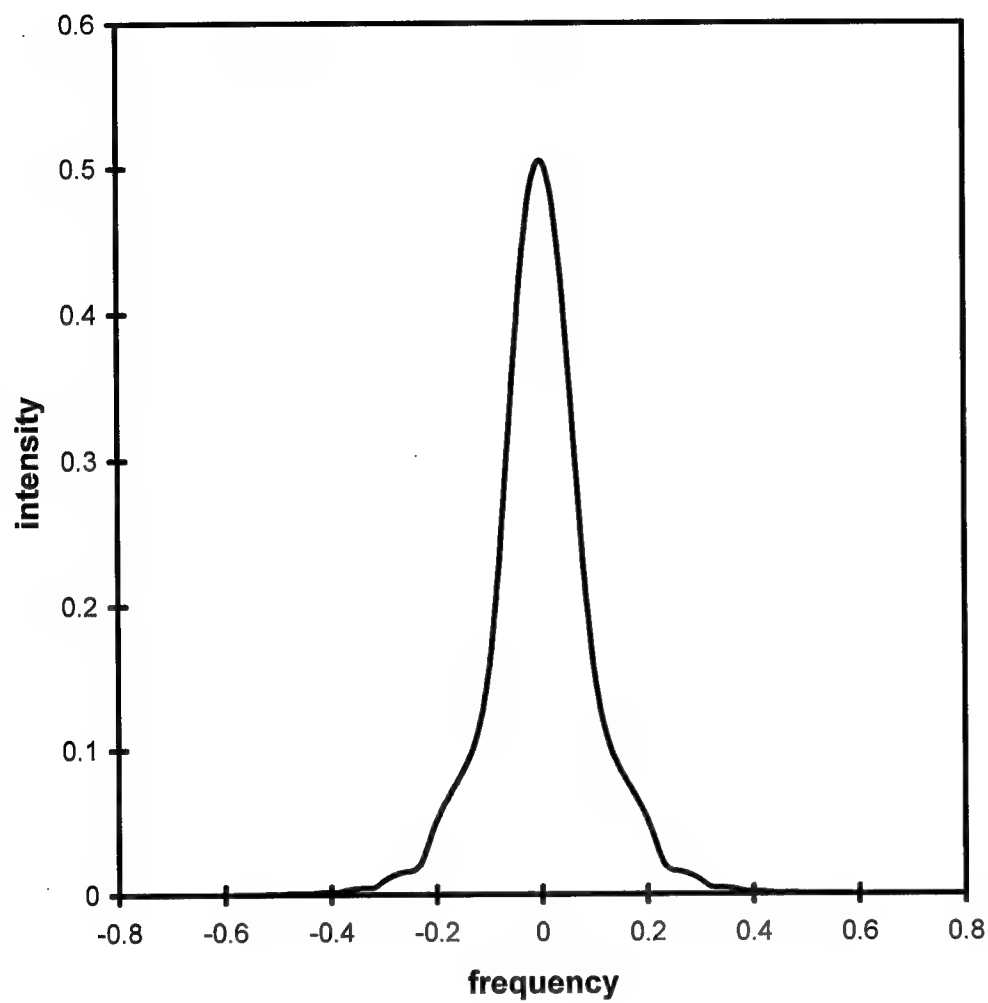
Figure 6.4 Pulse shape in a nonbirefringent NOLM laser with a 60/40 beamsplitter, and a 4 soliton period long loop mirror. The output coupling is 10%. The amplifier is 0.1 dispersion lengths long. The power of the pulse is shown as a function of frequency. Both are in soliton units.
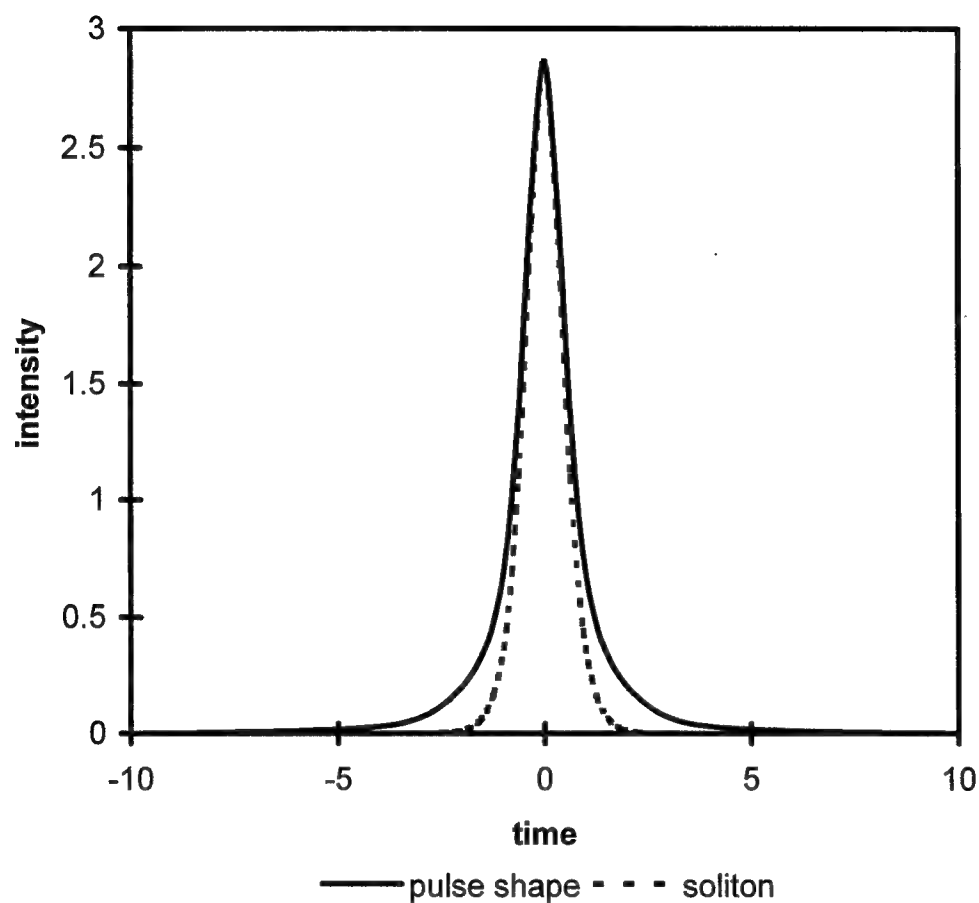
Figure 6.5 Pulse shape in a nonbirefringent NOLM laser with a 60/40 beamsplitter, and a 4 soliton period long loop mirror. The output coupling is 10%. The amplifier is 0.8 dispersion lengths long. The power of the pulse is shown as a function of time. Both are in soliton units.
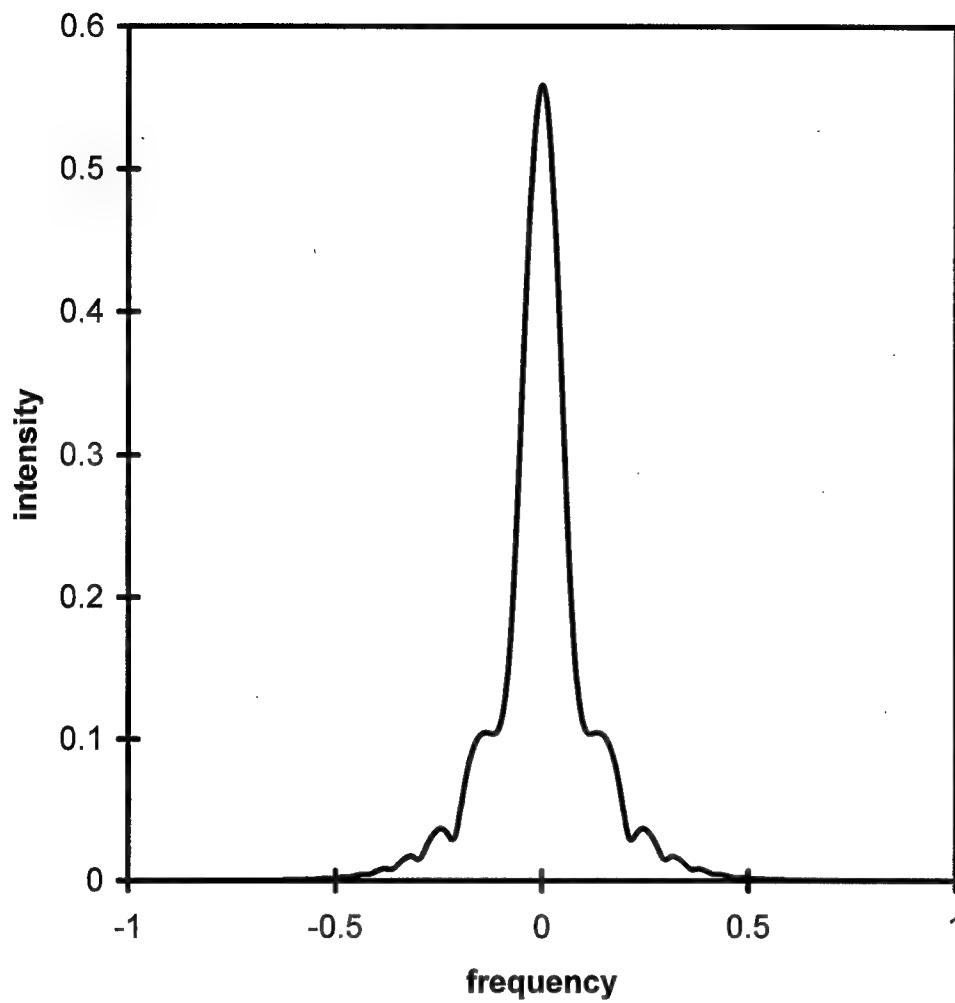
Figure 6.6 Pulse shape in a nonbirefringent NOLM laser with a 60/40 beamsplitter, and a 4 soliton period long loop mirror. The output coupling is 10%. The amplifier is 0.8 dispersion lengths long. The power of the pulse is shown as a function of frequency. Both are in soliton units.

Simulation Results: Dispersion Balanced Figure Eight Laser

The analysis given above suggests that to improve laser operation, one should

design a laser in which this pulse distortion is minimized. One possible means of doing

this is by using a different value of β_2 in the amplifier and in the loop mirror. The value of dispersion should be chosen so that the output pulse from the NOLM is a fundamental soliton in the amplifier fiber. According to Equation 2.6, the parameters controlling the relation between the width of a fundamental soliton and its height are

$$1 = \frac{\gamma\, P_0\, T_0^{\,2}}{|\beta_2|}.$$

(6.7)

The parameter γ is not in general, easily changed. It is dependent on the nonlinear properties of the fiber and on its effective core area. The first is a basic material property of silica and the second tends to be driven by the necessities of good amplifier design. Dispersion, however, can be controlled and dispersion shifted fiber is available. It is therefore plausible to consider changing this parameter. In the case of a four soliton period long loop, the pulse width is not altered by transmission through the NOLM. This means that we want T_0 to be unaltered by propagation in the amplifier fiber. The output pulse has in the case we are examining a peak intensity 2.2 times that of a unit fundamental soliton. Since γ and T_0 are held constant, the only way for Equation 6.7 to be true in the amplifier is if the dispersion is multiplied by a factor of about 2.2.

In order to examine this possible solution, Equation 2.36, the normalized nonlinear Schrodinger equation must be changed. The starting point for this is Equation 2.35, the unnormalized NLSE. This has the form, if we ignore higher order terms

$$\frac{\partial A}{\partial z} + \frac{\alpha}{2} A + \frac{i}{2}\beta_2 \frac{\partial^2 A}{\partial T^2} - \frac{1}{6}\beta_3 \frac{\partial^3 A}{\partial T^3} = \ i\gamma\left[|A|^2 A\right].$$

(6.8)

If the dispersion term is multiplied by a factor K and the equation is normalized as in section 2, the resulting equation is

$$i\frac{\partial U}{\partial \xi} + \frac{K}{2}\frac{\partial^2 U}{\partial \tau^2} - i\delta \frac{\partial^3 U}{\partial \tau^3} = -N^2\left[|U|^2 U\right].$$

(6.9)

In the case we are examining, this means that the linear propagation parameters will be multiplied by the factor K.

If propagation in the fiber amplifier is modified in this way, the result is quite striking. The stable gain region is shown in Figure 6.5. This simulation did not exhibit a maximum amplifier length as in Figure 6.1. This occurred even when the simulation was taken out to about 30 times the amplifier length examined in the noncompensated case. In addition this curve does not exhibit length dependent loss to any great extent.
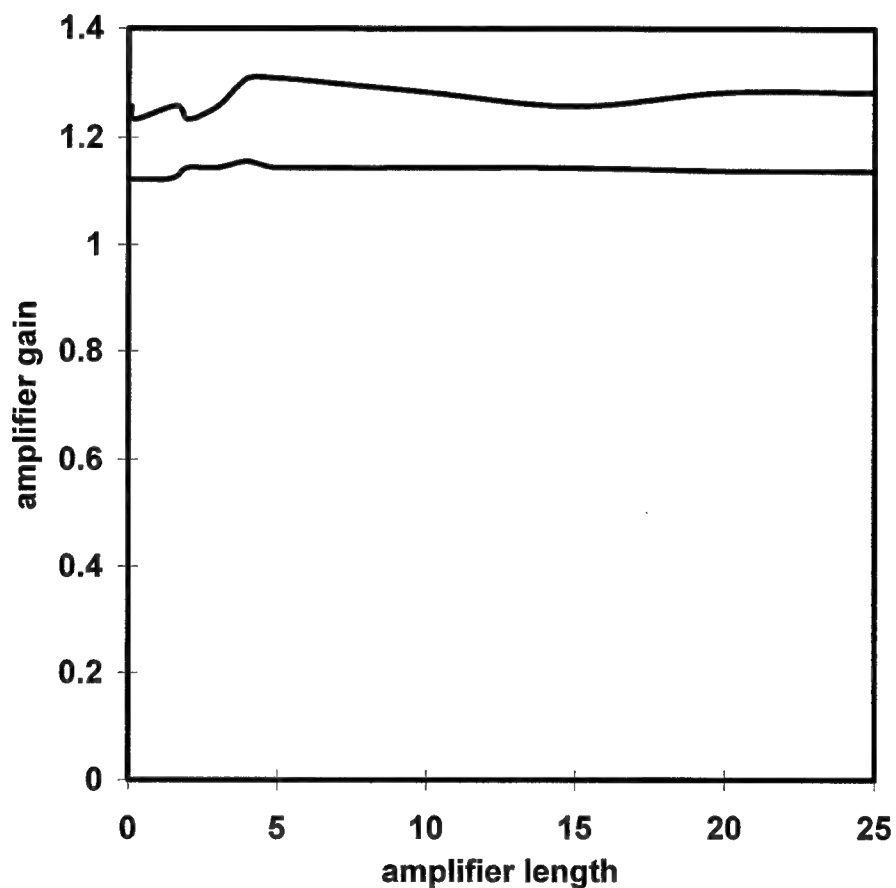
Figure 6.7 Stable pulse formation could take place between the curves in a nonbirefringent dispersion balanced NOLM laser with a 60/40 beamsplitter, and a 4 soliton period long loop mirror. The output coupling is 10%. The dispersion in the amplifier is 2.2 times that in the loop. Amplifier length is given in dispersion lengths.

The shape of the pulse is shown in Figure 6.8 and 6.9. The pulse shape in time space has the correct soliton shape. This is to be expected since the amplification is extremely gradual and the pulse can easily be shaped into a soliton by the fiber. The pulse displays very little chirp. The pulse in frequency space is totally dominated by the sidebands. The location of the sidebands is summarized in Figure 6.10. The dependent variable is Ψ which is defined to by

$$\Psi = \left(\frac{\delta\Omega}{2\pi}\right)^2.$$

(6.10)

From Equation 6.5, we see that the sideband theory predicts that

$$\Psi = \frac{1}{4\pi^2}\left(\frac{4m\pi L_D}{L} - 1\right),$$

(6.11)

where m is the order of the side band. The variable Ψ increases linearly with the order, and Figure 6.10 shows this relationship. The slopes of the lines can be used to compute an effective length of the cavity, L_{eff}, as the amplifier length is varied. This computation is made easier if the sidebands are compared to the location of the first sideband. If m is the order of the first sideband and n is the order of the one to which it is being compared, one obtains

$$\Psi_n - \Psi_m = \frac{1}{4\pi^2}\frac{4m\pi L_D}{L_{eff}}(n - m).$$

(6.12)

By examining how Ψ changes as the difference in order changes, we may obtain an effective cavity length in dispersion lengths. We see in figure 6.10 how the slope of the line changes as the length of the amplifier changes. The effective length is the length of the amplifier that would produce the sideband spacing observered.

It is interesting to do linear regression analysis on the relationship between the effective length and the length of the amplifier. This will help us to relate the effective length of the loop to the actual length. The results of this analysis are displayed in Figure 6.11. If a linear regression is performed on the data, one obtains

$$L_{eff} = 2.70L_{amp} - 2.62,$$ (6.13)

where L_{amp} is the length of the amplifier in dispersion lengths for a soliton of unit amplitude. The relationship between the dispersion length and physical length is the key to understanding this relationship. From equation 2.36 we see that

$$P_0 \propto \frac{|\beta_2|}{T_0^2} = \frac{1}{L_D}.$$

This indicates that we can relate a change in the peak intensity of a soliton directly to a change in its dispersion length. The peak intensity of the pulse is 2.66 for all lengths of the amplifier. If the peak intensity after the output coupler was 2.66, the intensity before would have been 2.96. Before the output coupler this intensity would have been 2.96. This means that the dispersion length of a soliton of unit amplitude should have a dispersion length 2.96 times that of the pulse at the end of a circuit of the laser, so the pulse should have been acting as if the amplifier was about 2.96 times longer than indicated. This explains the slope in equation 6.13. The linear regression disagrees with this by 17%. The NOLM is 2π dispersion lengths long. This length agrees approximately with the effective length for short amplifiers. This is to be expected since for a short amplifier most of the length of the laser is in the NOLM, where the pulse has a peak intensity of about 1 in the units used here.
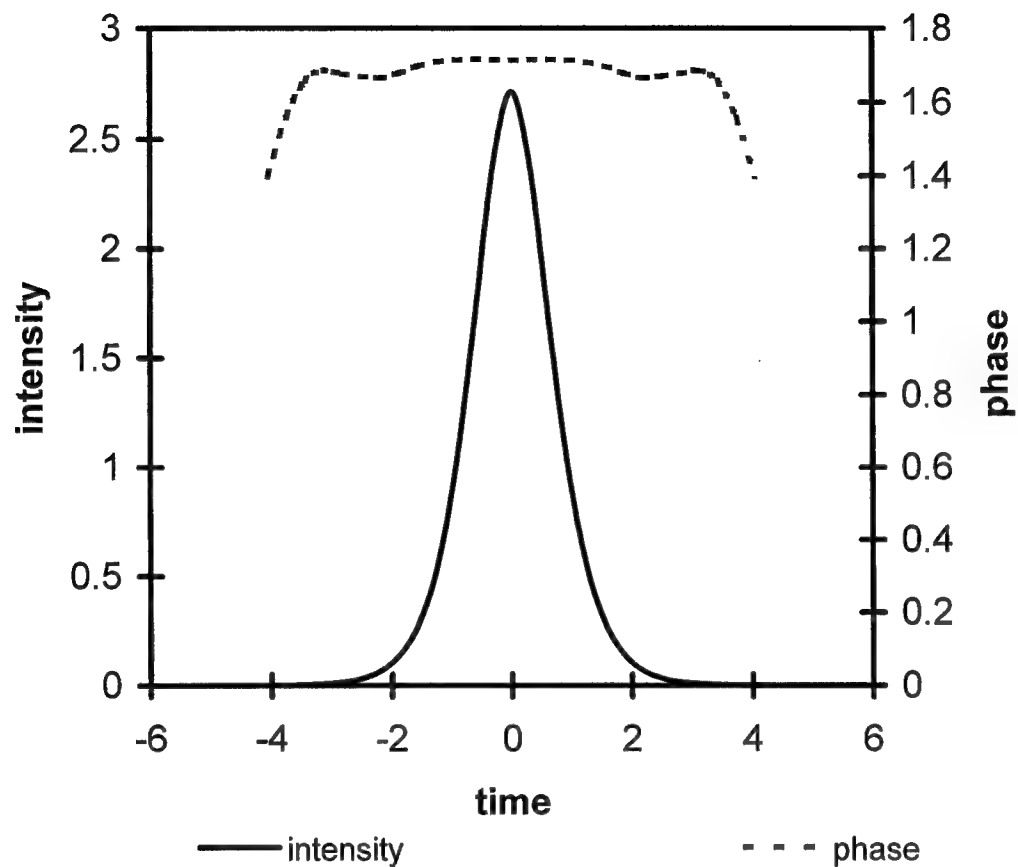
Figure 6.8 Pulse shape in a nonbirefringent dispersion balanced NOLM laser with a 60/40 beamsplitter, and a 4 soliton period long loop mirror. The output coupling is 10%. The dispersion in the amplifier is 2.2 times that in the loop. The pulse intensity is given as a function of time. Both are in soliton units.
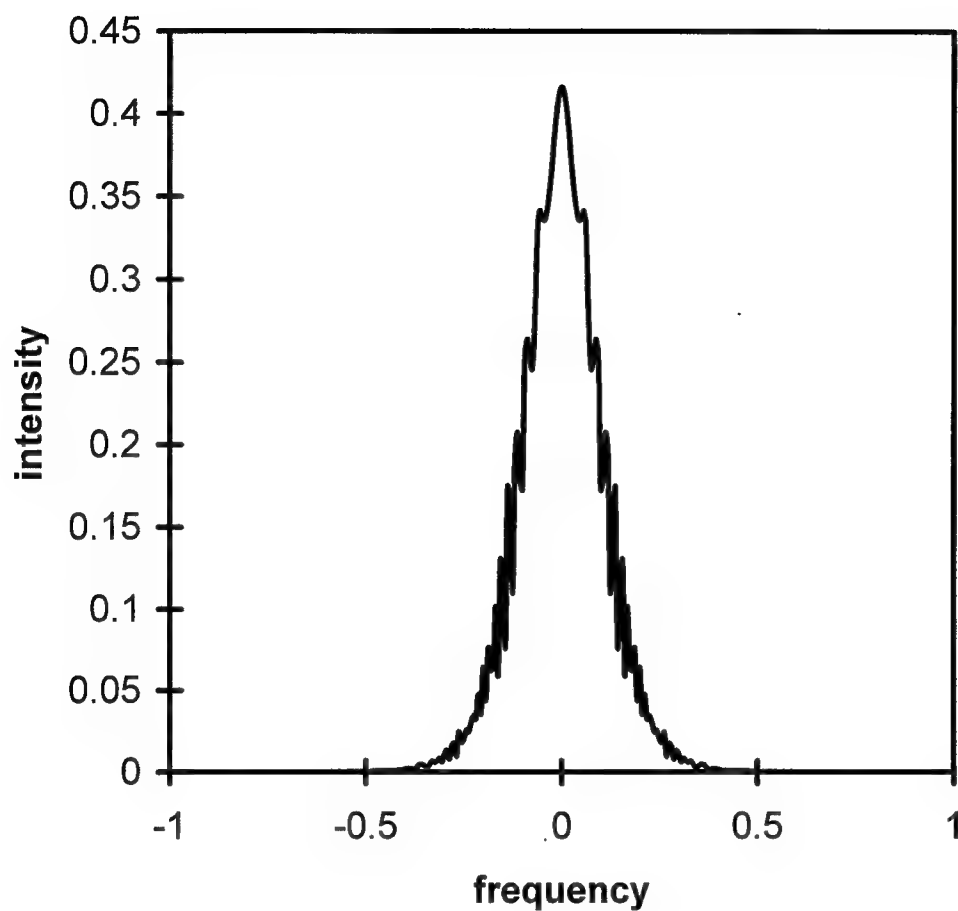
Figure 6.9 Pulse shape in a nonbirefringent dispersion balanced NOLM laser with a 60/40 beamsplitter, and a 4 soliton period long loop mirror. The output coupling is 10%. The dispersion in the amplifier is 2.2 times that in the loop. Pulse intensity is given as a function of frequency. Both are in soliton units.
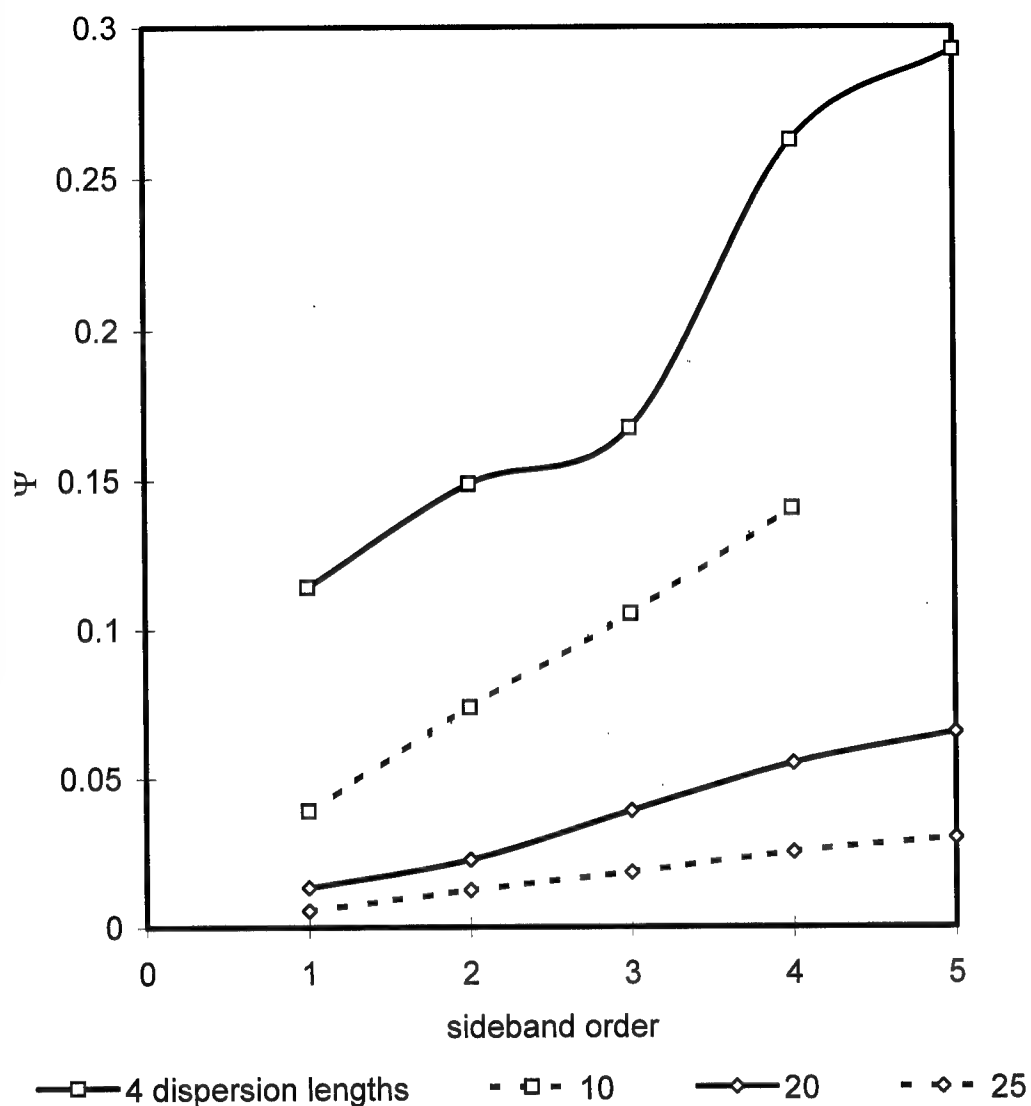
Figure 6.10 Sideband spacing in a nonbirefringent dispersion balanced NOLM laser with a 60/40 beamsplitter, and a 4 soliton period long loop mirror. The output coupling is 10%. The dispersion in the amplifier is 2.2 times that in the loop. The parameter Ψ is defined in Equation 6.10. The figure shows the effect of changing the length of the amplifier.

Figure 6.11 L_{eff} **as computed by means of Equation 6.12. The laser is a nonbirefringent dispersion balanced NOLM laser with a 60/40 beamsplitter, and a 4 soliton period long loop mirror. The output coupling is 10%. The dispersion in the amplifier is 2.2 times that in the loop**

The effect of changing the splitting ratio of the directional coupler in the NOLM was examined. The splitting ratio in the simulation was changed to 55/45. The loop was lengthened to 8 soliton periods. This meant that the input pulse energy for maximum transmission was unchanged. The two counter propagating pulses were approximately

unit solitons. The linear dispersion was 2.2 times greater in the amplifier than in the loop. The resulting stability curve is shown in Figure 6.12. The dispersion balancing scheme works for this case as well. The laser will form stable pulses for very long amplifiers.
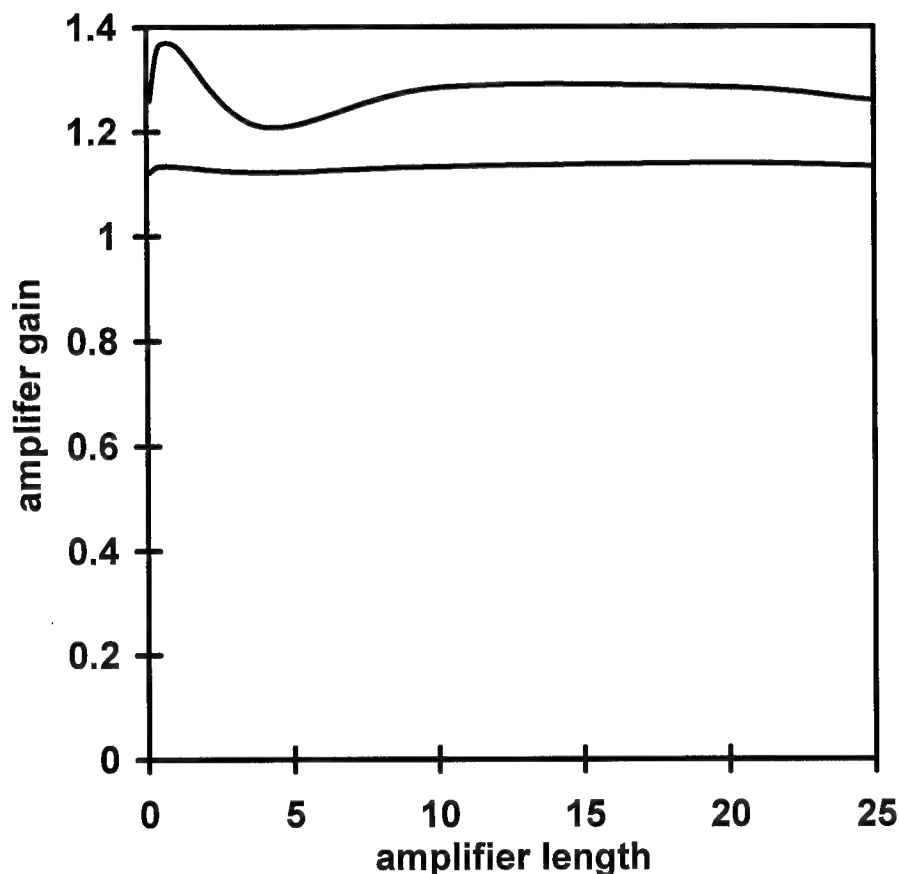
Figure 6.12 Stable pulse formation could take place between the curves in a nonbirefringent dispersion balanced NOLM laser with a 55/45 beamsplitter, and a 8 soliton period long loop mirror. The output coupling is 10%. The dispersion in the amplifier is 2.2 times that in the loop. Amplifier length is given in dispersion lengths.

The shape of the pulse for this laser is shown in Figure 6.13. This is for a 20 dispersion length amplifier with near minimum stable amplification. There is again very little chirp. It should be noted that side bands form in the case of the 55/45 directional

coupler in much the same way as they did for the 60/40 directional coupler. It appears that the sidebands are larger than those in the case of the laser with the 60/40 beamsplitter. This is of interest since the counterpropagating pulses in this case should have an initial form closer to that of a fundamental soliton. It would seem that pulse reshaping in the NOLM is not the major source of dispersive wave shedding of light from the pulses since the pulses were closer to being solitons in this case.

The location of the sidebands can also be analyzed as in the case of the 60/40 laser. The relationship between Ψ and the sideband order is shown in Figure 6.15 for lasers with various amplifier lengths. The relationship between the computed L_{eff} and the length of the amplifier is shown in figure 6.16. The resulting formula for the effective length, in dispersion lengths, for this laser is

$$L_{eff} = 2.29L_{amp} + 2.373 \qquad (6.14)$$

The peak intensity for this laser is 2.52. Before the 10% output coupler the peak would have been 2.80. As was argued before when describing equation 6.13, the slope should be around this value. In this case the difference between this figure and the slope is 17%. The NOLM is now 4π dispersion lengths long and this is about the effective length for a laser with a short amplifier.
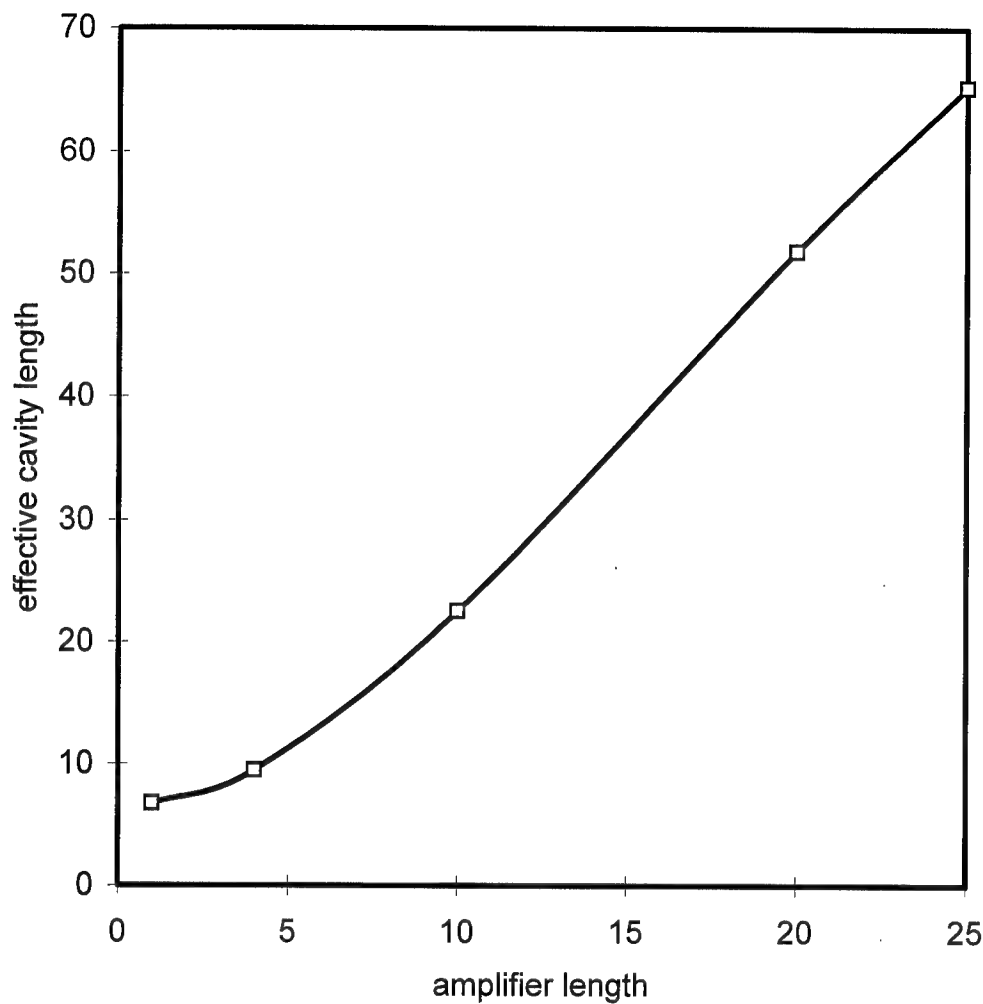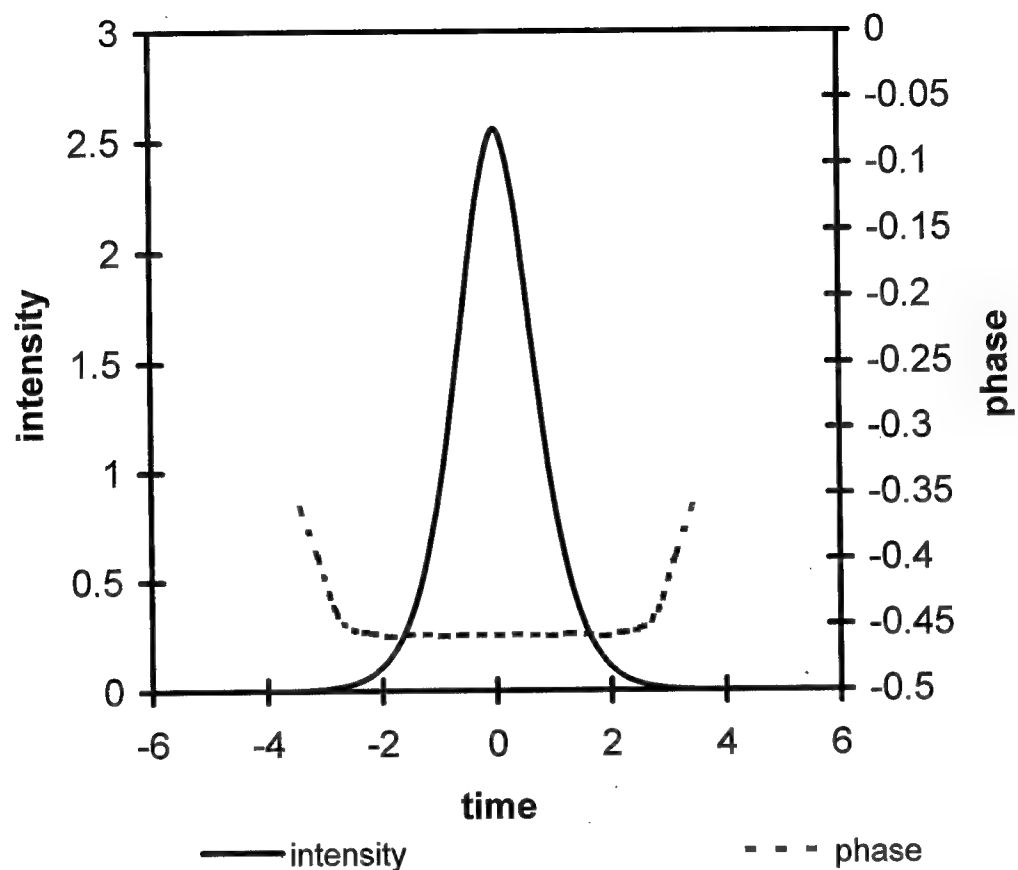
Figure 6.13 Pulse shape in a nonbirefringent dispersion balanced NOLM laser with
a 55/45 beamsplitter, and a 8 soliton period long loop mirror. The output coupling
is 10%. The dispersion in the amplifier is 2.2 times that in the loop. Pulse intensity
is given as a function of time. Both are in soliton units.
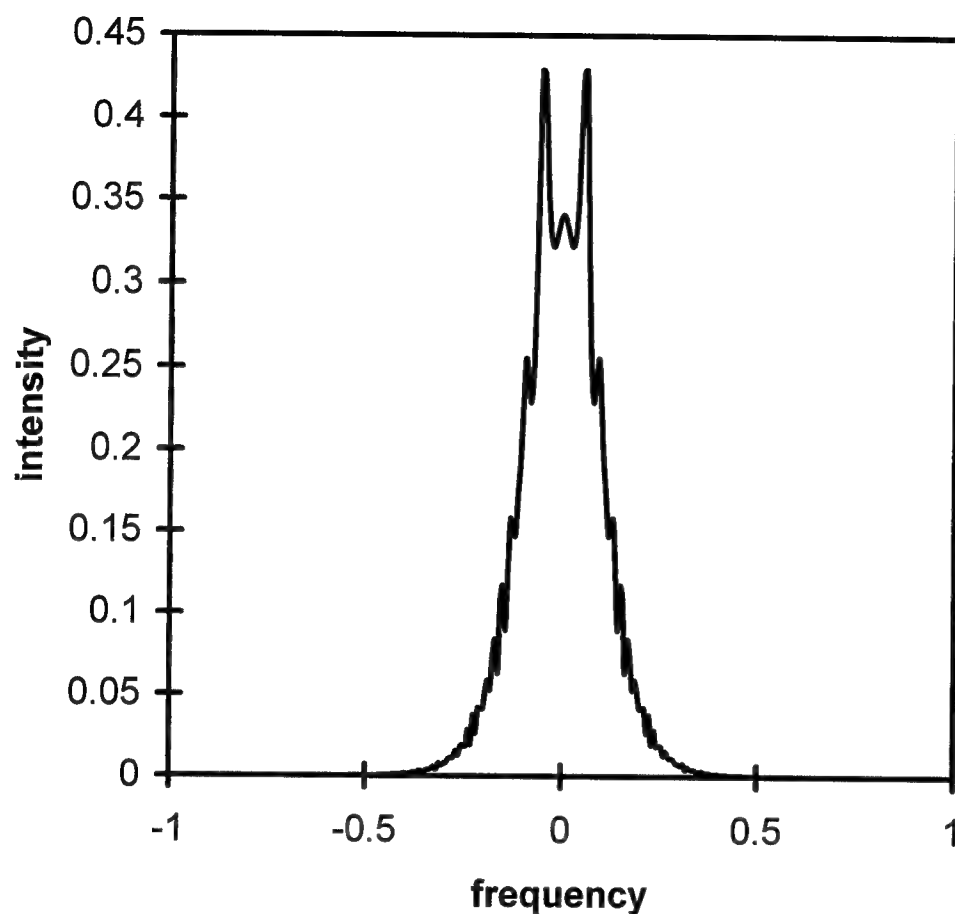
Figure 6.14 Pulse shape in a nonbirefringent dispersion balanced NOLM laser with a 55/45 beamsplitter, and a 8 soliton period long loop mirror. The output coupling is 10%. The dispersion in the amplifier is 2.2 times that in the loop. Pulse intensity is given as a function of frequency. Both are in soliton units.
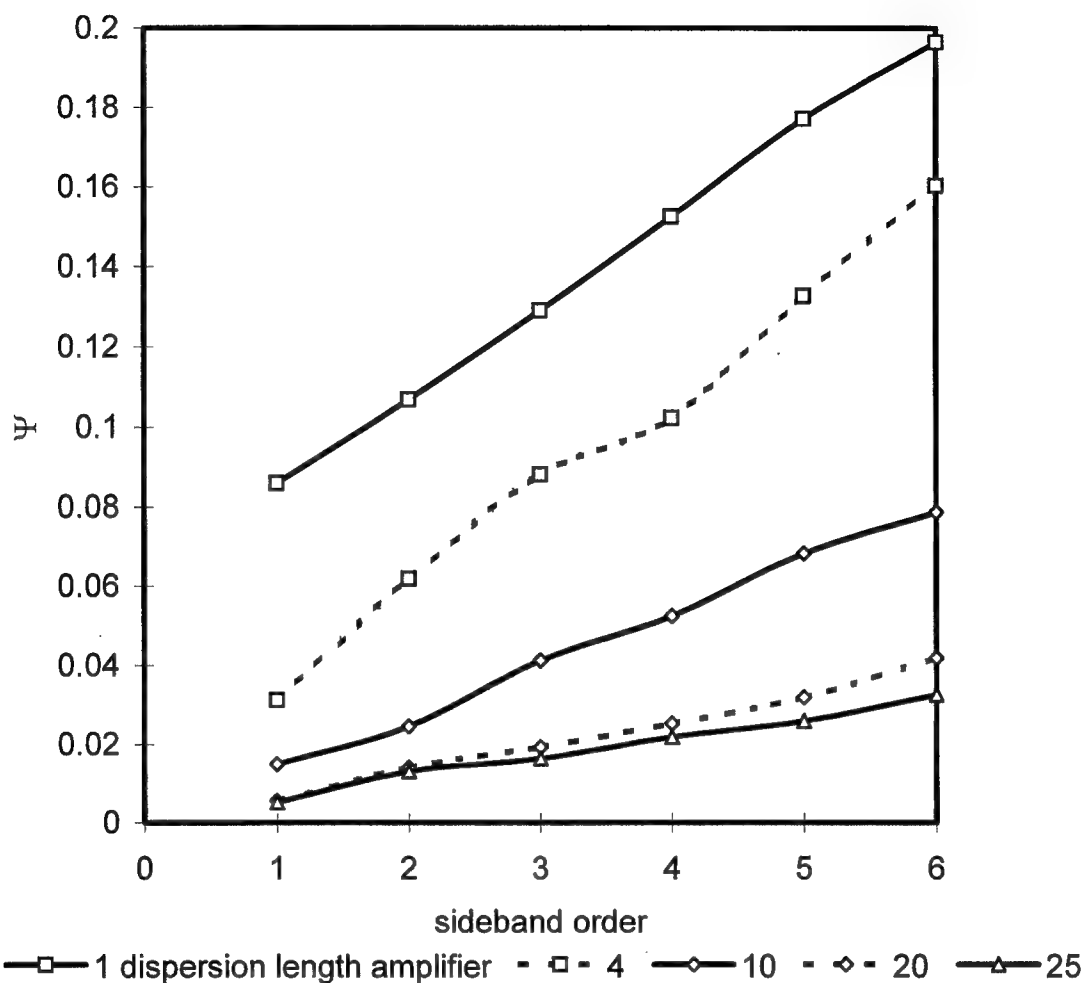
Figure 6.15 Sideband spacing in a nonbirefringent dispersion balanced NOLM laser with a 55/45 beamsplitter, and a 8 soliton period long loop mirror. The output coupling is 10%. The dispersion in the amplifier is 2.2 times that in the loop. The parameter Ψ is defined in Equation 6.10. The figure shows the effect of changing the amplifier length.
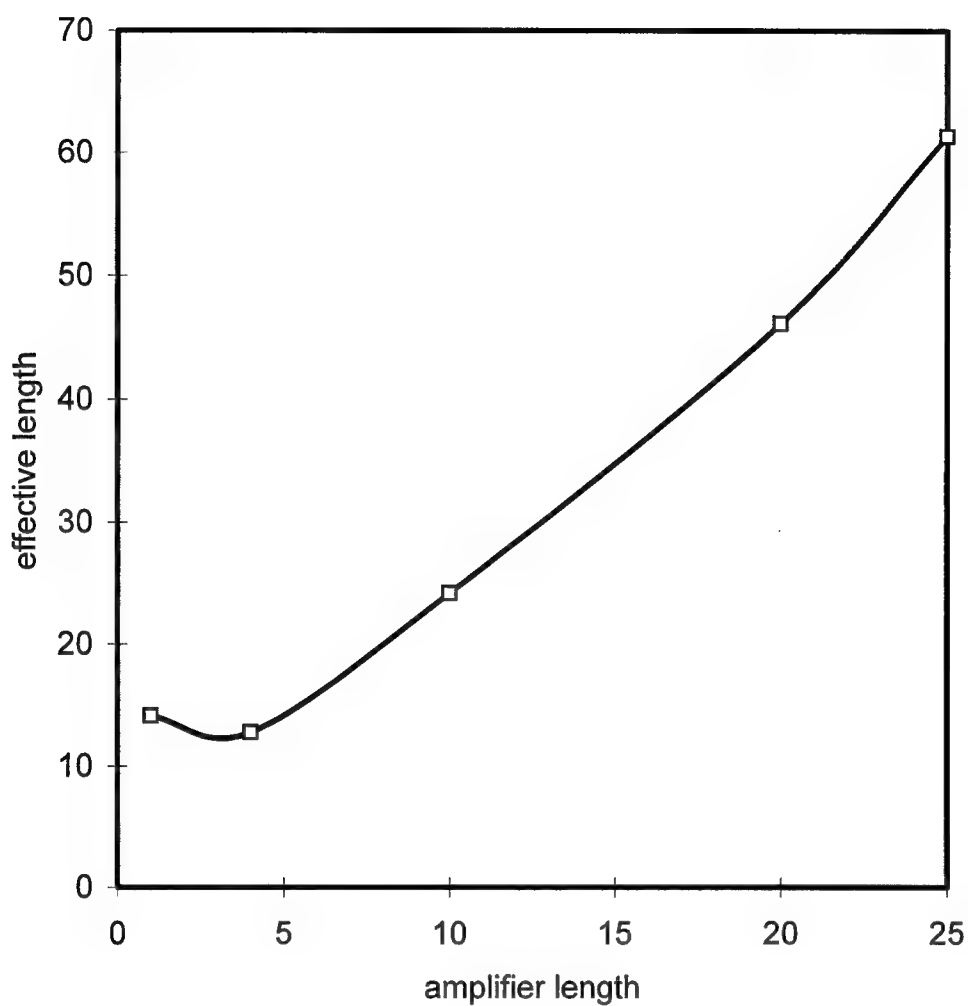
Figure 6.16 L_{eff} as computed by means of Equation 6.12. The laser is a nonbirefringent dispersion balanced NOLM laser with a 55/45 beamsplitter, and a 8 soliton period long loop mirror. The output coupling is 10%. The dispersion in the amplifier is 2.2 times that in the loop. All lengths are in dispersion lengths.
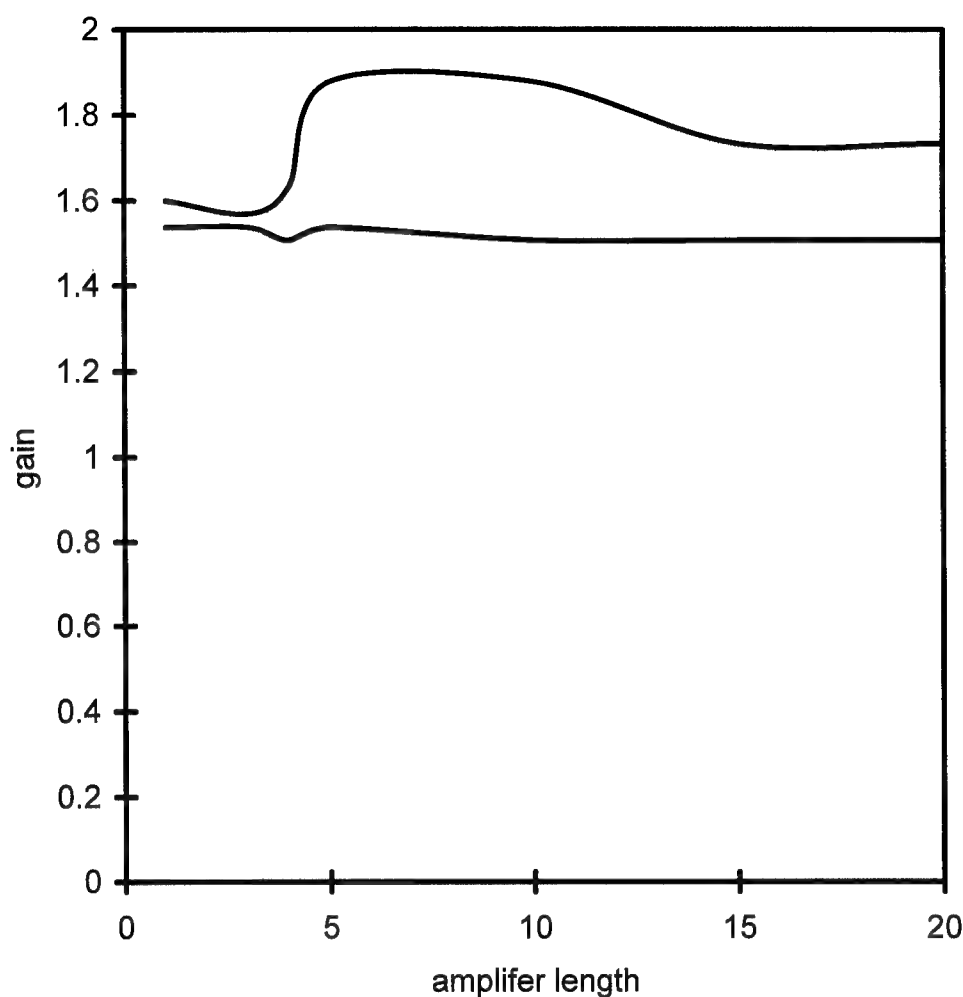
Figure 6.17 Stable pulse formation could take place between the curves in a nonbirefringent dispersion balanced NOLM laser with a 60/40 beamsplitter, and a 4 soliton period long loop mirror. The output coupling is 30%. The dispersion in the amplifier is 3.0 times that in the loop. Amplifier length is given in dispersion lengths.

The effect of increasing the output coupling was examined by changing the coupling to 30%. The central beamsplitter ratio was left at 60/40. The loop was 4 soliton periods long. Finding a value of birefringence for the amplifier that would work in this case proved to be challenging. The laser was first simulated with a dispersion

compensation value of 2.2. This was increased and the rate at which the pulse in the laser was amplified was observed. The amplification was highest when the dispersion in the amplifier was three times that in the loop. The result of simulating a laser with this configuration is shown in Figure 6.17. Again, long cavities can be achieved. The need to increase the dispersion in this configuration is to be expected. The amplifier section of the laser is immediately followed by the output coupler. Since the pulse must be amplified enough so that it has sufficient energy to be transmitted by the NOLM even after losing 30% of its energy to the output coupler. This means that a value of dispersion must be chosen such as to obtain the right pulse shape even after amplification.

The sidebands in this case are extremely pronounced as can be seen in Figure 6.19. This occurs due to the larger perturbations the laser imposes on the soliton like pulses. This make the sideband analysis easy and the sideband spacing information is summarized in Figure 6.20. Linear regression was used to find the effective length as a function of the amplifier length. This process yields the curve in Figure 6.21. Again, all these functions appear to be approximately linear. The form of the line in Figure 6.21 is

$$L_{eff} = 3.29L_{amp} - 1.1087.$$ (6.15)

The pulse peak intensity is 2.60. This is just after the output coupler and before the 30% output, so before the couple the intensity would have been 3.71. This means that the nonlinear length should have been the same. This value is about 19% larger than the slope in Equation 6.14. It is interesting to note that the slopes were all smaller than the expected values based on the peak laser intensities by about the same amount. This may imply that there is in fact some simple explanation possible for the disagreement.

As was mentioned before, the length of fiber lasers has been assumed to be limited to about 8 soliton periods. Using this length in Equation 6.15, we see that this corresponds to an effective length of 4.02 dispersion lengths. When Figure 6.17 is examined, this length is found to be where a large broadening of the stable gain region

occurs. Equations 6.13 and 6.15 can be used to compute the amplifier lengths corresponding to 8 soliton periods in the cases seen in Figures 6.7 and 6.12. The computed values are 5.3 and 5.2 dispersion lengths respectively. In both cases, the lasers appear to have some change in the stable gain curve near this point though its character is much less dramatic than in the laser with high output. This indicates that while these lasers do not cease functioning with an effective length of 8 soliton periods they do undergo some shift in their operation.
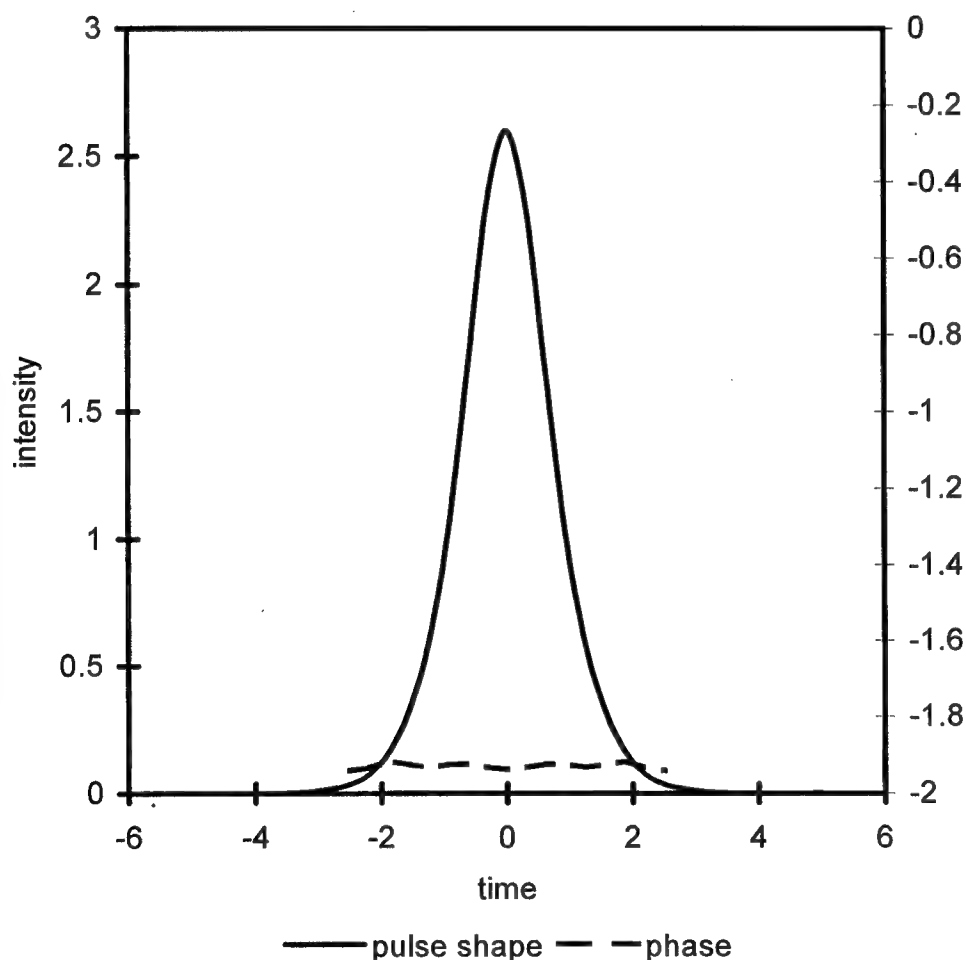
Figure 6.18 Pulse shape in a nonbirefringent dispersion balanced NOLM laser with a 60/40 beamsplitter, and a 4 soliton period long loop mirror. The output coupling is 30%. The dispersion in the amplifier is 3.0 times that in the loop. Pulse shape is given as a function of time. Both are in soliton units.
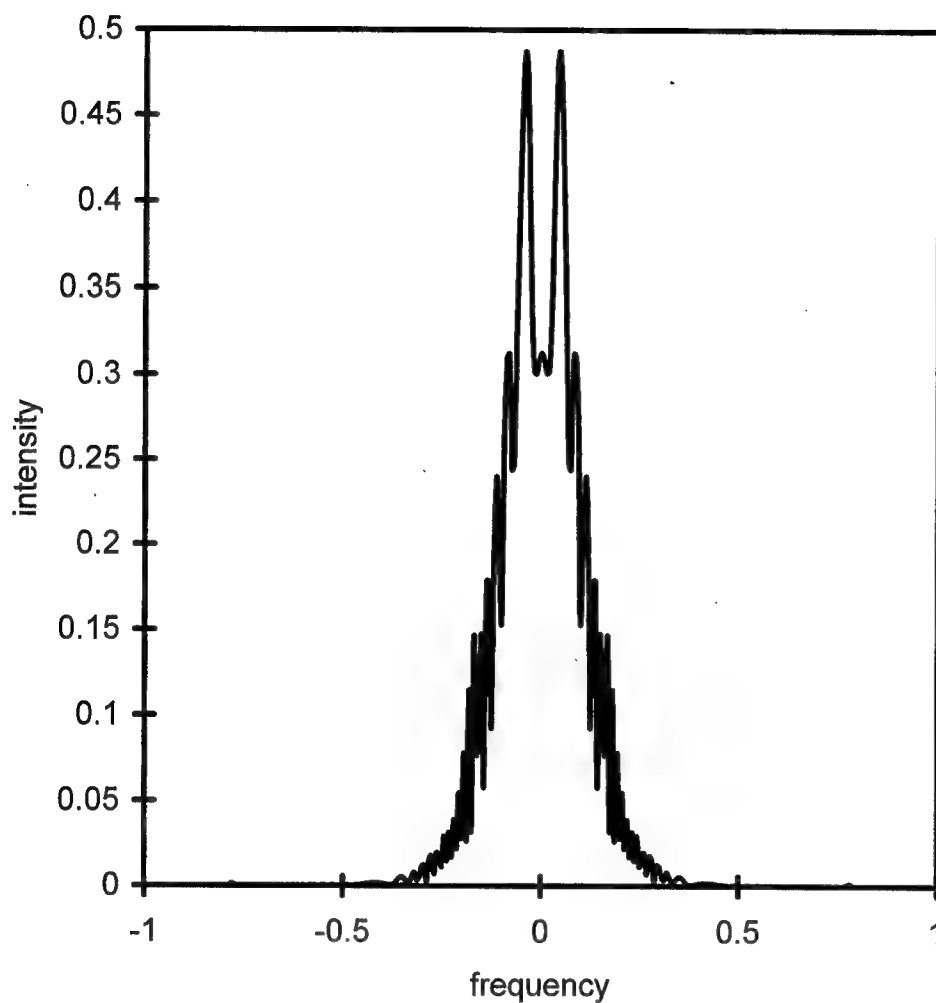
Figure 6.19 Pulse shape in a nonbirefringent dispersion balanced NOLM laser with a 60/40 beamsplitter, and a 4 soliton period long loop mirror. The output coupling is 30%. The dispersion in the amplifier is 3.0 times that in the loop. Pulse shape is given as a function of frequency. Both are given in soliton units.
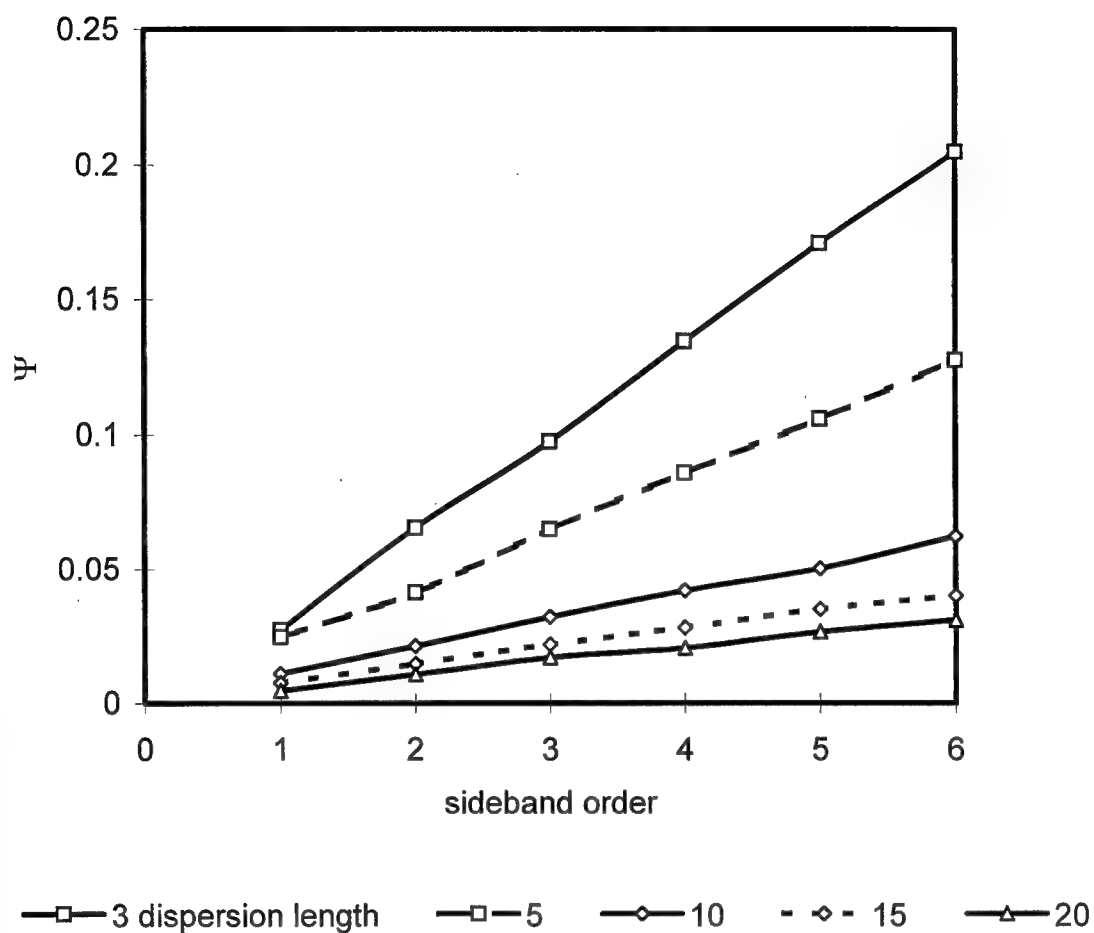
Figure 6.20 Sideband spacing in a nonbirefringent dispersion balanced NOLM laser with a 60/40 beamsplitter, and a 4 soliton period long loop mirror. The output coupling is 30%. The dispersion in the amplifier is 3.0 times that in the loop. The parameter Ψ is defined in Equation 6.10. The figure shows the effect of changing the amplifier length.
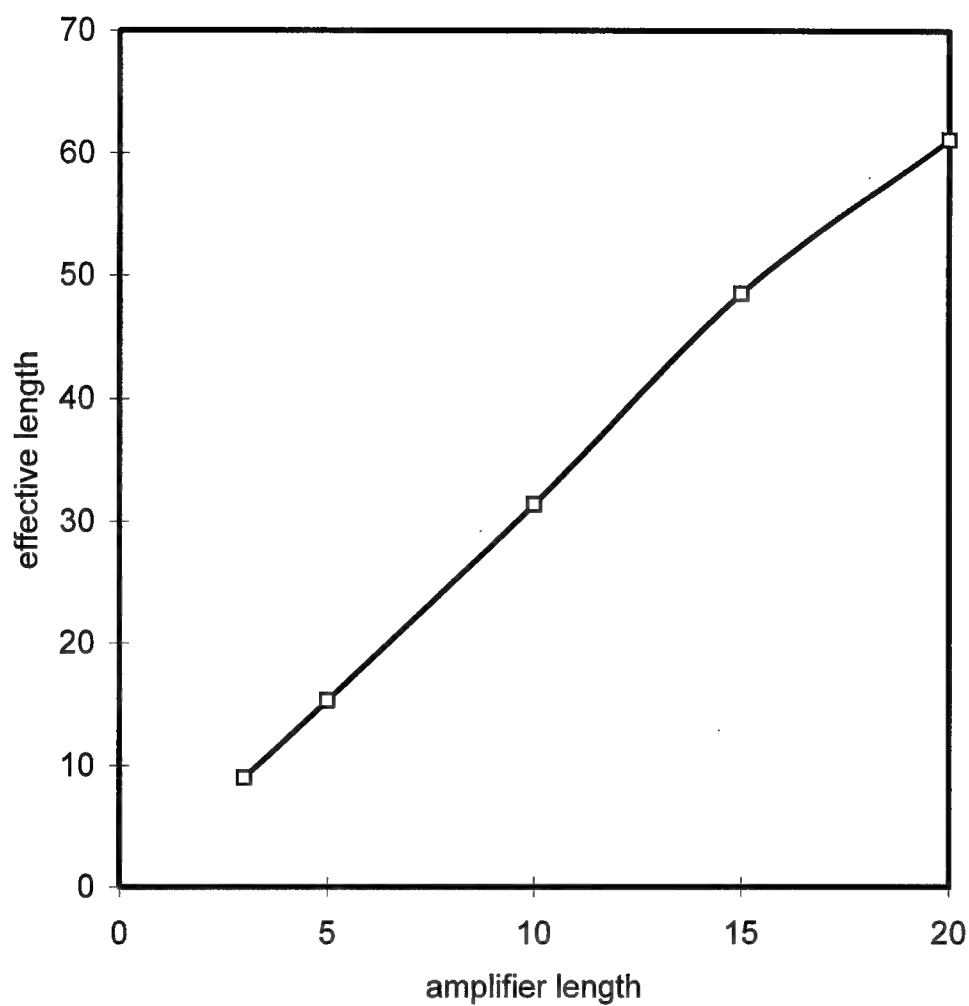
Figure 6.21 L_{eff} as computed by means of Equation 6.12. The laser is a nonbirefringent dispersion balanced NOLM laser with a 60/40 beamsplitter, and a 4 soliton period long loop mirror. The output coupling is 30%. The dispersion in the amplifier is 3.0 times that in the loop. Lengths are given in dispersion lengths.

Two situations were simulated in which the lasers were assumed to have birefringent fiber. The first was the case in which all of the starting pulse energy was on the slow birefringent axis and the plane of the loop tilted by $\pi/4$ radians from this direction. In the second, the pulse was a vector soliton and had equal amplitudes along both axes. The plane of the loop was along the slow axis. These cases were chosen because they appeared to offer the possibility of controlling the NOLM switch by adjusting the polarization controller. This was discussed in the chapter on the NOLM.

The results are displayed in Figures 6.22-6.24. The dispersion in the amplifier was made to be 2.2 times that in the loop. The pulse in the laser is again a nearly unchirped soliton. The shift of the pulse center in time is due to the fact that it is propagating predominately on the slow axis. Essentially none of the light leaked into the orthogonal polarization. In frequency space, the location of the maximum of the pulse has not changed, but the pulse has become asymmetric and the location of the sidebands have shifted.

A laser with a vector soliton trial pulse was simulated. The results are in Figures 6.25-6.27. The dispersion in the amplifier was again increased by 2.2. The laser pulse is found to maintain its polarization. In frequency space, one observes that the two polarizations couple with each other. This is also the explanation of the chirp that develops in the phase and the shift observed in the central frequencies.

When a phase shift of $\pi/4$ was imposed with the polarization controller no stable operating configuration could be found. This was true for both of the cases examined in which birefringence was considered. As described in the last section, the polarization controller reshapes the pulse. The same effects that lead to poor two-pass transmission in the case of the NOLM lead to excessively high loss in the laser. It was found that this loss could not be compensated with additional amplification. The pulse would stabilize for a pass and then decay away.
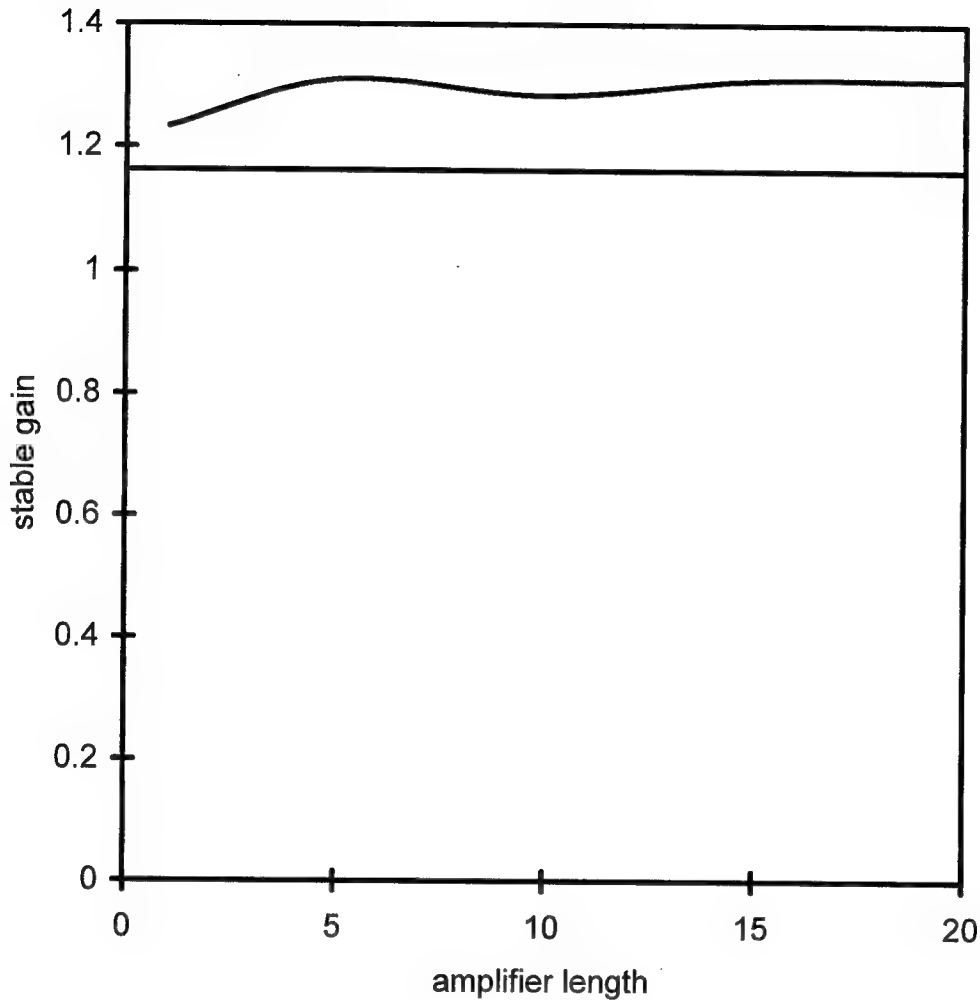
Figure 6.22 Stable pulse formation could take place between the curves in a birefringent NOLM laser with a 60/40 beamsplitter, and a 4 soliton period long loop mirror. The output coupling is 10%. The birefringence parameter is $\delta=0.1$. The input pulse and the slow axis of the polarization controller are aligned with the slow birefringent axis. The plane of the loop has a $-\pi/4$ angle with the slow axis. The dispersion in the amplifier is 2.2 times that in the loop. The amplifier length is given in dispersion lengths.
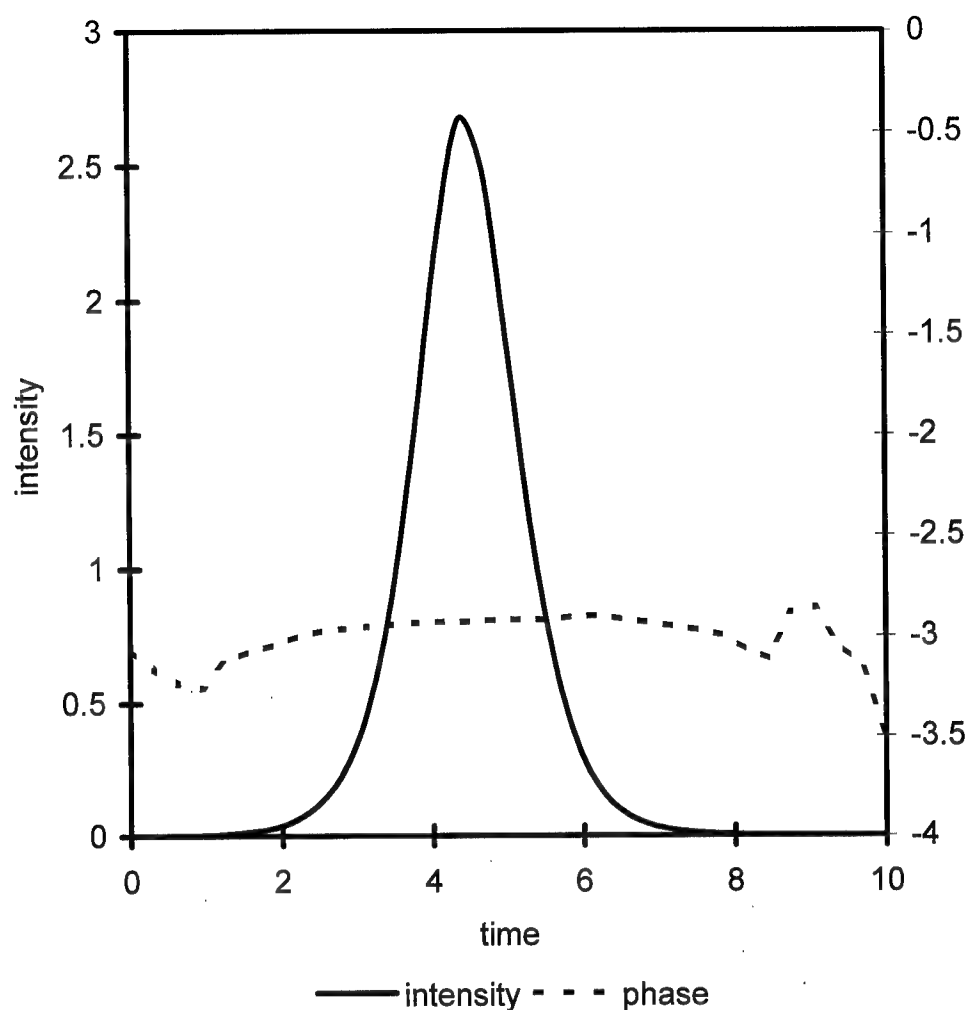
Figure 6.23 Pulse shape in a birefringent NOLM laser with a 60/40 beamsplitter, and a 4 soliton period long loop mirror. The output coupling is 10%. The birefringence parameter is δ=0.1. The input pulse and the slow axis of the polarization controller are aligned with the slow birefringent axis. The plane of the loop has a -π/4 angle with the slow axis. The dispersion in the amplifier is 2.2 times that in the loop. Pulse intensity is given as a function of time. Both are given in soliton units.
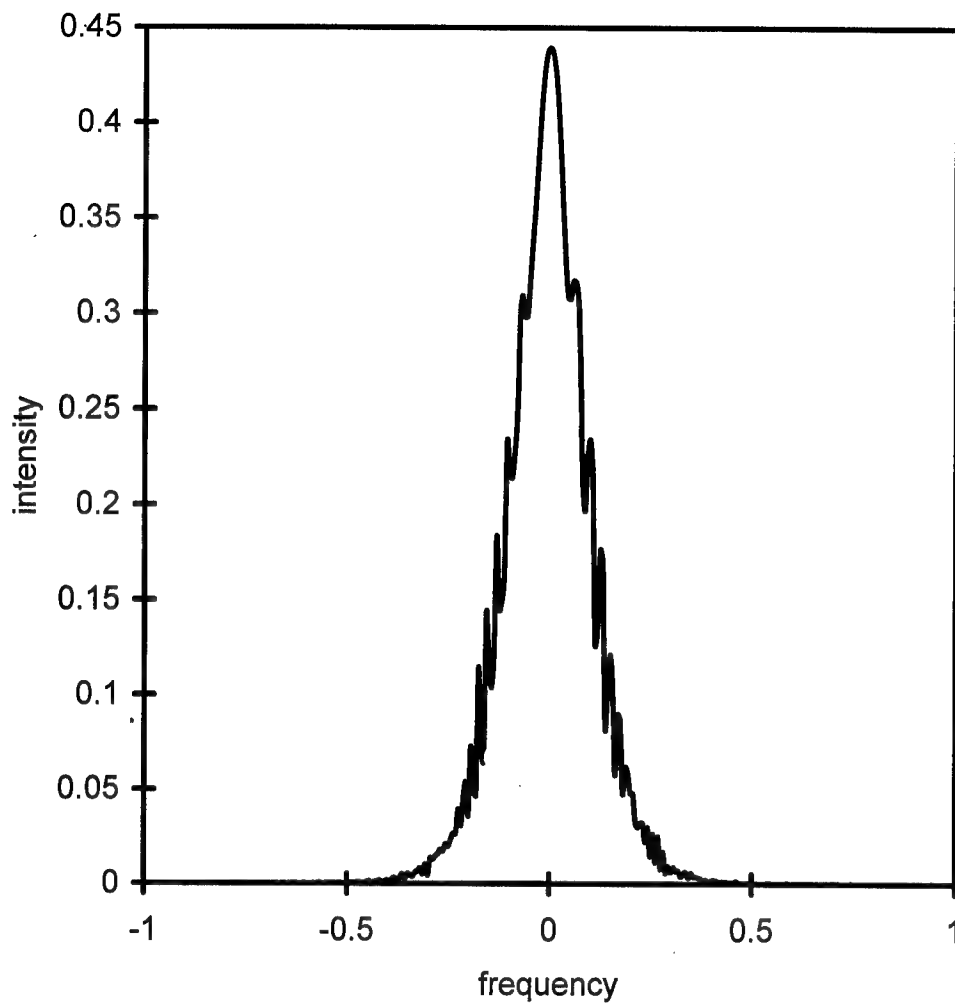
Figure 6.24 Pulse shape in a birefringent NOLM laser with a 60/40 beamsplitter, and a 4 soliton period long loop mirror. The output coupling is 10%. The birefringence parameter is δ=0.1. The input pulse and the slow axis of the polarization controller are aligned with the slow birefringent axis. The plane of the loop has a -π/4 angle with the slow axis. The dispersion in the amplifier is 2.2 times that in the loop. Pulse intensity is given as a function of frequency. Both are in soliton units.

Figure 6.25 Stable pulse formation could take place between the curves in a birefringent NOLM laser with a 60/40 beamsplitter, and a 4 soliton period long loop mirror. The output coupling is 10%. The birefringence parameter is $\delta=0.1$. The input pulse and the slow axis of the polarization controller are at an angle of $\pi/4$. with the slow birefringent axis. The plane of the loop is aligned with the slow axis. The dispersion in the amplifier is 2.2 times that in the loop
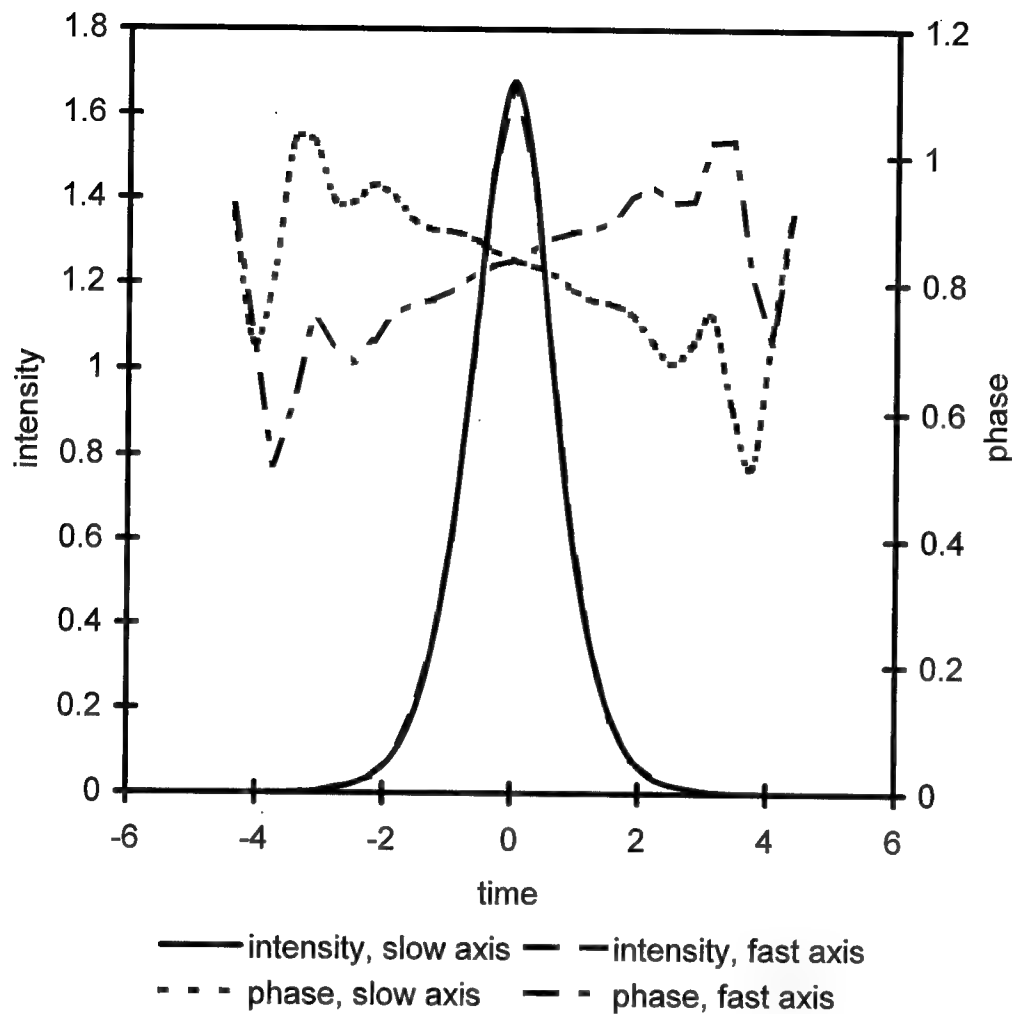
Figure 6.26 Pulse shape in a birefringent NOLM laser with a 60/40 beamsplitter, and a 4 soliton period long loop mirror. The output coupling is 10%. The birefringence parameter is δ=0.1. The input pulse and the slow axis of the polarization controller are at an angle of π/4. with the slow birefringent axis. The plane of the loop is aligned with the slow axis. The dispersion in the amplifier is 2.2 times that in the loop. Pulse intensity is given as a function of time. Both are given in soliton units.
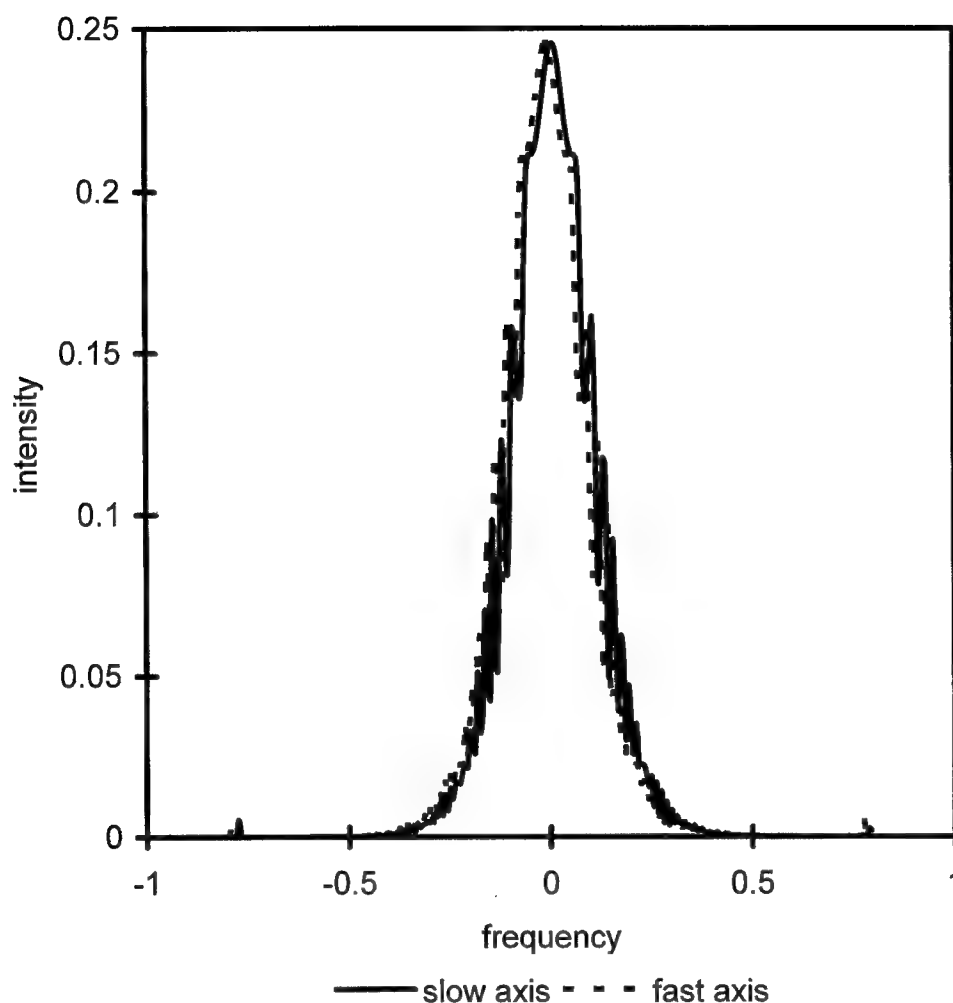
Figure 6.27 Pulse shape in a birefringent NOLM laser with a 60/40 beamsplitter, and a 4 soliton period long loop mirror. The output coupling is 10%. The birefringence parameter is $\delta=0.1$. The input pulse and the slow axis of the polarization controller are at an angle of $\pi/4$ with the slow birefringent axis. The plane of the loop is aligned with the slow axis. The dispersion in the amplifier is 2.2 times that in the loop. Pulse intensity is given as a function of frequency. Both are given in soliton units.

The conclusion of the results appears to be that the NOLM figure eight laser can function in a number of ways depending upon the amount of loss in the system. The loss can be introduced into the system in a number of ways. In the results above, we have

seen that it can be introduced by pulse reshaping in the amplifier, by birefringence reducing transmission through the NOLM, or by linear loss in the output coupler. If loss in all of these are low, then it is possible to make the laser cavity very long. Sidebands will build up, but they will not be great enough to make the laser stop working. If the laser has more loss in it, then it will function in a fashion described before by other in which the growth of the side bands creates a limit to how long the laser cavity can be made.

Haus[116] introduced the idea of inserting normal dispersion. This was described as a means of reshaping the pulse and they said that they optimized the results by computer simulation. Dulling did extensive experiments based on the idea of reducing total dispersion in the cavity. The new idea which is introduced here is that in a figure eight laser this balancing can be done by actually increasing dispersion. Dennis andDulling[120] did not invoke the idea of pulse reshaping nor did he describe where he inserted the positive dispersion fiber. I have been able to take the pulse reshaping ideas of Haus and extend them in a creative way to deal with the specific dynamics of the figure eight configuration.

The most straightforward experimental comparison is to the work of Dennis and Dulling.[120] They did experiments with an NALM mode-locked figure eight laser. They experimentally confirmed a relationship between the total length of the laser and the minimum producable pulse width. The relationship is given by

$$\tau_{min} \propto \sqrt{L\overline{\beta_2}} \, ,$$

as above. This result is consistent with the observation here that there is a limit to how long the amplifier can be made. Since the length is given in soliton units, the length of the cavity, and the width of the pulses is linked by this equation. They also observed the formation of sidebands. The sideband theory has been verified for ring lasers.[111] It appears that the predictions of the simulations given here agree as long as the effective

length of the loop is adjusted to take into account the fact that the pulse has a different energy in different parts of the loop.

Chapter Seven : Conclusions

The research described in this thesis has extended understanding of fiber optic devices and lasers. The work has been principally concerned with applying existing models to give a more detailed understanding of their operation. Much of this work has centered upon birefringence in optical fibers. Some important new ideas have emerged about nonbirefringent figure eight lasers, as well.

New results have been obtained concerning the amplification of pulses in birefringent optical amplifiers. The simulations showed that, for high amplification, the pulse broke up into many pulses, and that the pulses formed tended to couple with pulses formed in the orthogonal polarization. This results in a train of coupled solitary waves propagating together. This coupling can be broken by a large amplifier saturation parameter.

The simulation of the nonlinear optical loop mirror (NOLM) was also extended into the birefringent case. Specifically, I studied the effect of birefringence on the function of the NOLM. Many of the same phenomena were found as in the nonbirefringent case. It was found that the length of the output pulse relative to the input pulse tends to increase with the length of the loop; however, the energy required for transmission decreases. I examined the effect of adjusting the polarization controller in the loop. The controller reduces the energy required for switching, and increases low intensity transmission. Unfortunately, it tends to distort pulses as well. This reduces the transmission of the pulses when reintroduced into a controller, and hence, the utility of the device. The problem is reduced if the birefringence in the loop is small. Since the values of birefringence examined here are fairly high, the technique may still have utility.

The work on the amplifier and on the NOLM was combined to study a figure eight laser mode-locked by an NOLM. The eight soliton period length limit found by other groups experimentally, and analytically by other means, reemerged in this simulation. A maximum gain for a stable pulse also was found. This limit puts a bound

on how powerful a pulse can become in a laser of this type. It also explains why pulses always break up into many smaller pulses, when pump power is increased.

It was demonstrated, for the first time, that the limit of the length of the loop could be eliminated by balancing the dispersion in the two parts of the figure eight laser. If the dispersion in the amplifier section is increased, so that the pulse is nearly a soliton in both parts of the laser, then the cavity can be made as long as one wishes. This method eliminates a design constraint for this type of laser.

The pulses in this simulation displayed frequency side-bands of the kind that are experimentally found. Their location agreed with experimental observations and analytical predictions. An effective length of the cavity was predicted. This effective length could be related to the physical length of the cavity, and to the relative pulse intensities in the different parts of the laser.

A laser with birefringence was simulated. It could be made to function when the polarization controller applied no phase delay along one birefringent axis relative to the other. When a phase delay was imposed, however, the controller created enough pulse distortion to cause the laser to never produce stable pulses. This implies that the behavior of the NOLM laser can not be controlled in this manner, unless the birefringence of the fiber is very small. If the birefringence is large, the controller must be adjusted so as to eliminate this phase delay.

The idea of dispersion balanced figure eight lasers has not been examined at all in the past. The method of increasing dispersion in one part of the fiber actually goes in the opposite direction of the methods used by other researchers. At the present time experiments to verify the predictions of the model are being considered.

Literature Cited

[1] G. P. Agrawal, *Fiber-Optic Communication Systems*. New York: Wiley, 1992.

[2] A. W. Snyder and J. D. Love, *Optical Waveguide Theory*. London: Chapman and Hall, 1983.

[3] A. Yariv, *Quantum Electronics*. New York: Wiley, 1989.

[4] G. P. Agrawal, *Nonlinear Fiber Optics*. San Diego: Academic Press, 1989.

[5] M. N. Islam, *Ultrafast Fiber Switching Devices and Systems* Cambridge: Cambridge University Press, 1992.

[6] M. J. F. Digonnet, Ed., *Rare-Earth Doped Fiber Lasers and Amplifiers*. New York: Dekker, 1993.

[7] E. Desurvire, *Erbium-Doped Fiber Amplfiers*. New York: Wiley, 1994.

[8] P. N. Butcher and D. Cotter *The Elements of Nonliner Optics*. Cambridge: Cambridge University Press, 1990.

[9] K. Otsuka, "Nonlinear antiresonant ring interferometer," *Opt. Lett.,* vol. 8, pp. 471-473, 1983.

[10] S. Trillo *et al,* "Soliton switching in fiber nonlinear directional couplers," *Opt. Lett.,* vol. 13, pp. 672-674, 1988.

[11] M. N. Islam, "Ultrafast all-optical logic gates based on soliton trapping in fibers," *Opt. Lett.* vol. 14, pp. 1257-1259, 1989.

[12] I. N. Duling III, "Subpicosecond all-fiber erbium laser," *Electron. Lett.,* vol. 27, pp. 544-545, 1991.

[13] M. Hofer *et al,* "Mode locking with cross-phase and self-phase modulation," *Opt. Lett.,* vol. 16, pp. 502-504, 1991.

[14] K. Tamura *et al,* "77-fs pulse generation from a stretched-pulse additive pulse mode locked all-fiber ring laser," *Opt. Lett.,* vol. 18, pp. 1080-1082, 1993.

[15] P. E. Langridge and W. J. Firth, "Doubly nonlinear fibre loop lasers," *Opt. Comm.,* vol. 86, pp. 170-176, 1991.

[16] A. Hasegawa, *Optical Solitons in Fiber.* New York: Springer-Verlag, 1989.

[17] B. E. A. Saleh and M. C. Teich, *Fundamentals of Photonics.* New York: Wiley, 1991.

[18] R. Courant and D. Hilbert, *Methods of Mathematical Physics.* New York: Wiley, 1983.

[19] A. Yariv, *Theory and Applications of Quantum Mechanics.* New York: Wiley,1982.

[20] Y. Kodama and A Hasegawa, "Nonlinear pulse propagation in a monomode dielectric guide," *IEEE J. Quantum Electron.,* vol. QE-23, pp. 510-524, 1987.

[21] A. Hasegawa and F. Tappert, "Transmission of stationary nonlinear optical pulses in dispersive dielectric fibers," *Appl. Phys Lett.,* vol. 23, pp. 142-144, 1973.

[22] A. Hasegawas, and Y. Kodama, "Signal transmission by optical solitons in monomode fiber," *Proc. IEEE,* vol. 69, pp. 1145-1150, 1981.

[23] G. Strang, *Introduction to Applied Mathematics.* Wellesley, MA: Wellesley-Cambridge Press, 1986.

[24] P. L. DeVries *A First Course in Computational Physics.* New York: Wiley, 1994.

[25] A. C. Newell and J. V. Moloney, *Nonlinear Optics.* Redwood City: Addison-Wesley, 1992.

[26] H. Liu and A. Puri, "Effect of higher-order group-velocity dispersion on ultrashort pulses propagation in optical fibers," *Opt. Comm.,* vol.99, p. 375, 1993.

[27] I. P. Kaminow, "Polarization in optical fibers," *IEEE J. Quantum. Electron,* vol. QE-17, pp. 15-22, 1981.

[28] C. R. Menyuk, "Nonlinear pulse propagation in birefringent optical fibers," *IEEE J. Quantum. Electon.,* vol. QE-23, pp. 174-179, 1987.

[29] C. R. Menyuk, "Pulse propagation in an elliptically birefringent Kerr medium," *IEEE J. Quantum. Electron.,* vol. QE-25, pp. 2674-2682, 1989.

[30] C. R. Menyuk, M. N. Islam, and J. P. Gordon, "Raman effect in birefringent optical fibers," *Opt. Lett.* vol. 16, pp. 566-568, 1992.

[31] M. V. Tratnik and J. E. Sipe, "Bound solitary waves in a birefringent optical fiber," *Phys. Rev. A*, vol. 38, pp. 2011-2016, 1988.

[32] D. N. Christodoulides and R. I. Joseph, "Vector solitons in birefringent nonlinear dispersive media," *Opt. Lett.,* vol. 13, pp. 53-55, 1988.

[33] R. S. Tasgal and M. J. Potasek, "Soliton solutions to coupled higher-order nonlinear Schrodinger equations," *J. Math. Phys.,* vol. 33, pp. 1208-1215. 1992.

[34] M. Haelterman et al. "Bound-vector solitary waves in isotropic nonlinear dispersive media," *Opt. Lett.,* vol. 18, pp. 1406-1408, 1993.

[35] T. Ueda and W. L. Kath, "Dynamics of coupled solitons in nonlinear optical fibers," *Phys. Rev. A,"* vol. 42, pp. 563-571. 1990.

[36] V. V. Afanasjev, "Soliton polarization rotation in fiber lasers," *Opt. Lett.,* vol. 20, 270-272, 1995.

[37] C. R. Menyuk, "Stability of solitons in birefringent optical fibers. I: Equal propagation amplitudes," *Opt. Lett.,* vol. 12, pp. 614-616, 1988.

[38] C. R. Menyuk, "Stability of solitons in birefringent optical fibers. II. arbitrary amplitudes," *J. Opt. Soc. Am. B,* vol. 5, pp. 392-402, 1988.

[39] Y. S. Kivshar, "Soliton stability in birefringent optical fibers: analytical approach," *J. Opt. Soc. Am. B,* vol. 7, pp. 2204-2209, 1990.

[40] K. J. Blow, N. J. Doran and D. Wood, "Polarization instabilities for solitons in birefringent fibers," *Opt. Lett.* , vol. 12, pp. 202-204, 1987.

[41] M. N. Islam, C. E. Soccolich, J. P. Gordon, and U. C. Paek, "Soliton intensity-dependent polarization rotation," *Opt. Lett.,* vol. 15, pp. 21-23, 1990.

[42] B. J. Ainslie, "A Review of the fabrication and properties of erbium-doped fibers for optical amplifiers," *J. of Lightwave Technol.,* vol. 9, pp. 220-227, 1991.

[43] M. Nakazawa, K. Kurokawa, H. Kubota, K. Suzuki, and Y. Kimura, "Femtosecond erbium-doped optical fiber amplifier," *Appl. Phys. Lett,* vol. 13, pp. 653-655, 1990.

[44] B. J. Ainslie *et. al*, "Femtosecond soliton amplification in erbium doped silica fibre," *Electon. Lett.*, vol. 26, pp. 186-188, 1990.

[45] Yu. Khrushcev *et al*, "Amplification of femtosecond pulses in Er^{3+} -doped single-mode optical fibres," *Electron. Lett.*, vol. 26, pp. 456-458, 1990.

[46] C. R. Giles and E. Desurvire, "Modeling erbium-doped fiber amplifiers," *J. Lightwave Tech.*, vol. 9, pp. 271-283, 1991.

[47] E. Desurvire, "Study of the complex atomic susceptibility of erbium-doped fiber amplifiers," *J. Lightwave Tech.*, vol. 8, pp. 1517-1527, 1990.

[48] I. V. Mel'nikov, R. F. Naviev and A. V. Nazarkin, "Coherent amplification of ultrashort solitons in doped fiber," *Opt. Lett.*, vol. 15, p. 1348, 1990.

[49] T. Wang and S. Chi, "Self-induced transparency in a dispersive and nonlinear Kerr host medium," *Opt. Lett.*, vol. 16, p. 1574, 1991.

[50] A. I. Maimistov, "On coherent amplification of optical solitons," *Opt. Comm.*, vol. 94, p. 33, 1992.

[51] I. R. Gabitov, M. Romagnoli, and S. Wabnitz, "Femtosecond soliton collapse and coherent pulse train generation in erbium-doped fiber amplifiers," *App. Phys. Lett.*, vol. 59, p. 1811, 1991.

[52] M. Nakazawa, E. Yamada, and H. Kubota, "Coexistence of self-induced transparency soliton and nonlinear Schrodinger soliton," *Phys. Rev. Lett.*, vol. 66, p. 2625, 1991.

[53] B. Gross and J. T. Manassah, "Numerical solutions of the Maxwell-Bloch equations for a fiber amplifier," *Opt. Lett.*, vol. 17, p. 350, 1992.

[54] W. Hodel, J Schutz, and H. P. Weber, "Limits to the amplification efficiency of ultrashort fundamental solitons using Er-doped fibers," *Opt. Comm.*, vol. 88, p. 173, 1992.

[55] W. Hodel, D. S. Peter and H. P. Weber, "Chirped pulse amplification in Er-doped fibers," *Opt. Comm.*, vol. 97, p. 233, 1993.

[56] L. Gagnon, and P. A. Belanger, "Adiabatic amplification of optical solitons," *Phys. Rev. A,* vol. 43, p. 6187, 1991.

[57]P. A. Belanger, L. Gagnon, and C. Pare, "Solitary pulses in an amplified nonlinear dispersive medium," *Opt. Lett.,* vol. 14, p. 943, 1989.

[58]M. Nakazawa, K. Kurokawa, H. Kubota, and E. Yamada, "Observation of the trapping of an optical soliton by adiabatic gain narrowing and its escape," *Phys. Rev. Lett.,* vol. 65, p. 1881, 1990.

[59]M. Romagnoli, F. S. Locati, F. Matera, M. Settembre, M. Tamburrini, and S. Wabnitz, "Role of pump-induced dispersion on femtosecond soliton amplification in erbium-doped fibers," *Opt. Lett.,* vol. 17, p. 923, 1992.

[60]M. Romagnoli, F. S. Locati, F. Matera, M. Settembre, M. Tamburrini, and S. Wabnitz, "Nonlinear nonreciprocity of soliton amplification with erbium-doped fibers," *Opt. Lett.,* vol. 17, p. 1456, 1992.

[61]G. P. Agrawal, "Amplification of ultrashort solitons in erbium-doper fiber amplifiers," *IEEE Phot. Tech. Lett.,* vol. 2, p. 875, 1990.

[62]G. P. Agrawal, "Optical pulse propagation in doped fiber amplifiers," *Phys. Rev. A,* vol. 44, p. 7493, 1991.

[63]G. P. Agrawal, "Effect of gain dispersion and stimulated Raman scattering on soliton amplification in fiber amplifiers," *Opt. Lett.,* vol. 16, p. 226, 1991.

[64] C. C. Yang and J. S. Wang, "Cross-polarization cross-phase modulation of femtosecond pulses in erbium-doped fiber amplifiers," *J. Opt. Soc. Am. B,* vol. 9, pp. 682-686, 1992

[65] E. Desurvire et al., "Design optimization for efficient erbium-doped fiber amplifiers," *J. Lightwave Technol.,* vol. 8, pp. 1730-1741, 1990.

[66] M. Ohahshi, "Design Considerations for an er^{3+} -doped fiber amplifier," *J. Lightwave Technol.,* vol. 9, pp. 1099-1104, 1991.

[67] B. Pedersen et al., "The design of erbium-doped fiber amplifiers," *J. Lightwave Technol.,* vol. 9, pp. 1105-1112, 1991.

[68] The. Pfeiffer and H. Bulow, "Analytical gain equation for erbium-doped fiber amplifiers including mode field profiles and dopant distribution," *IEEE Phonics Technol. Lett.,* vol. 4, pp. 447-451, 1992.

[69] N. J. Doran and D. Wood, "Nonlinear-optical loop mirror," *Opt. Lett.*, vol. 13 pp. 56-58, 1988.

[70] D. A. Pattison et al., "Bandpass switching in a nonlinear-optical loop mirror," *Opt. Lett.*, vol. 20, pp. 362-364, 1995.

[71] M. E. Fermann et al., "Nonlinear amplifying loop mirror," *Opt. Lett.*, vol. 15, pp. 752-754, 1990.

[72] K. J. Blow, N. J. Doran and B. K. Nayar, "Experimental demostration of optical solitons switching in an all-fiber nonlinear Sagnac interferometer," *Opt. Lett.*, vol. 14, pp. 754-756, 1989.

[73] M. Jinno and T. Matsumoto, "Nonlinear Sagnac interferometer switch and its applications," *IEEE J. Quantum. Electron.*, vol. 28 pp. 875-882, 1992.

[74] B. -E. Olsson and P. A. Andrekson, "Extinction ratio improvement using the nonlinear optical loop mirror," *IEEE Photonics Technol. Lett.* vol. 7, pp. 120-122, 1995.

[75] B. -E. Olsson and P. A. Andrekson, "Noise filtering with the nonlinear optical loop mirror," *J. Lightwave Technol.*, vol. 13, pp. 213-215, 1995.

[76] S. V. Chernikov and J. R. Taylor, "Multigigabit/s pulse source based on the switching of an optical beat signal in a nonlinear fibre loop mirror," *Electron. Lett.*, vol. 29, pp. 658-660, 1993.

[77] M. Matsumoto et al., "Adiabatic amplification of solitons by means of nonlinear amplifying loop mirrors," *Opt. Lett.*, vol. 19, pp. 1019-1021, 1994.

[78] I. N. Duling, III, C. -J. Chen, P. K. A. Wai, and C. R. Menyuk, "Operation of a nonlinear loop mirror in a laser cavity," *IEEE. J. Quantum Electron.*, vol. 30, pp. 200-208, 1994.

[79] K. J. Blow, N. J. Doran, and S. J. D. Phoenix, "The soliton phase," *Opt. Comm.*, vol. 88, pp. 137-140, 1992.

[80] T. A. Birks and P. Morkel, "Jones calculus analysis of single-mode fiber Sagnac reflector," *Appl. Opt.*, vol. 27, pp. 3107-3113, 1988.

[81] D. B. Mortimore, "Fiber Loop Reflectors," *J. Lightwave Technol.,* vol. 6, pp. 1217-1224, 1988.

[82] N. Finlayson, B. K. Nayar, and N. J. Doran, "Switch inversion and polarization sensitivity of the nonlinear-optical loop mirror," *Opt. Lett.,* vol. 17, pp. 112-114, 1992.

[83] H. Lin et al., "Optimizing polarization states in a figure-8 laser using a nonreciprocal phase shifter," *J. Lightwave Technol.,* vol. 12, pp. 1121-1128, 1994.

[84] B. L. Heffner, "Deterministic, analytcally complete measurement of Polarization-dependent transmission through optical devices," *IEEE Photonics Technol. Lett,* vol. 4, pp. 451-454, 1992.

[85] K. Smith, N. J. Doran, and P. G. J. Wigley, "Pulse shaping, compression, and pedestal suppression employing a nonlinear-optical loop mirror," *Opt. Lett.,* vol. 15, pp. 1294-1296, 1990.

[86] I. N. Duling III, C. -J. Chen, P. K. A. Wai, and C. R. Menyuk, "Operation of a nonlinear loop mirror in a laser cavity," *IEEE J. Quantum Electron.,* vol. 30, pp. 194-199, 1994.

[87] B. K. Nayar, N. Finlayson and N. J. Doran, "Concatenated all-optical loop mirror switches," *J. Mod. Opt.,* vol. 40, pp. 2327-2332, 1993.

[88] H. Avramopoulos et al., "Passive modelocking of an erbium-doped fiber laser," *Optical Amplifiers and Their applications, Technical Digest Series,* vol. 19, PDP8, 1990.

[89] S. Wu et al. "High-power passively mode-locked Er-doped fiber laser with a nonlinear optical loop mirror," *Opt. Lett.,* vol. 18, pp. 1444-1446, 1993.

[90] I. N. Duling III, "All-fiber ring soliton laser mode locked with a nonlinear mirror," *Opt. Lett.,*vol. 16, pp. 539-541, 1991.

[91] D. J. Richardson et al. "Selfstarting, passively modelocked erbium fiber ring laser based on the amplifying Sagnac switch," *Electron. Lett.,* vol. 27, pp. 542-544, 1991.

[92] N. Nakazawa, E. Yoshida and Y. Kimura, "Generation of 98 fs optical pulses directly from and erbium-doped fibre ring laser at 1.57 μm," *Electron. Lett.,* vol. 29, pp. 63-65, 1993.

[93] D. J. Richardson et al., "Pulse repetition rates in passive, selfstarting femtosecond soliton fiber laser,"*Electron. Lett.,* vol. 27, pp. 1451-1453, 1991.

[94] A. E. Siegman, *Lasers.* Mill Valley, CA: University Science Books, 1986.

[95] E. Yoshida et al., "Laser diode-pumped femtosecond erbium-doped fiber laser with a sub-ring cavity for repetion rate control," *Appl. Phys. Lett.,* vol. 60, pp. 932-934, 1992.

[96] N. Park et al., "Frequency locking of an erbium-doped fiber ring laser to an external fiber Fabry-Perot resonator," *Opt. Lett.,* vol. 18, pp. 879-881, 1993.

[97] G. T. Harvey and L. F. Mollenauer, "Harmonically mode-locked fiber ring laser with an internal Fabry-Perot stabilizer for soltion transmission," *Opt. Lett.,* vol. 18, pp. 107-109, 1993.

[98] M. L. Dennis and I. N. Duling III, "High repetition rate figure eight laser with extracavity feedback," *Electon. Lett.,* vol. 28, pp. 1894-1896, 1992.

[99] X. Shan et al., "Stabilising Er fibre soliton laser with pulse phase locking," *Electron. Lett.,* vol. 28, pp. 182-184, 1992.

[100] A. B. Grudinin et al., "Passive harmonic modelocking of a fibre soliton ring laser," *Electron. Lett.,* vol. 29, pp. 1860-1861, 1993.

[101] Hofer *et al*, "Characterization of ultrashort pulse formation in passively mode-locked fiber lasers," *IEEE J. Quantum Electron.,* vol. 28, pp. 720-728, 1992.

[102] A. G. Bulushev et al., "Self-starting mode-locked laser with a nonlinear ring resonator," *Opt. Lett.,* vol. 16, pp. 88-90, 1991.

[103] A. J. Stentz and R. W. Boyd, "Polarization effects and nonlinear switching in fiber figure-eight lasers," *Opt. Lett.,* vol. 19, pp. 1462-1464, 1994.

[104] V. Tzelpis et al., "Analysis of a passively mode-locked self-starting all-fiber soliton laser," *J. Lightwave Technol.,* vol. 11, pp. 1729-1736, 1993.

[105] C. -J. Chen et al., "Soliton fiber ring laser," *Opt. Lett.,* vol. 17, pp. 417-419, 1992.

[106] D. J. Richardson *et al*, "Amplification of femtosecond pulses in a passive all-fiber soliton source," *Opt. Lett.,* vol. 17, pp. 1596-1598, 1992.

[107] S. M. J. Kelly, "Characteristic sideband instability of periodically amplified average soliton," *Electron. Lett.* vol. 28, pp. 806-808, 1992.

[108] K. J. Blow and N. J. Doran, "Average soliton dynamics and the operation of soliton systems with lumped amplifiers," *IEEE Photonics Technol. Lett.,* vol. 3, pp. 369-371, 1991.

[109] S. M. J. Kelly, et al., " Average soliton dynamics of a high-gain erbium fiber laser," *Opt. Lett.,* vol. 16, pp. 1337-1339, 1991.

[110] N. J. Smith et al., "Sideband generation through perturbations to the average soliton model," *J. Lightwave Tech.,* vol. 10, pp. 1329-1333, 1992.

[111] D. U. Noske, et al. "Source of spectral and temporal instability in soliton fiber lasers," *Opt. Lett.,* vol. 17, pp. 1515-1517, 1992.

[112] M. L. Dennis and I. N. Duling III, "Role of dispersion in limiting pulse width in fiber lasers," *Appl. Phys. Lett.,* vol. 62, pp. 2911-2913, 1993.

[113] H. A. Haus, E. P. Ippen, K. Tamura, "Additive-pulse modelocking in fiber lasers," *IEEE J. Quantum Electron.,* vol. 30, pp. 200-208, 1994.

[114] H. A. Haus and E. P. Ippen, "Self-starting of passively mode-locked lasers," *Opt. Lett.,* vol. 16, pp. 1331-1333, 1991.

[115] H. A. Haus et al., "Effect of third-order dispersion on passive mode locking," *Opt. Lett.,* vol. 18, pp. 51-53, 1993.

[116] H. A. Haus et al., "Stretched-pulse additive pulse mode-locking in fiber ring lasers: theory and experiment," *IEEE J. Quantum Electron.,* vol. 31, pp. 591-598, 1995.

[117] P. F. Curley et al., "Periodic pulse evolution in solitary lasers," *J. Opt. Soc. Am. B,*" vol. 10, pp. 1025-1028, 1993.

[118] C.-J. Chen et al. "Stability of passively mode-locked fiber lasers with fast saturable absorption," *Opt. Lett.,* vol. 19, pp. 198-200, 1994.

[119] A. I. Chernykh and S. K. Turitsyn, "Soliton and collapse regimes of pulse generation in passively mode-locked laser systems," *Opt. Lett.,* vol. 20, pp. 398-400, 1995.

[120] M. L. Dennis and I. N. Duling III, "Experimental study of sideband generation in femtosecond fiber lasers," *IEEE J. Quantum Electron.,* vol. 30, pp. 1469-1477, 1994.

[121] N. J. Smith and N. J. Doran, "Picosecond soliton propagation using nonlinear optical loop mirrosrs as intensity filters," *Electron. Lett.,* vol. 30, pp. 1084-1085, 1994.

[122] M. L. Dennis and I. N. Duling III, "Third-order dispersion in femtosecond fiber lasers," *Opt. Lett.,* vol. 19, pp. 1750-1752, 1994.

[123] J. P. Gordon, "Dispersive petrubations of solitons of the nonlinear Schrodinger equation," *J. Opt. Soc. B*, vol. 9, pp. 91-97, 1992.

MISSION OF ROME LABORATORY

Mission. The mission of Rome Laboratory is to advance the science and technologies of command, control, communications and intelligence and to transition them into systems to meet customer needs. To achieve this, Rome Lab:

a. Conducts vigorous research, development and test programs in all applicable technologies;

b. Transitions technology to current and future systems to improve operational capability, readiness, and supportability;

c. Provides a full range of technical support to Air Force Material Command product centers and other Air Force organizations;

d. Promotes transfer of technology to the private sector;

e. Maintains leading edge technological expertise in the areas of surveillance, communications, command and control, intelligence, reliability science, electro-magnetic technology, photonics, signal processing, and computational science.

The thrust areas of technical competence include: Surveillance, Communications, Command and Control, Intelligence, Signal Processing, Computer Science and Technology, Electromagnetic Technology, Photonics and Reliability Sciences.